UC San Diego
UC San Diego Electronic Theses and Dissertations

Title
Coordinated Voltage Regulation of Distribution Networks

Permalink
https://escholarship.org/uc/item/09x7234m

Author
Li, Changfu

Publication Date
2020

Peer reviewed|Thesis/dissertation

UNIVERSITY OF CALIFORNIA SAN DIEGO

Coordinated Voltage Regulation of Distribution Networks

A dissertation submitted in partial satisfaction of the
requirements for the degree
Doctor of Philosophy

in

Engineering Sciences (Mechanical Engineering)

by

Changfu Li

Committee in charge:

Professor Jan Kleissl, Chair
Professor Raymond de Callafon
Professor Hamed Mohsenian-Rad
Professor Eugene R. Pawlak
Professor Nanpeng Yu
Professor Paul Yu

2020

The dissertation of Changfu Li is approved, and it is acceptable in quality and form for publication on microfilm and electronically:

_____

_____

_____

_____

_____

Chair

University of California San Diego

2020

DEDICATION

献给我的父母和姐姐.

To my parents and sister.

TABLE OF CONTENTS

LIST OF TABLES

ACKNOWLEDGEMENTS

Last but not least, I would like to express gratitude to my families. Thank you for your continuous love and support, without which this dissertation would have not be completed.

The text and data in Chapter 2, in full, is a reprint of the material as it appears in Optimal OLTC Voltage Control Scheme to Enable High Solar Penetrations, Li, C., Disfani, V.R., Pecenak, Z.K., Mohajeryami, S., Kelissl, J., *Electric Power Systems Research*, 2018. The dissertation author is the primary investigator and author of this article.

The text and data in Chapter 3, in full, is a reprint of the material as it appears in Coordination of OLTC and Smart Inverters for Optimal Voltage Regulation of Unbalanced Distribution Networks, Li, C., Disfani, V.R., Haghi, H.V., Kelissl, J., *Electric Power Systems Research*, 2020. The dissertation author is the primary investigator and author of this article.

The text and data in Chapter 4, in full, is submitted to *Journal of Renewable and Sustainable Energy* under the title Data-Driven Online PV Smart Inverter Coordination using Deep Reinforcement Learning, Li, C., Chen, Y., Jin, C., Sharma, R., Kelissl, J.. The dissertation author is the primary investigator and author of this article.

VITA

2014   B. E. in Thermal Energy & Power Engineering, Huazhong University of Science and Technology, Wuhan, China

2015   M.S. in Engieering Sciences (Mechanical Enginering) University of California San Diego, La Jolla, CA, USA

2020   Ph. D. in Engineering Sciences (Mechanical Engineering), University of California San Diego, La Jolla, CA, USA

SELECTED PUBLICATIONS

C. Li, Y. Chen, C. Jin, R. Sharma, and J. Kleissl , "Data-Driven Online PV Smart Inverter Coordination using Deep Reinforcement Learning", *Journal of Renewable and Sustainable Energy*, submitted, 2020.

C. Li, V. R. Disfani, H. V. Haghi, and J. Kleissl, "Coordination of OLTC and Smart Inverters for Optimal Voltage Regulation of Unbalanced Distribution Networks", *Electric Power Systems Research*, 187, 2020.

Z. K. Pecenak, H. V. Haghi, **C. Li**, M. J. Reno, V. R. Disfani, and J. Kleissl, "Aggregation of Voltage-Controlled Devices During Distribution Network Reduction", *IEEE Transactions on Smart Grid*, 2020.

C. Li, V. R. Disfani, H. V. Haghi, and J. Kleissl, "Optimal Voltage Regulation of Unbalanced Distribution Networks with Coordination of OLTC and PV Generation", *IEEE PESGM*, 2019.

C. Li, C. Jin, and R. Sharma, "Coordination of PV Smart Inverters Using Deep Reinforcement Learning for Grid Voltage Regulation", *IEEE ICMLA*, 2019.

C. Cortés, H. V. Haghi, **C. Li**, and J. Kleissl, "Dynamic Weight-Based Collaborative Optimization for Power Grid Voltage Regulation ", *ISES Solar World Congress*, 2019.

C. Li, V. R. Disfani, Z. K. Pecenak, S. Mohajeryami, and J. Kleissl, "Optimal OLTC Voltage Control Scheme to Enable High Solar Penetrations", *Electric Power Systems Research*, 160, 2018.

C. Li, E. Ratnam, and J. Kleissl, "Distribution Feeder Hotspots", *California Solar Initiative RD&D Program, Technical Report*, 2016.

ABSTRACT OF THE DISSERTATION

Coordinated Voltage Regulation of Distribution Networks

by

Changfu Li

Doctor of Philosophy in Engineering Sciences (Mechanical Engineering)

University of California San Diego, 2020

Professor Jan Kleissl, Chair

Electrical power grid is one of the most complex engineering systems. The conventional power grid is designed with centralized power plants and unidirectional electricity flow from plants to consumers on the distribution network. However, there has been increasing adoption of renewable distributed energy resources (DERs) like solar Photovoltaics (PV) generation on the distribution power grid due to their associated environmental and economical benefits. Fluctuating and distributed solar generation can lead to power ramps and two-way power flows, potentially driving the service voltage out of

acceptable ranges. Advanced coordinated voltage regulation is needed to integrate high solar penetrations into distribution networks.

In this dissertation, three different coordinated voltage regulation methods are proposed to tackle the voltage regulation challenges arising from increasing solar generation.

The first one optimizes legacy voltage regulation devices (on-load tap changers (OLTCs)). Linearizations are proposed to to reduce computation burden. Comprehensive simulations show that the proposed method enables 67% more PV connection comparing to conventional autonomous OLTC control.

The second one investigates coordination between legacy OLTCs and emerging PV smart inverters with optimization. Nonlinear constraints are relaxed through proposed linearization techniques. Simulations demonstrate improved voltage profiles and significant reduction of OLTC operations from intelligent coordination between OLTCs and SIs. Robustness against forecasting errors (up to 30%) is also validated.

Finally, a data-driven framework using deep reinforcement learning (DRL) is introduced for PV smart inverters coordination. The reward scheme is carefully designed to balance voltage regulation and reactive power generation. Comprehensive tests prove a well-trained DRL agent can achieve near optimal performance with over 99% reduction in computation time comparing to optimization approach.

Chapter 1

Introduction

As one of the most complex infrastructures ever built by human beings, the electrical power grid is essential to the functioning of our society and daily life. Conventional power networks consist of large power plants producing electric power, high voltage transmission networks transferring electricity from generation centers to consumption centers, and distribution networks that deliver electric power to individual customers (see Fig. 1.1).

1.1   Voltage Regulation in Distribution Networks and New Challenges

Since end customers are directly connected to distribution networks, it is essential to maintain distribution network voltages within acceptable levels. Both under-voltages and over-voltages can be problematic for end users by causing inappropriate and inefficient equipment operation. Under-voltages could lead to overheating of induction motors

Figure 1.1: Electricity generation, transmission, and distribution.

while over-voltages can damage equipment through insulation impairment and incur higher transformer losses [10]. In the United States, voltages at user meters are required to be maintained within [0.95, 1.05] p.u. ($\pm 5\%$ of nominal voltages) following the ANSI voltage standards [7] .

1.1.1   Conventional Autonomous Voltage Regulation

Traditionally, grid operators rely on legacy voltage regulation devices to maintain appropriate voltage profiles on the distribution networks. For example, on-load tap changers (OLTCs) adjust the turn ratio of transformers, shunt capacitors can inject reactive power, while shunt reactors can absorb reactive power. With conventional central supply of power, simple autonomous voltage regulation can maintain satisfactory voltages since the voltage typically drops monotonously along the distribution network due to unidirectional power flow from substations to the end points of the distribution network. Legacy
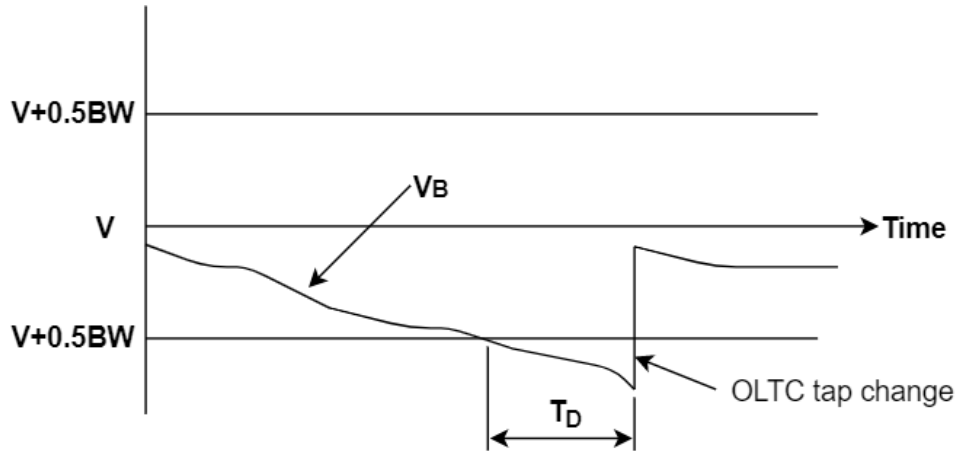
Figure 1.2: Illustration of autonomous operation of OLTCs. The OLTC monitors its local bus voltage V_B. If the local bus voltage deviates from the preset reference voltage V outside of the allowable range ($0.5BW$, half of dead band) for a duration longer than the time delay (T_D), the OLTC will adjust its tap position to bring the local voltage back within $V \pm 0.5BW$.

devices operate autonomously based on local measurements without coordination with other devices. Fig. 1.2 illustrates the autonomous operation of OLTCs. Given the controllability of conventional generators and predictable and relatively slow changes in power demand, traditional voltage regulation devices typically operate only a few times per day [11].

1.1.2 Increasing Solar Penetrations and New Voltage Regulation Challenges

Driven by efforts to fight climate change and continuous price drop of solar PV, there has been close to exponential growth of PV deployment globally for over two decades (Fig. 1.3). Large portions of the installations are rooftop/distributed PVs. The presence of a high share of solar generators on the distribution network can lead to reverse power

3
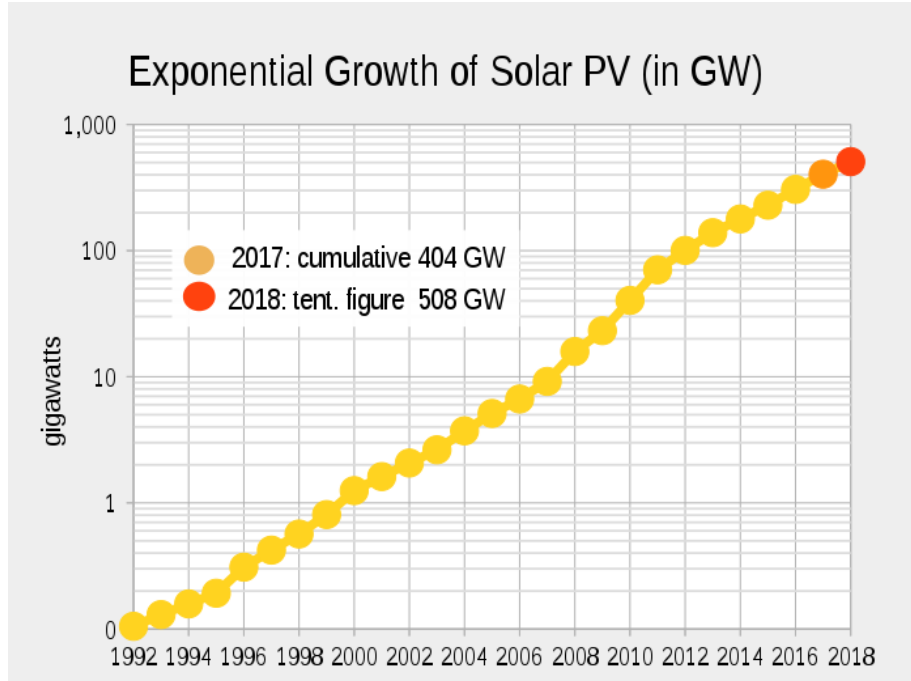
Figure 1.3: History of cumulative PV capacity worldwide (adapted from [1]).

flow during periods with excessive solar generation, causing voltage violations on the distribution network (Fig. 1.4).

Besides potential voltage violations, frequent solar power output ramps resulting from moving clouds can cause increased equipment operations, leading to shortened lifespan of voltage regulation devices [12]. Proper coordination between voltage regulation devices is vital to address these challenges.

1.1.3 Smart Inverter Voltage Regulation

Historically, PV systems (and other DERs) have been required to immediately disconnect during grid disturbances; however, disconnection of a large amount of DERs

4
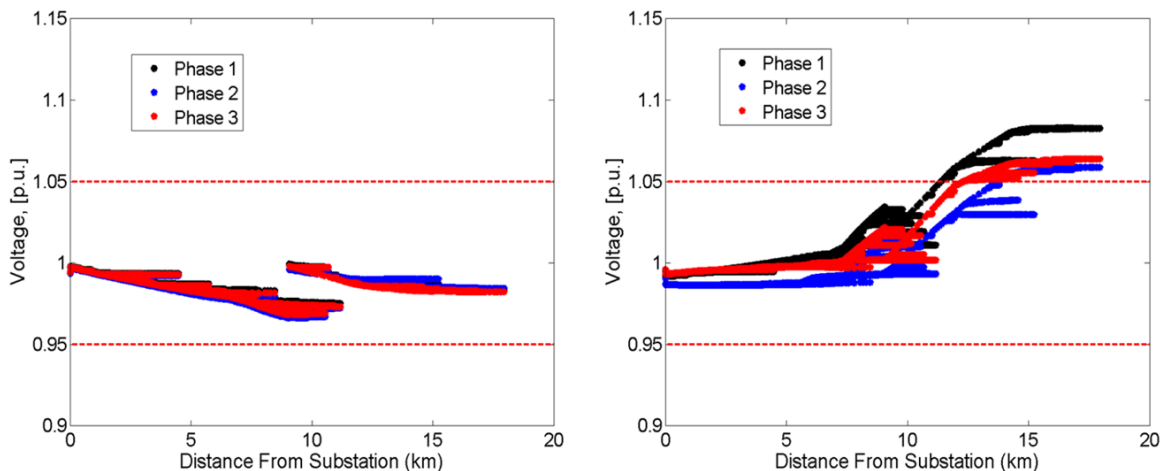
Figure 1.4: Voltage profile of the distribution feeder in the middle day with 0% (left) and 150% (right) PV penetration using autonomous voltage regulation. The red dash lines indicate the [0.95, 1.05] p.u. ANSI limits. The substation is at the feeder head and PVs are located downstream on the feeder. PV penetration is defined as the ratio of total PV installation capacity and peak demand on the distribution feeder.

at once could further destabilize the grid during contingency events such as losses of large conventional generators or transmission lines. Under the revised IEEE 1547 standards [13], DERs coupled with smart inverters (SIs) are mandated to stay connected and participate in grid regulation through different smart functions. California utilities have been leading the way to implement the new standards through CA Rule 21 [14].

The Volt-Var function is one of the common SI capabilities to provide autonomous voltage regulation. It determines the reactive power absorption/injection based on the voltage at the point of common coupling (PCC) according to a predefined droop curve. SIs have a distinct advantage in voltage regulation in that they can respond much faster (essentially instantaneously) compared to legacy regulation devices (OLTCs, capacitors, reactors, etc.).

1.2 Coordinated Voltage Regulation of Distribution Networks

There has been extensive research on improving traditional autonomous voltage control to tackle voltage regulation challenges arising from growing connection of renewable DERs.

Many aim to improve autonomous control of legacy devices by incorporating more downstream feeder information through either measurements or estimates [15, 16, 17, 18, 19]. Voltage measurements [15, 16, 17] and voltage estimates [18, 19] of remote points instead of local voltages are input to OLTC tap control for better voltage regulation. Although those improved autonomous rules help achieve better voltage regulation and are relatively simple in deployment, they still suffer from a lack of coordination with other devices and especially SIs.

Optimization based approaches/optimal power flow (OPF) can determine the optimal coordination between different devices. Some works aim to improve coordination of legacy devices to regulate voltage while reduce device wear and tear resulted from PV fluctuations. In [20], OLTCs, shunt capacitors (SCs), shunt reactors (ShRs), and static var compensator (SVC) are optimally dispatched hourly to minimize voltage deviation and energy losses. Reference [21, 22] coordinate OLTCs and SVCs to minimize energy losses and TOs. Despite showing promising results, a few gaps exist: 1) lack of demonstration on real distribution feeders with large numbers of PV systems using realistic high temporal and spatial resolution PV profiles despite the importance is shown in [23]; 2) lack of

consideration of OLTC physical switch speed which could lead to unrealistic decisions; 3) fast solution speed to regulate sub-minute solar ramps.

The contributions of the work in Chapter 2 include :1) a novel linearization technique to represent the OLTC tap position and feeder voltage as a convex optimization problem which is solvable in an operational time scale at high-resolution (30 s); 2) coordination between multiple OLTCs; 3) demonstration of the method in realistic conditions on real feeders; 4) using realistic OLTC switching limits.

PV SIs provide an alternative method for fast-response voltage regulation comparing to legacy devices like OLTCs. Yet the cooperation among SIs is essential to achieve optimal performances while coordination between SIs and other legacy devices is also important to avoid undesirable interactions [24]. However, non-linear AC power flow constraints render optimization problems nonconvex and computationally intensive for large distribution networks, numerous studies have been done to address this concern.

Reference [25] formulates the OPF problem using second order cone program (SOCP) after convex relaxation to dispatch SI real and/or reactive power dispatch of SIs for minimizing losses while eliminating voltage violations. Semi-definite programming (SDP) relaxation is leveraged for optimal dispatch of SI real and reactive power in [26] and DGs in [27]. Reference [9] formulates the OPF as a quadratic constrained quadratic program (QCQP) by leveraging a linear approximation of power flow equations. LinDistFlow [11] is adopted to formulate OPF for SI reactive power optimization in [28]. Alternating direction method of multipliers (ADMM) based algorithms are used to solve the OPF in a distributed manner in [26, 27, 28, 9], which offers more robustness against communication

failures. In these works, however, cooperation amongst SIs is studied without taking other voltage regulation devices including OLTCs into account, which could result in undesired interactions [24]. Morever, decentralized OPF formulation requires the global objective to be separable, which does not extend to coordination of SIs and OLTCs for TO minimization.

Other works optimize cooperation between other devices as well as SIs [29, 30, 31, 8] in a centralized fashion. OLTC tap positions and SI outputs in [29] are optimized concurrently to minimize voltage deviations, assuming all OLTCs are located at the substation. DGs and OLTCs are coordinated through optimization to minimize voltage deviations and network losses in [30] using sensitivity coefficients, the computation burden of the coefficient calculation can increase substantially due to exponentially growing tap position combination of more OLTCs. SIs, OLTCs, and ShCs are coordinated in [31] to meet voltage operation limits. Despite delicate computaional strategies are introduced to reduce computation cost, its non-linear and non-convex formulation could lead to either local solutions or convergences issues [31, 32, 33]. In [8], the big bang-big crunch optimization is used to improve convergence speed. However, the computation time can still be up to 40 s for the small IEEE 33-bus feeder with only 3 DGs, 1 OLTC and 2 ShCs, which makes the optimization technique not applicable for distribution systems with hundreds and thousands of nodes.

The work in chapter 3 fill the gaps mentioned above by proposing a new linearization method to linearize power flow equations and to convexify the problem, which guarantees convergence of the optimization and less computation costs. The optimization is modeled

and solved using mixed-integer linear programming (MILP) to coordinates both OLTCs and SIs. The contributions of the work inculudes: 1) it addresses coordination of OLTCs and SIs for optimal voltage regulation; 2) a novel linearization technique is proposed to convexify the optimization problem for higher computational efficiency; 3) it guarantees convergence and leads to more accurate voltage estimates; 4) it is robust against forecast errors; 5) it is scalable to handle multiple OLTCs and SIs coordination regardless of OLTC location.

While OPF approaches ensure optimal coordination, they rely on accurate distribution network models which are not necessarily available [34]. and they are computationally intensive. The recent success of AlphaGo [35] has sparked applications of intelligent grid operations using reinforcement learning (RL), which is time-efficient and model free. Many applies RL/DRL for control legacy voltage regulation devices with discrete settings (i.e. generator voltage set points, OLTC tap positions, capacitor switches) [36, 37, 38, 39, 40, 41].

SIs are more suitable for mitigating frequent PV generation fluctuations due to their continuous outputs and fast response in comparison to legacy voltage regulation devices. While references [42, 43, 44] coordinate SIs with DRL, PV active power curtailment is not considered in the reward function design in [42, 43], which can lead to excessive curtailment. Reference [44] balances active power curtailment and voltage regulation. However, instead of directly determining optimal active and reactive power set points, incremental changes are employed, which can lead to insufficient responses to large PV ramps. Moreover, the performance is not validated against OPF.

The work in chapter 4 proposes a DDPG-based algorithm to coordinate multiple SIs with continuous outputs. The reward is carefully designed to balance voltage regulation and active power curtailment, in contrast to [42, 43] and is validated against OPF (contrary to [44]) with comprehensive tests.

1.3   Dissertation Overview

Although the cited works have contributed significantly to coordinated voltage regulation of distribution networks, there still exist a number of gaps. They include (1) coordination of multiple OLTCs using OPF; (2) validation on realistic feeders with realistic PV conditions considering OLTC switching limits; (3) coordination of legacy devices like OLTCs with emerging SIs by OPF; (4) reduction of computation costs of OPF to be able to respond faster to solar ramps; (5) application of RL for real-time SI coordination considering solar power curtailment.

In this dissertation, we investigated three different coordinated voltage regulation methods to improve voltage profiles of distribution networks to enable higher solar penetrations. In Chapter 2, we address coordination of multiple OLTCs through traditional optimization. Linearization techniques are proposed to speed up the solution. The techniques are expanded in Chapter 3 to the coordination of legacy OLTCs and SIs. The proposed three works are summarized in Table. 1.1. In Chapter 4, a data-driven framework is introduced for online SI coordination using deep reinforcement learning. Conclusions and future work are summarized in Chapter 5.

Table 1.1: Summary of proposed works.

Proposed method	Approach	OLTCs	SIs	Distribution network model
OTC (Chapter 2)	optimization	tap optimized	unity power factor	yes
AVR (Chapter 3)	optimization	tap optimized	Q optimized	yes
DDPG (Chapter 4)	reinforcement learning	N/A	Q coordinated	no

Chapter 2

Optimal OLTC Voltage Control Scheme to Enable High Solar Penetrations

2.1 Introduction

The amount of variable distributed generation (VDG) such as solar PV being con-
nected to the grid continues to increase each year as a result of their many technical,
economic, and environmental benefits [45]. However, existing distribution networks may
not be capable of handling large amounts of VDG since they are initially designed assuming
centralized off-site generation.

Variability and intermittency of VDGs, in particular, present significant challenges
to voltage regulation in distribution systems [46]. Traditionally, to address the voltage

issues on the distribution system, OLTCs and voltage regulators are typically employed to maintain the voltage on the secondary side of power transformers within regulatory limits.

Conventional ATC of OLTC maintains a fixed voltage at the transformer's secondary side based on measured local busbar voltage, a line-drop compensator, or remote voltage measurements [47]. As OLTCs are typically configured assuming a voltage drop along the feeder, a voltage rise caused by reverse power flow during periods with low demand and high solar power feed-in can lead to overvoltages [48]. Moreover, with high PV penetration on a distribution system, high frequency solar ramping caused by fast-moving clouds can result in excessive TOs [49].

In order to solve voltage problems resulting from high penetration of VDG on distribution systems, various advanced control methods have been proposed. Several researchers applied rule-based control of OLTCs by replacing local busbar voltage with voltage measurements or estimates from feeder end points and/or critical nodes as the control signal [47, 15, 50, 18]. However, in these works, the voltage measurements/estimates are only used to control tap position of substation OLTC and coordination between multiple OLTCs is not studied. Therefore, these methods suffer from lack of scalability and are not applicable to feeders with multiple OLTCs.

Other researchers exploited the capability of devices other than OLTCs. A DSTATCOM was used in [12] to damp impacts of residential PV power fluctuations on the OLTC operation. However, the study is done on a small balanced network and no coordination is considered between DSTATCOM and OLTCs. Coordination between energy storage systems and OLTC is studied in [51] for peak load shaving, power loss reduction, and

tap changer stress relief (reduction in TO and reducing operations close to tap limits). However, the proposed solution requires adoption of costly battery storage systems and does not consider coordination of multiple OLTCs. The authors in [52] have studied voltage control by using faster static var compensator (SVC) and slower-responding OLTC to limit SVC reactive power output and reset voltage reference after disturbances for effective voltage support. However, the control is only based on local voltage measurements and as a result the SVC and OLTC are not truly coordinated in an optimal way. Moreover, only one OLTC is used in this work, which makes the scalability of the proposed approach questionable.

A central control methodology can achieve coordinated control of different voltage regulation devices and optimize their operations over a time horizon by taking advantage of load and solar forecast. In [20], OLTCs, shunt capacitors (SCs), shunt reactors (ShRs), and SVC are optimally dispatched hourly to minimize voltage deviation and energy losses. Similarly, reference [53] updates optimal tap position of OLTC and reactive power output of PV inverters every 50 s to minimize voltage deviation. Simulation results in both studies show that the proposed methods are able to achieve the desired objectives. However in both works, a genetic algorithm is used to search for the optimal solution, which can be time-consuming considering the extensive search space for the coordinated control of different devices.

Reference [21] presents a two-stage approach for solving the optimal voltage regulation problem with coordination between OLTC and SVC. The optimization problem is solved hourly to minimize power losses and TO based on one hour ahead forecasts.

The two-stage method is also adopted to solve the coordination problem of more devices including OLTC, SC, and SVC under load and distributed generation uncertainty in [22]. Although the proposed method already improves the solution time by a large margin comparing to existing methods, it still takes around 25 s to solve the problem for one time step on the small IEEE 123-bus system in [21] and the solution time increases to 58 s in [22] which has more devices on the same test feeder. Since PV variability in partly cloudy conditions over a distribution system typically occurs on the order of a few minutes, an hourly time step is insufficient. Rather sub-minute time steps are recommended and therefore this two-stage approach is still questionable for high-resolution application for real distribution feeders, which usually contain thousands of buses. Reference [54] proposes and successfully demonstrates a coordinated reactive power control of PV to minimize TO and avoid operating the OLTC at its control limits. However, only coordination of PV and substation OLTC is considered, while the two other OLTCs operates autonomously.

Despite showing promising results, all of the optimal control methods in [20, 53, 21, 22, 54] are tested on simple distribution networks with only a few or evenly-distributed PV systems. In terms of PV generation profiles, only reference [53] adopts the required sub-minute generation profile during partly cloudy conditions while low-resolution (1 h) generation profiles for a clear-sky day are used in [20, 21, 22]. Reference [54] applies PV profiles with 30 s resolution but it is also for clear day without solar ramps. Morever, the same generation profile is used for all PVs in these studies even though it is very critical to use unique and realistic generation profiles for each PV, and the importance of applying realistic individual PV generation profiles has been demonstrated in [23].

In addition, TO step limits between two consecutive simulation time steps have not been considered which could lead to unrealistic operating decisions of OLTC. For example, reference [21] provides an additional test case to show the proposed method's ability of dealing with fast-moving clouds effects, however, the results shows that one OLTC would need to switch by eight steps in less than 1 minute, which is a challenging and arguably impractical task for conventional OLTC with slow mechanical switching gear and the typical 30 to 60 s time delay [55].

In summary, application of existing optimal control methods to sub-minute high-resolution applications are questionable. Potential issues include large computation time, lack of consideration of realistic OLTC switch limits, limited testing on large real distribution feeder and realistic representation of distributed PV characteristics like random deployments and fast ramping events. To tackle these issues, we propose a multi-horizon, central optimization of OLTC tap position to minimize voltage deviation maxima throughout the feeder and minimize the number of TOs.

High temporal and spatial resolution PV forecasts are employed to reflect a realistic picture of a feeder with high penetration of distributed VDGs.

The contributions of this paper to improve the state-of-the-art in optimal voltage control are:

1. A novel linearization technique to represent the OLTC tap position and feeder voltage as a convex optimization problem which is solvable in an operational time scale at high-resolution (30 s).

2. Coordination between multiple OLTCs

3. A flexible optimization platform that can be easily expanded to consider other optimization objectives and coordinated control of other devices including SCs and ShRs.

4. Demonstration of the method in realistic conditions on real feeders.

5. Using realistic OLTC switching limits.

The proposed method is firstly benchmarked against an advanced rule-based control method that is found in the literature and proven to be effective through simulations and field deployments. Since the rule-based control method does not coordinate multiple OLTCs, the proposed method is further compared against a conventional autonomous control method. These studies are carried out through simulations on two disparate California distribution feeders.

The rest of the paper is organized as follows. Section 2.2 discusses the tap operation and their effects on feeder voltages. Section 2.3 introduces the optimization platform. Section 2.4 provides details of the test feeder models, control concepts, and simulation scenarios. Section 2.5 presents simulation results followed by conclusions and future work in section 2.6.

2.2 Linearized Model of Tap Operation Voltage Impacts

2.2.1 Voltage Effects of OLTC Tap Operation

OLTCs are indispensable in regulating voltage. They include a moving connection point (called tap) along a transformer winding which allows discrete numbers of turns to be selected. Along the transformer winding, the residing points for taps are called tap positions and denoted by τ. OLTCs regulate voltage by altering the tap position and thus changing the ratio of secondary voltage with respect to the primary voltage. The ratio is referred as tap ratio a. The tap positions are numbered such that $a = 1$ when $\tau = 0$.

The net node current injections of the distribution feeder (I) can be represented by the following equation,

$$I = YV, \tag{2.1}$$

where Y is the admittance matrix of the feeder and V is the complex vector of node voltages (one node corresponds to one phase of a bus/a three-phase bus has three nodes). Similarly, the vector of node voltages can be written as a function of injected currents as

$$V = ZI, \tag{2.2}$$

where $Z = Y^{-1}$ is the feeder impedance matrix.

A linear approximation of the perturbations in node voltage due to changes in

impedance and current $(\partial V/\partial(ZI))$ leads to

$$\Delta V = \Delta Z \cdot I + Z \cdot \Delta I. \tag{2.3}$$

To make the problem mathematically tractable, it is assumed that $\Delta I = 0$, and with this assumption the second term on the RHS of Eq. (2.3) will become zero. $\Delta I = 0$ means that the current injection is fixed at each time step as used in [56]. The reason behind this assumption is that loads and PVs, i.e. current sources, are not controlled in this optimization problem. Even if their current injections changes, they are negligible and due to voltage change caused by tap changes from initial tap positions. In Section 3.5.1, a sensitivity analysis is performed to verify the accuracy of this assumption, and it is shown that this assumption is valid.

To proceed, a model to determine the impacts of TO on ΔZ is required. We propose a novel method to modeling effects of tap position on ΔZ. Assuming a OLTC is connected between the node i of the primary side and node j of the secondary side, a change in the tap position of OLTC affects only the elements of the admittance matrix corresponding to these two nodes as

$$Y_{ii} = a^2/z_T + \sum_{k \neq j} 1/z_{ik} \tag{2.4}$$

$$Y_{ji} = Y_{ij} = -a/z_T \tag{2.5}$$

$$Y_{jj} = 1/z_T + \sum_{k \neq i} 1/z_{jk}, \tag{2.6}$$

where z_T is the equivalent impedance of the transformer on the winding connected to node i, z_{ik} is the impedance connected between two arbitrary nodes i and k $(i \neq k)$, and z_{ii} is

the impedance connected from the node i to ground (one node corresponds to one phase of a bus/a three-phase bus has three nodes).

Let us define Y_0 and $Z_0 = Y_0^{-1}$ as the admittance and impedance matrices for the initial tap ratio a_0. Similarly, V_0 and $I_0 = Y_0 V_0$ denote the resulting node voltage and injected current for a_0. According to Eq. (2.1), any change in injected current can be represented as

$$\Delta I = Y_0 \cdot \Delta V + \Delta Y \cdot V_0. \tag{2.7}$$

Under the assumption of fixed current injection from loads and PVs, change of current injections are equal to zero. Therefore, Eq. (2.7) is equal to zero yielding,

$$\Delta V = -Y_0^{-1} \cdot \Delta Y \cdot V_0 \tag{2.8}$$

Similarly, since ΔI equals to zero, Eq. (2.3) can be written as,

$$\Delta V = \Delta Z \cdot I_0. \tag{2.9}$$

Combining Eq. (2.8) and Eq. (2.9), the matrix ΔZ becomes

$$\Delta Z = -Y_0^{-1} \cdot \Delta Y \cdot Y_0^{-1}, \tag{2.10}$$

which is input to Eq. (2.9) to determine ΔV.

2.2.2 Linearization of ΔY

From Eq. (2.9), ΔV can be determined if ΔZ is known. Therefore, ΔZ is used for voltage control in the optimization. And the control of ΔZ is achieved by control

of ΔY via changing tap position. We design the voltage control platform as a convex optimization problem to reduce computational expense and achieve global optimality. To achieve convexity, the objective function and optimization constraints have to be linearized.

The admittance matrix depends non-linearly on tap position as some elements are a function of a^2 (see Eq. (2.4)). A tap change from a_0 to a yields $\Delta Y_{ii} = (a^2 - a_0^2)/z_T$. To remove the non-linearity, a Taylor series expansion is performed for a^2 around a_0. Replacing a^2 with $2aa_0 - a_0^2$ yields a linear expression $\Delta Y_{ii} = (2aa_0 - 2a_0^2)/z_T$.

2.2.3 Linearization of voltage magnitudes

Node voltages are the main control parameters in the voltage control algorithm. Magnitude of node voltages expressed as complex numbers can be calculated using their real parts and imaginary parts by the following equation,

$$|v|^2 = v_d^2 + v_q^2, \tag{2.11}$$

where $v = v_d + jv_q$ is the complex voltage of an arbitrary node in the feeder.

The magnitudes of node voltages in Eq. (2.11) are linearized around the operation point (i.e. $v_0 = v_{d_0} + jv_{q_0}$) as

$$|v_0|\Delta|v| = v_{d_0}\Delta v_d + v_{q_0}\Delta v_q \tag{2.12}$$

and then,

$$|v| = |v_0| + \Delta|v| = |v_0| + |v_0|^{-1}(v_{d_0}\Delta v_d + v_{q_0}\Delta v_q). \tag{2.13}$$

21

This definition for voltage magnitudes of all nodes sets up an affine relation between the voltage magnitude and the OLTC tap position and makes the optimization problem convex.

2.3 Feeder-Wide Optimal Tap Changer Control

2.3.1 Optimal OLTC Control Structure

In the future smart grid, smart meters, synchrophasors, and communication platforms enable distribution system operator (DSO) to be aware of the system states (voltage magnitudes and angles) of all buses of the feeder [57]. Moreover, solar and demand forecast can provide insights of future conditions of the grid.

We propose that non-local information could be used by DSO to develop a central or feeder-wide optimal voltage control platform, which can monitor direct effects of OLTC tap position on the voltage profile of the entire feeder.

Fig. 2.1 shows the central control platform. The control center obtains voltage states (V_0) at the linearization point from power flow run by OpenDSS [2]. The solution of the optimization problem for the control horizon using PV and load forecasts then yields optimal tap positions of all OLTCs. The optimal tap positions are then delivered back to each OLTC without communication delay. For readability only a single OLTC is shown, but the method can handle any number of OLTCs.

Due to the discrete nature of tap positions as the main decision variables, the corresponding optimization problem is a mixed-integer programming problem. To minimize
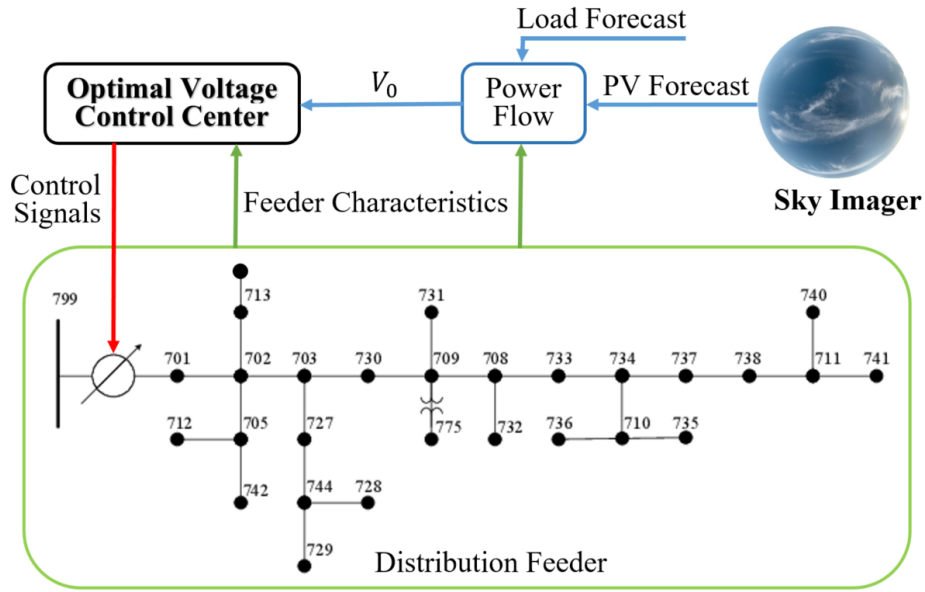
Figure 2.1: Structure for proposed optimal voltage control.

the number of TO in the control objectives, the optimization problem is defined over a 5 min horizon. The 5 min horizon is chosen in accordance with the Sky Imager's forecast horizon, which can provide forecast of PV availability for up to 10 mins The forecast resolution is 30 s. The optimization horizon can assume any value shorter than the forecast horizon. Details regarding the sky imager forecasting can be found in [58, 59]. Historical measurements provided from the utility are used as perfect load forecast, which is also the practice in [20, 53]. The forecasted conditions allow the tap position to be optimized based on present and future grid states.

2.3.2 Optimization Model

Objective Functions

Since the goal is to improve feeder voltage profile while minimizing tap operations, two objective functions are defined. The first objective function (J_1) minimizes the voltage deviations on the feeder during the optimization horizon. The specific parameter selected is the maximum voltage deviation,

$$J_1 = \max_{t \in T} \left\{ \max \left\{ | |V_t| - \mathbf{1} | \right\} \right\}, \tag{2.14}$$

where T is the set of time steps in the optimization horizon, $|V_t|$ denotes the vector of voltage magnitude of all nodes at time step t, and $\mathbf{1}$ is a vector with all its components being equal to 1 p.u.. Minimizing the maximum voltage deviation across the feeder from 1 p.u. centers the max and min voltage of the feeder around 1 p.u. to keep the voltage of the entire feeder within the 0.95 to 1.05 p.u. ANSI limits [7].

The second objective function (J_2) counts the number of TO as,

$$J_2 = \sum_{t \in T} \sum_{p \in P} |\tau_{p,t+1} - \tau_{p,t}|, \tag{2.15}$$

where P is the set of all OLTCs and $\tau_{p,t}$ denotes the tap position of OLTC p at time step t. All tap changes over any two consecutive time steps over a defined time horizon T are aggregated in J_2.

Constraints

To ensure that the final solution meets the feeder power flow, the linearized power flow (Eq. (2.8)) is an equality constraint. Further, the equality constraint in Eq. (3.20)

relates the voltage magnitudes to the real and imaginary parts of the node voltages. Tap positions τ are integer values in the range of $[-\tau_{\max}, \tau_{\max}]$. Assuming that the selection of $\tau_{p,\max}$ for OLTC p leads to a tap ratio equal to $a_{p,\max}$, its tap ratio at time t can be represented as an affine function of $\tau_{p,t}$ as

$$a_{p,t} = 1 + \frac{\tau_{p,t}}{\tau_{p,\max}}(a_{p,\max} - 1) \tag{2.16}$$

for any $t \in T$ and $p \in P$. Therefore, Eq. (2.16) must be included in the optimization model as an equality constraint.

To avoid unrealistic tap operation as reported in [21] and to consider TO delays, the optimization problem restricts the number of TO between two consecutive time to be less than $\Delta TO_{\max}$, which is set to be 1 in the paper.

Optimization Formulation

Combining the two objective functions, the optimal voltage control problem is

$$\min \qquad J = w_1 J_1 + w_2 J_2 \tag{2.17}$$

$$\text{s.t.} \qquad (2.8), (3.20), (2.16)$$

$$\tau_{p,t} \in \mathbb{Z} \qquad \forall_{p \in P} \ \forall_{t \in T}$$

$$-\tau_{p,\max} \leq \tau_{p,t} \leq \tau_{p,\max} \qquad \forall_{p \in P} \ \forall_{t \in T}$$

$$\left| \tau_{p,t} - \tau_{p,t-1} \right| \leq \Delta TO_{p,\max} \qquad \forall_{p \in P} \ \forall_{t \in T}$$

The weighting factors, w_1 and w_2 are chosen to be 1 and 0.01, respectively. The reason behind the selection of these values are fully elaborated in Section 2.4.4.

Proof of Convexity

Since absolute values, maximum values, and summation of convex functions are still convex, we claim that the objective functions J_1 and J_2 and their sum are convex. Moreover, all the constraints are affine functions. These two characteristics preserve the convexity of the optimization problem. Therefore, its convergence to the global optimal solution is guaranteed in polynomial time.

2.4   Case Study

2.4.1   Distribution Feeder Models

To evaluate the proposed OTC method, quasi-steady state simulations are carried out for two real California distribution feeders. The feeders, referred to as feeder A and B in this paper, correspond to feeder 2 and feeder 5 in [23], where more details regarding feeder models, load data, and PV generation data can be found. Feeder topologies of the chosen are displayed in Fig. 2.2. And table 2.1 summarize feeder characteristics.

Feeder A and B are chosen to represent feeders with a single OLTC and multiple OLTCs, respectively. Feeder A is equipped with a single OLTC at the substation. Feeder B has one OLTC installed at the substation and a second OLTC located in the middle of the feeder as shown in Fig. 2.2. Tap position of all OLTCs can vary from -16 to +16 with voltage regulation capability of [0.9 1.1] p.u..

Capacitors are removed from the circuits due to convergence issues at high PV

penetration, and thus the feeder under ATC experiences under-voltage problems in the morning and evening independent of PV penetration. Under high PV penetration the maximum voltage on the feeder always occurs in the middle of the day regardless of the tap control method. The capacitors would have little effect (if any) on the voltage in the middle of the day with high PV penetration since the capacitors typically switch off or operate with small VArs at those times. Since the ATC undervoltages would not occur in reality on these two feeders with capacitors, the comparison of the three control methods is only based on over-voltages.

2.4.2 Tap Control Schemes

In this paper, OTC is firstly benchmarked against an advanced rule-based VLC found in literature. Since the VLC does not coordinate multiple OLTCs, the OTC is then compared with a basic rule-based ATC. Details regarding these three control schemes are provided below.

Autonomous Tap Control (ATC)

ATC denotes the widely used conventional OLTC operation where the OLTCs only monitor their local busbar voltage and change tap to keep the deviation of the local busbar voltage from the preset reference voltage within certain limits. To avoid excessive TOs, a tap change is only triggered when the measured voltage is out of range for a certain period of time. The minimum time period is called tap time delay. A shorter time delay will provide better voltage regulation but at a cost of more TOs, and vice versa. In this

paper, ATC is only applied to feeder B for comparison with OTC when there are multiple OLTCs. The reference voltages of both OLTCs on feeder B are set to 0.99 p.u. and the voltage regulation bandwidth is 0.0167 p.u.. The tap time delay is set to 60 s based on the utility setting. All other OLTC parameters are kept as default OpenDSS [2] values.

Voltage Level Control (VLC)

VLC denotes the method adapted from [15] which controls OLTCs based on voltage measurements from critical nodes of the feeder. This advanced rule-based control method has proven to be effective in simulation as well as field test [15, 50]. When there are over- or under-voltage problems on a feeder, VLC dynamically sets a reference voltage based on voltage measurements using the equation:

$$U_{\text{new}} = U_{\text{UL}} - \frac{\text{VB} - \text{Rng}}{2} - (u_{\text{max}} - U_{\text{old}}), \tag{2.18}$$

where U_{new} is the new reference voltage. U_{UL} is the voltage upper limit, which is 1.05 p.u., VB $= 0.1$ p.u. is the allowable voltage band which is the difference between voltage upper and lower limits, and Rng is the difference between the highest (u_{max}) and lowest (u_{min}) measured voltage. The old reference voltage U_{old} is modified by changes in tap position. The relationship of reference voltage and tap position (τ) is:

$$U_{\text{new}} = 1 + \frac{(1.1 - 0.9)\tau}{32}, \tag{2.19}$$

The initial (at midnight of each day) reference voltage is 1 p.u..

Optimal Tap Control (OTC)

OTC determines optimal control tap of OLTCs based on the feeder-wide voltage profile. Tap position are the outputs of the optimization problem proposed in Section 2.3. OLTCs will follow the optimal tap position schedule to maintain the voltage symmetric about 1 p.u. and a reference voltage therefore does not need to be specified. The number of tap changes is limited to one step per simulation time step (30 s); that is, $\Delta\mathrm{TO}_{\max} = 1$ in Eq. (2.17). The same constraint on tap changes between two consecutive time steps is also considered in ATC and VLC.

2.4.3   Simulation Setup

Since VLC is limited to feeders with a single OLTC, feeder A is simulated with VLC and simplified OTC (see Section 2.5.1 for more details) to benchmark OTC against the established rule-based VLC. Meanwhile, feeder B is simulated with ATC and complete OTC to show OTC's ability of coordinating multiple OLTCs to improve the voltage profile.

Feeder A and feeder B are simulated on selected days from the 94 day period spanning December 10, 2014 to March 14, 2015. 28 days are chosen to cover different weather conditions (clear, partly cloudy, overcast) and days when the feeders showed the largest voltages in [60].

The performance of OTC are evaluated for different amounts of PV generation. Here PV penetration is defined as (2.20).

$$PV_{\mathrm{Pen}} = \frac{P_{\mathrm{pv\_peak}}}{P_{\mathrm{load\_peak}}} \times 100\% \tag{2.20}$$

where $P_{\text{pv\_peak}}$ is the total rated AC power of all PV units, and $P_{\text{load\_peak}}$ is the peak feeder load. The desired PV penetration level is achieved by scaling the rated output of existing PV systems. Each feeder is simulated from 0% to 200% PV penetration with 25% increments.

Both feeders experience very high voltages on March 14, 2015 in [60], a partly cloudy day with large solar ramps. Therefore March 14, 2015 is used to illustrate voltage and tap change results. Simulations for March 14, 2015 showed that the minimum and maximum voltages at different times of the day occur at just 30 out of the 2,844 nodes of feeder A and 67 out of 4,869 nodes of feeder B. To reduce the computational cost, the objective function J_1 considers only the nodes with maximum and minimum voltage deviations and the OLTC nodes.

2.4.4   Selection of Weighting Factors of OTC

Since the optimization objective J is a weighted sum of J_1 and J_2, heavy weighting on J_1 will improve the voltage profile at the cost of more TOs and vice versa. Therefore, appropriate weighting factors should be chosen to achieve desired trade-off between voltage profile and number of TOs. Several combinations of weighting factors (w_1, w_2) are tested with simulations on feeder B on March 14, 2015 with 150% PV penetration (Table 3.3).

As expected, larger weighting factors (w_2) on J_2 cause decreases in total TO, while maximum voltages generally increase. When there is no penalty on TO (i.e. $w_2 = 0$), the maximum voltage on the feeder remains low at 1.049 p.u. as the OLTC moves the taps as often as needed to reduce voltage deviation.
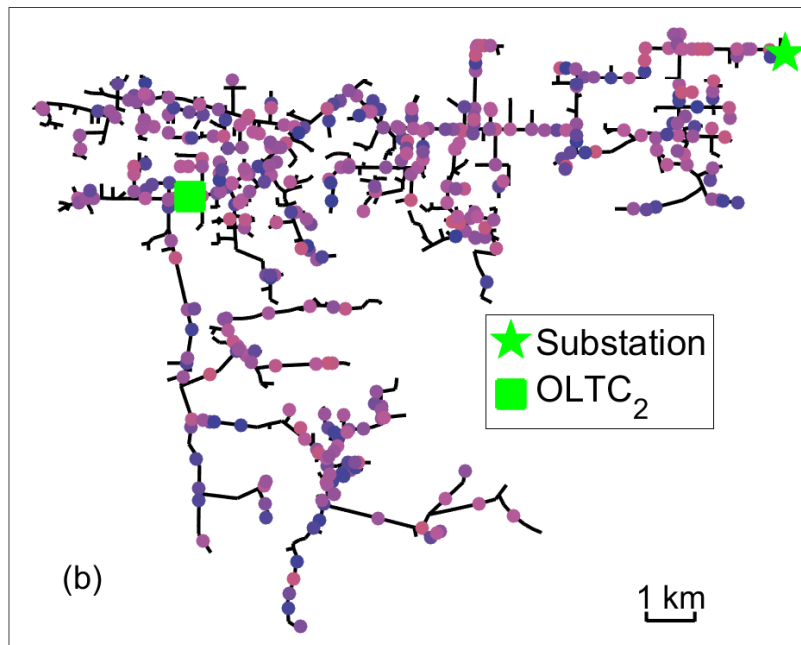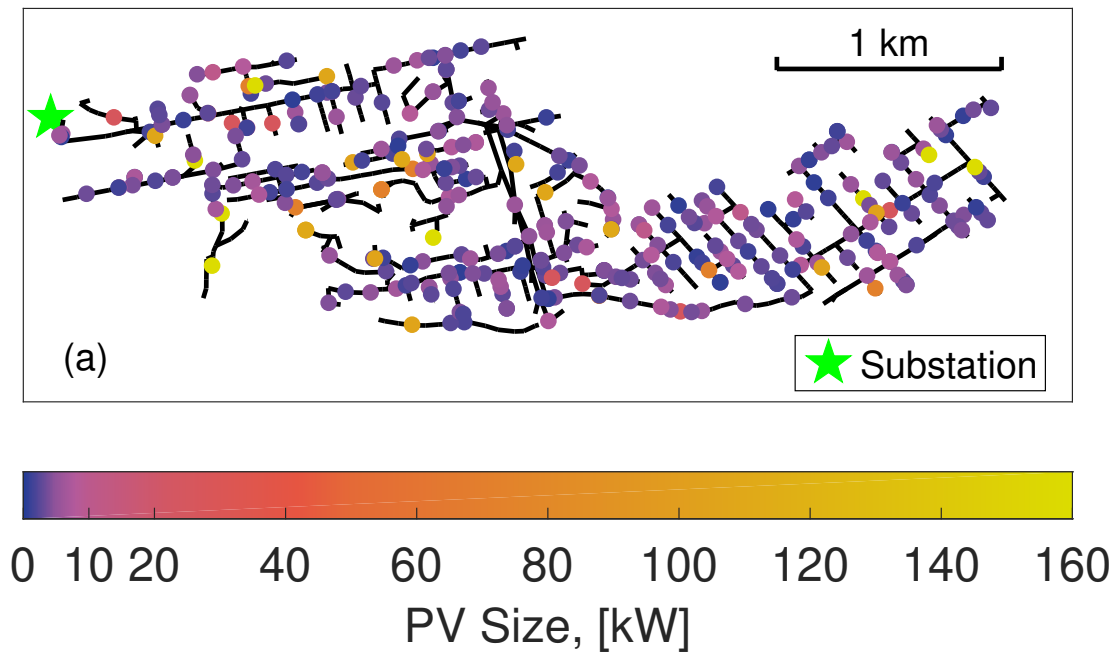
Figure 2.2: Feeder topologies of feeder (a) A and (b) B. Black lines represent feeder lines. Each dot is a PV system and its color indicates its AC power rating. The substation is marked with a green star and the green square marks the additional OLTC of feeder B.

Table 2.1: Feeder Properties.

Feeder	A	B
Type	Urban	Rural
Voltage Level (kV)	12	12
Total Length (km)	40	115
Peak Load (MVA)	8.4	6.3
# of Loads	3761	1169
# of PV System	340	387
# of OLTCs	1	2
# of Buses	948	1623
# of Nodes	2844	4869

Table 2.2: Case study of different objective function weights w_2 on feeder B with 150% PV penetration on March 14, 2015. w_1 is fixed at 1.

w_1	w_2	Max Volt (p.u.)	Total TO
	0	1.049	1569
	0.005	1.049	101
1	0.01	1.055	80
	0.02	1.059	68
	0.04	1.156	38

Relative to the case with $w_2 = 0$, $w_2 = 0.005$ provide a large reduction in TO without increase in maximum voltage. If $w_2 > 0.005$, the maximum voltage increases without much TO reduction for the feeder studied. Therefore, $w_2 = 0.005$ is used hereinafter.

The desirable combination of w1 and w2 for different feeders may vary due to the preferences of the DSO between better voltage regulation or less TO, different locations of OLTCs, feeder topologies, distribution of PVs, etc. Local adjustments of the weighting factors are therefore recommended.

2.4.5 Sensitivity Analysis

Given that predicted node voltages determine the OLTC tap operations, a sensitivity analysis examines the errors resulting from fixed current injections, the linearization of admittance matrix and voltage magnitude in Eq (2.8). Errors are defined as the differences in voltage magnitude calculated from Eq (3.20) versus the (non-linear) power flow results

in OpenDSS:

$$E(t)_j = V_{\text{calculated}}(t)_j - V_{\text{OpenDSS}}(t)_j, \tag{2.21}$$

where j stands for a node and t stands for a time step. The calculated voltage incorporates all error sources resulted from fixed current injection assumption and linearization of admittance matrix and voltage magnitude.

Fig. 3.5 presents error distribution based on simulations on feeder B with 150% PV penetration. For time steps in the time horizon without tap changes, errors are nearly identical to zero. Therefore, the figure only shows errors from time horizons with tap changes. The results show that the calculated voltages almost match the simulated ones. Thus, it can be concluded that the proposed voltage model represents voltage magnitudes very accurately; the maximum error magnitude is 0.0016 p.u. and the mean absolute error magnitude is only 9.10e-5 p.u..

2.5 Distribution Feeder Simulations Results

2.5.1 Single OLTC Without Forecasting (Benchmark)

The OTC approach is benchmarked against the established VLC. Two simplifications are made to OTC for the purpose of making a fair comparison. Firstly, since VLC only changes the tap settings after voltage violations, the simplified OTC platform also changes tap position only if the feeder experiences a voltage violation. In other words the optimal tap position output from OTC is used only if there is voltage violations. Secondly,
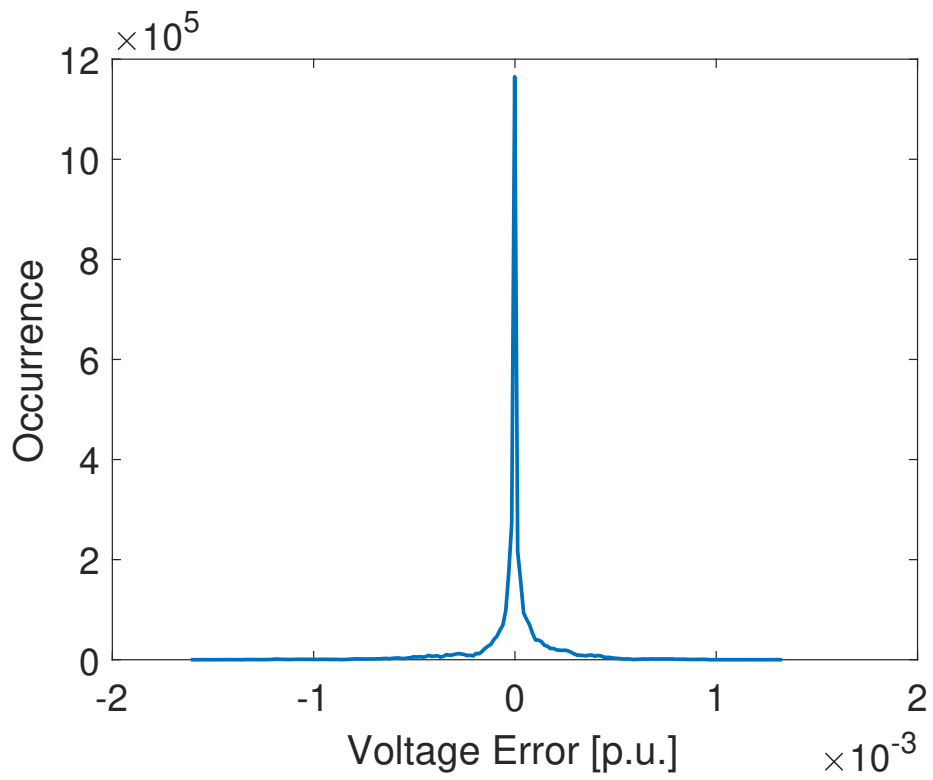
Figure 2.3: Distribution of voltage errors from the fixed current injection assumption, linearization of admittance matrix, node voltages. The distribution is created from simulations for feeder B with 150% PV penetration.

since VLC can't integrate PV and load forecast to optimize future operations, the OTC control actions are also only based on current conditions. In this way, the basic OTC only calculate tap positions for next time step if needed and therefore TO reduction is not considered. Since both simplified OTC and VLC operate the OLTC to achieve symmetry of maximum and minimum voltage around 1 p.u., OLTC operations under control of both methods are expected to be the same.

Fig. 2.4 displays the time series of the OLTC tap position on feeder A under VLC and simplified OTC with 200% PV penetration on March 14, 2015. The peak output of PV on feeder A is 15.4 MW. The OLTC behaves the same during the whole day under VLC and simplified OTC, resulting in 9 TOs. Therefore, the feeder voltage profiles must also be identical. Simulations for other PV penetration levels show similar results. The OTC and VLC voltages of each node are identical at all PV penetration levels (0%–200%). Therefore, the simplified OTC platform avoids voltage violations as effectively as VLC.

2.5.2 Coordination of Multiple OLTCs Considering Forecasting

To demonstrate OTC's ability of coordinating multiple OLTCs, simulations are carried out for another real California distribution feeder (feeder B) with two OLTCs. Since VLC is unable to coordinate multiple OLTCs, we compare against ATC.

In this comparison, the complete OTC platform described in section 2.3 is used. OTC optimizes tap position for the next 5 min based on solar and load forecast by balancing the sometimes conflicting objectives of minimum voltage extrema and minimum number of TOs. Further, OTC minimizes voltage deviation extrema even if there is no
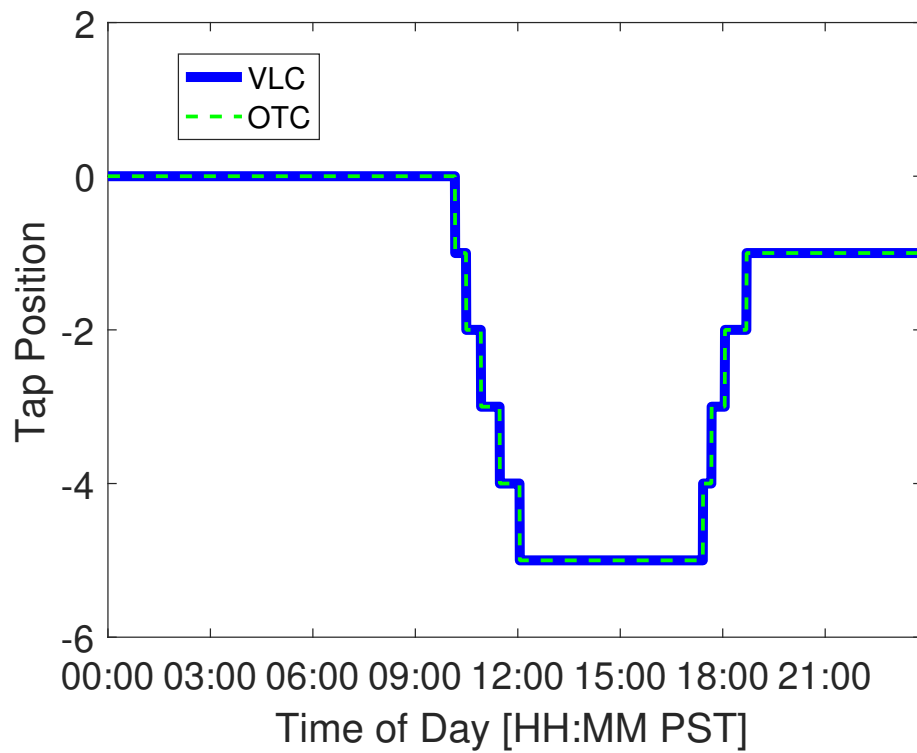
Figure 2.4: Time series of the tap position on feeder A with 200% PV penetration on March 14, 2015.

over- or under-voltage problem.

Voltage Profile

Fig. 2.5 presents the time series of maximum and minimum voltage for feeder B with high PV penetration on March 14. The peak output of the PV fleet on the feeder B is 7.6 MW at a time when the load is only 1.8 MW.

The highest and lowest voltages on the feeder are 1.089 p.u. and 0.912 p.u. when the OLTCs are controlled by ATC. With OTC being applied, the highest voltage on feeder A is reduced to 1.049 p.u. and lowest voltage is increased to 0.950 p.u. Although it is expected that maximum and minimum voltage magnitudes deviate symmetrically from 1 p.u., they are slightly asymmetric here (+0.049 p.u. vs. -0.050 p.u.) due to the effect of TO minimization in the objective function and the fact that tap positions are discrete variables.

With ATC, the highest voltage typically occurs near noon when solar irradiance is greatest and the lowest voltage occurs in the evening under high load and low solar irradiance. With OTC, both the highest and lowest voltages occur in the middle of day. The shift of voltage minima from the evening to the middle of the day is due to the OTC tap position reducing voltage in response to high voltages in the middle of the day. At night the OTC counteracts the voltage drop (caused by increasing load) without support from solar generation, thus the voltage profile is raised. In other words, the minimum and maximum voltages occur at the same time as the largest voltage magnitude change across the feeder. At very high solar penetration the voltage increase across the feeder at midday

is larger in magnitude than the voltage drop in the evening.

Fig. 2.6 presents the maximum and minimum voltage on the feeder on March 14 as a function of PV penetration level for feeder B. For ATC, maximum voltage increases with PV penetration, while minimum voltage remains constant. The maximum voltages are greater for OTC than ATC at low to moderate PV penetrations ($0\%-75\%$). This is due to the fact that at low PV penetrations OTC corrects for low voltages by raising the tap position. However, at high PV penetration ($>75\%$), OTC maximum voltage becomes lower than for ATC, since OTC reduces over-voltages due to PV generation.

In general, OTC minimizes voltage deviations from 1 p.u., resulting in a voltage profile symmetric about 1 p.u. per the objective function J_1, which is the optimal way to maintain feeder voltage within ANSI limits. Feeder B experiences over-voltage violations starting with around 90% PV penetration under ATC, while over-voltages do not occur until around 150% PV penetration with OTC. The OTC scheme therefore allows a 67% increase in installed PV comparing to the ATC case. The proposed OTC method successfully mitigates over-voltage problems resulting from large amounts of distributed PV generation.

Tap Operations

The average number of TO per day for each OLTC during the 28 day simulation period for ATC and OTC is shown as a function of PV penetration in Fig. 2.7. The OLTC at the substation ($OLTC_1$) has low TO for all PV penetrations under ATC while OTC operates $OLTC_1$ more to correct the voltage at the expense of increased TOs. In contrast,
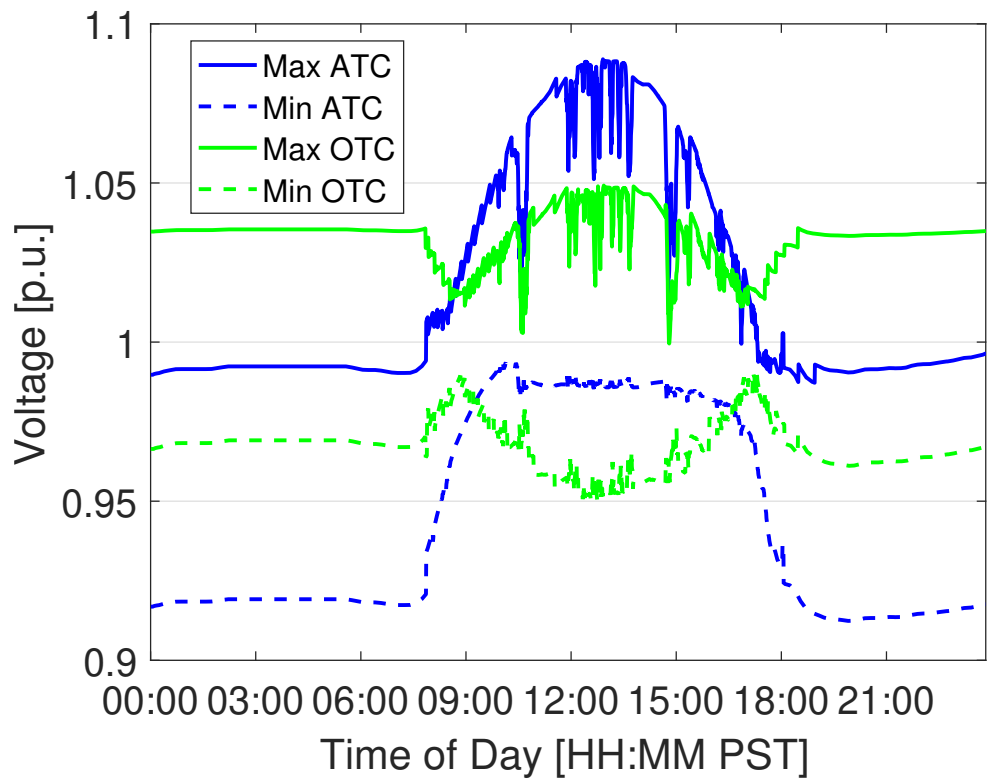
Figure 2.5: Time series of maximum and minimum voltage of feeder B with 150% PV penetration on March 14, 2015.
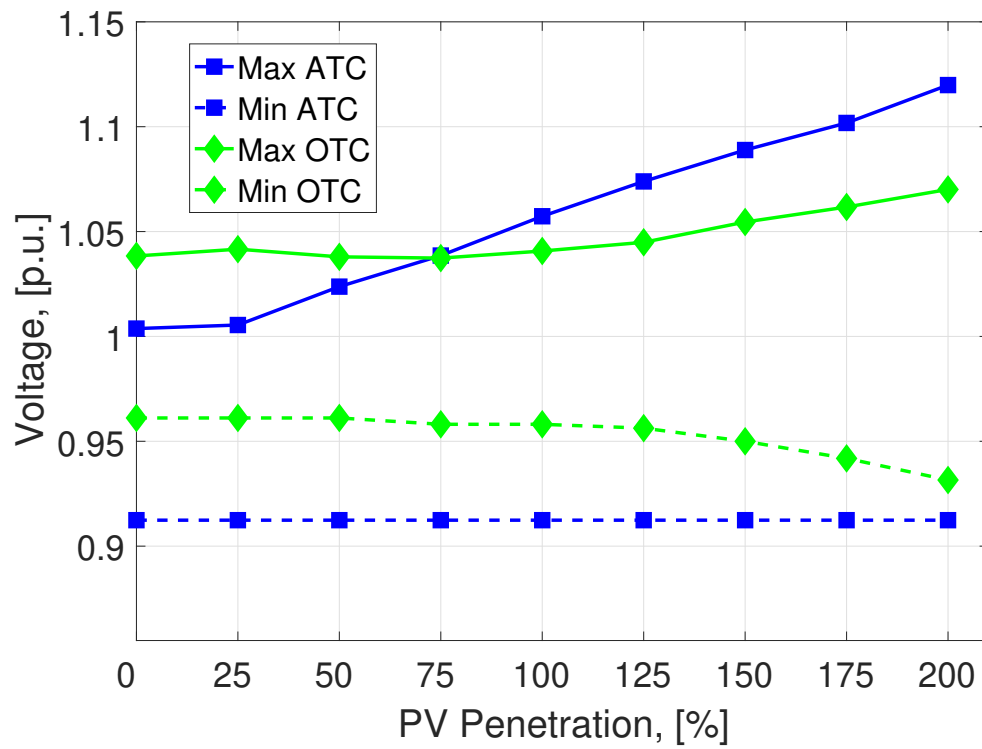
Figure 2.6: Maximum and minimum voltage as a function of PV penetration level on March 14 2015 for feeder B.

OLTC$_2$ generally incurs about the same TOs with OTC.

TOs could be reduced by applying a larger weight w_2 in Eq. (2.17) as shown in Table 3.3.

OTC optimizes the voltage on the entire feeder and increases TOs of OLTCs located near the substation, while the number of TOs of the downstream OLTC remains around the same. J_2 is designed to reduce aggregated TOs of all OLTCs. When OTC detects large voltage deviation on the feeder, it operates OLTCs that are best able to reduce the voltage deviation with a minimum number of TOs. In general, the proposed OTC method can provide a better coordination between OLTCs on the feeder to improve the voltage profile.

Even with PV penetration as high as 200%, the largest number of TO is observed to be around 50 TO/day for all OLTCs on the feeder. Assuming a lifespan of tap changers of 1 million TO [61], the OLTC will last for about 55 years. According to [62], the OLTC can perform 600,000 switching operations without maintenance, therefore even the OLTC with maximum TOs under 200% PV penetration can operate for around 33 years without maintenance.

Computation Time

Solving the optimization problem at an operational timescale would enable the control to be used in real time applications. To demonstrate the scalability and computational efficiency of proposed OTC, we add up to six OLTCs on feeder B and perform a series of simulations on a PC with an Intel(R) Core(TM) i7-4700MQ 2.8-GHz processor and 16GB
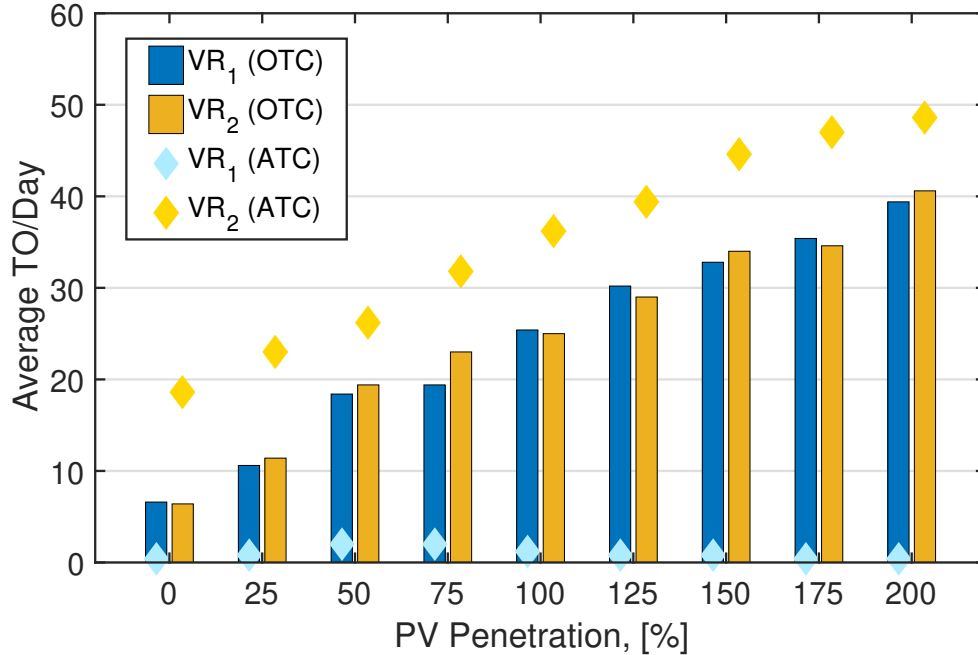
Figure 2.7: Average TO/day of each OLTC on feeder B over the 28 day simulation period as a function of PV penetration.

RAM.

Fig. 3.4 displays computation time for one time step and two to eight OLTCs together with a curve fit. The expression of the fitted curve is: $y = 0.0379 \cdot x^3 - 0.2254 \cdot x^2 + 0.7310 \cdot x - 0.6309$ (s), where x is the number of OLTC and y is the solution time for one time step. Since the convexity of the optimization problem has been proven in Section 2.3.2, the solution time of the optimization problem should be polynomial, which is consistent with the fitted expression we get.

The proposed OTC solves the optimization problem efficiently. For a large distribution feeder with 4 OLTCs and 1623 buses the solution time for one simulation time step is 1.1 s . Even with 8 OLTCs, the solution time for one step is still just 10.2 s. In comparison, the method in [54] takes 25 s to solve the formulated problem for one step on
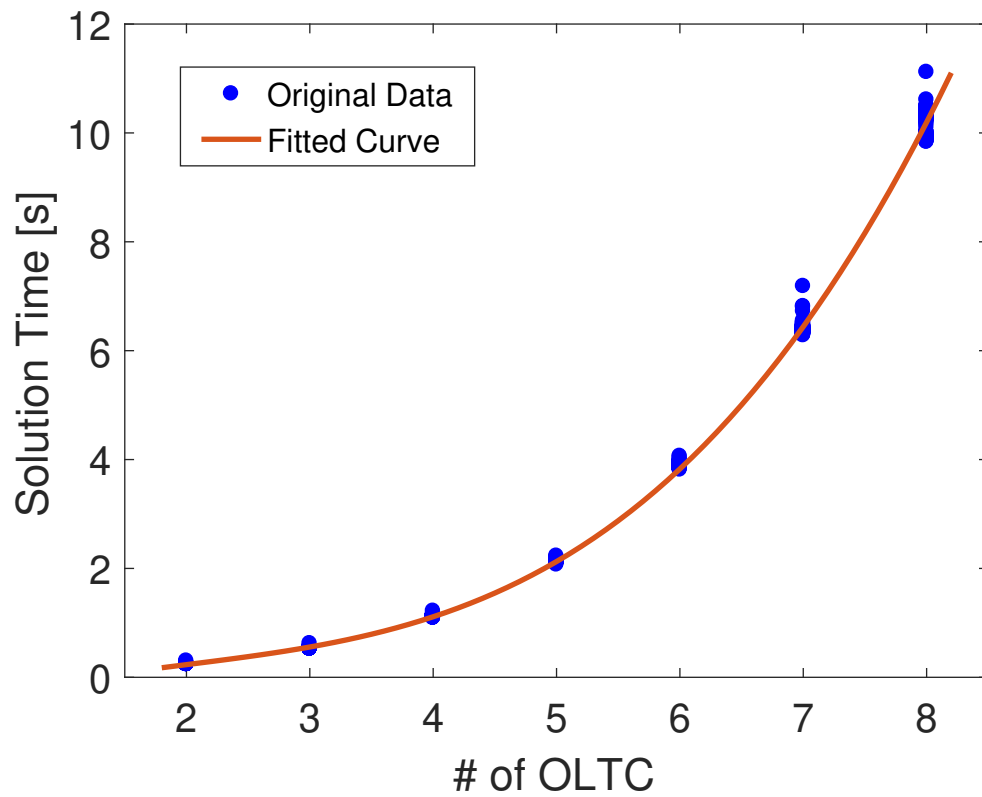
Figure 2.8: Computation time for the optimization (excluding power flow) for one time step as a function of total number of OLTCs.

a PC with Intel Xeon E5420 2.5-GHz CPU, 4-GB memory for a feeder with only 4 OLTCs and 123 buses.

2.6 Conclusions and Future Work

A novel control platform for optimal tap control of OLTC for voltage regulation was proposed. OTC is capable of coordination between multiple OLTCs. OTC is compared against two established rule-based tap control methods through simulations on two real California distribution feeders using high temporal and spacial resolution PV forecast. Results show the OTC can solve the optimization problem in an operational time scale.

Benchmarking showed a simplified OTC to be as effective as an advanced rule-based method in terms of avoiding voltage violations on a feeder with a single OLTC. However, the OTC is more advanced compared to VLC as it considers coordination between two or more OLTCs and integrates forecasts to optimize tap operations.

In the exhibition of the method on a feeder with multiple OLTCs, the complete OTC algorithm outperforms ATC in voltage regulation. Improved voltage regulation enables higher PV hosting capacity on distribution feeders. Comparing to ATC, the feeder tested can accommodate 67% more PV without over-voltage problem under the control of OTC. This is achieved by operating OLTCs in an effective way that reduces voltage deviation with minimum TOs. In this case, we estimate the life time of the OLTC with most TOs will be around 55 years even with 200% PV penetration under highly variable solar ramping scenarios. And the OLTC is expected to be able to operate for 33 years without

maintenance.

Future work will include other voltage regulation devices like shunt capacitors, shunt reactors as well as voltage support from PV inverters via reactive power output control. Since OTC relies on accurate solar and power demand forecast to optimize tap positions of OLTCs, its effectiveness of voltage regulation may be compromised by forecasts with low accuracy. The robustness of OTC to deal with forecast error will be another focus of future work.

The text and data in Chapter 2, in full, is a reprint of the material as it appears in Optimal OLTC Voltage Control Scheme to Enable High Solar Penetrations, Li, C., Disfani, V.R., Pecenak, Z.K., Mohajeryami, S., Kelissl, J., *Electric Power Systems Research*, 2018. The dissertation author is the primary investigator and author of this article.

Chapter 3

Coordination of OLTC and Smart Inverters for Optimal Voltage Regulation of Unbalanced Distribution Networks

3.1 Introduction

Penetration of variable distributed generation connecting into distribution systems has increased significantly in recent years. In California, specifically solar photovoltaics (PV) has shown such growth predominantly. While PV brings economic and environmental benefits, it presents voltage regulation challenges in distribution systems due to the variability in the solar resource [49, 51, 63, 64].

Conventionally, utility devices such as on-load tap changers (OLTCs), shunt capacitors (ShCs), and shunt reactors regulate the voltage within operation limits. These devices are usually limited in number of switches and slow in response time, and hence less effective in regulating feeder voltage during periods of minute-by-minute PV variability. In contrast, PV smart inverters (SIs) provide an alternative method for fast-response voltage regulation by modulating real and/or reactive power of PV systems [46]. Moreover, all these devices typically operate autonomously based on pre-defined rules or curves to regulate voltage. These autonomous control schemes are based on local measurements requiring no communications. The lack of coordination between these devices leads to sub-optimal system performance.

Numerous research works in the literature have studied coordination of SIs for voltage regulation [25, 28, 65, 66, 26, 9]. In [25], optimal power flow (OPF) problems is formulated considering feeder-wide constraints and then solved to determine the optimal real and/or reactive power dispatch of SIs for minimizing losses while eliminating voltage violations. Through convex relaxation, the OPF is formulated as a second order cone program, and reactive power of SIs is optimized to reduce line losses and energy consumption. The alternating direction method of multipliers (ADMM) is used to solve the OPF and find the optimal SI reactive power for reducing losses in [28] and for voltage regulation in [65]. ADMM-based algorithms are also employed in [66] to determine optimal SI real and reactive power set points for voltage regulation. In [26], semi-definite programming relaxation is leveraged for optimal dispatch of SI real and reactive power. A linear approximation of the power flow equations is used in [9] to optimize SI real and reactive

powers efficiently. In these works, however, cooperation amongst SIs is studied without taking other voltage regulation devices including OLTCs into account. Uncoordinated operation of OLTCs and SIs may cause unintended OLTC tap operations [24] leading to higher OLTC wear and tear and less effective voltage regulation.

Various studies have improved coordination between SIs and other voltage regulation devices for better voltage regulation performance. Some works improve the basic autonomous rule based methods [17, 19, 67]. Reference [17] replaces the local OLTC bus voltage with feeder end measurement for the control of tap switching to improve the visibility of downstream voltage. SIs dynamically adjusts their power factor per autonomous curves. OLTC voltage set points are dynamically adjusted based on voltage estimates from sensitivity matrix to accommodate SI outputs in [19]. OLTC and SIs are coordinated by iteratively updating their settings to achieve target local voltage at the SI [67].

The improved rule based methods are relatively simple to implement and can accomplish partial coordination between devices. However, optimization based approaches can achieve optimal coordination to ensure optimal voltage regulation performances for distribution feeders with complicated voltage profiles caused by fluctuating distributed energy resources [29, 34, 30, 31, 8]. In [29], SI real and reactive power and OLTC tap positions are optimized simultaneously to minimize voltage deviations. A robust optimization model is developed in [34] to schedule real and reactive power of distributed generators (DGs) and OLTCs for production cost minimization while ensuring acceptable network voltage profiles. DGs and OLTCs are coordinated through optimization to minimize voltage deviations and network losses in [30]. The optimization in [31] also coordinates SIs,

OLTCs, and ShCs while meeting voltage operation limit constraints. Reactive power of SIs, ShCs and OLTC tap position are optimized to eliminate voltage violations in [8].

Since non-linear AC power flow constraints render optimization problems non-convex and computationally intensive for large distribution networks, different linearization techniques have been applied in the literature to address this concern. In [29], an analytical approach is proposed to calculate sensitivity coefficients of node voltages to approximate voltage change as a function of SI real power, reactive power, and OLTC tap positions. Since [29] assumes that OLTCs are located at the substation, the method is not directly applicable to distribution feeder with OLTC in the middle of the feeder [29, 34]. In [30], the sensitivity coefficients for OLTC tap position are determined by summing real and reactive power coefficients at all buses due to each OLTC variation. The computational burden of the method could increase substantially due to exponentially growing tap position combinations with more OLTCs. Linearized power flow equations are exploited for computational efficiency in [9]. The solution, however, does not coordinate SIs and OLTCs and is not validated on multi-phase and unbalanced distribution feeders. Furthermore, the voltage estimate from the linear approximation differs substantially from the actual system voltage.

SIs, OLTCs, and ShCs are coordinated in [31] and the method is tested on unbalanced feeders. The optimization problem is non-linear and non-convex without relaxation of AC power flow constraints. While computational strategies are introduced to reduce computation cost, this non-linear and non-convex formulation could lead to either local solutions or convergence issues [31, 32, 33]. In [8], the big bang-big crunch optimization

50

is used to improve convergence speed. However, the computation time can still be up to 40 s for the small IEEE 33-bus feeder with only 3 DGs, 1 OLTC and 2 ShCs, which makes the optimization technique not applicable for distribution systems with hundreds and thousands of nodes.

In the authors' prior work [68], coordination of multiple OLTCs for voltage regulation is studied. Voltage violations are mitigated and the method is proven to be computationally efficient. However, it does not address coordination between OLTCs and SIs, which can lead to the higher OLTC wear and less effective voltage regulation as discussed in [24].

As a follow-on work, this paper proposes an optimization-based voltage control strategy to coordinate OLTCs and SIs in operable time scales. It proposes a new linearization method to linearize power flow equations and to convexify the problem, which guarantees convergence of the optimization and less computation costs. The optimization is modeled and solved using mixed-integer linear programming (MILP). Since the linearization technique convexifies the optimization problem, convergence are guaranteed in contrary to [31]. By relaxing the non-linear AC power flow constraints, fast solutions can be achieved in a regular PC, unlike [8]. Also, the proposed method addresses OLTCs which are located within the feeder–not necessarily on substation–which differentiates this paper from [29, 34]. The proposed formulation is scalable and can be easily applied to distribution networks with any number of OLTCs in contrast to [30]. A sensitivity study shows that voltage estimation is more accurate with a maximum error of 0.009 p.u. compared to around 0.1 p.u. in [9]. The method is also applicable to unbalanced feeders. It

is demonstrated on the highly-unbalanced modified IEEE 37 bus test network. And it is robust against forecast errors as demonstrated by simulations. The scalability of the method is also tested on a real California utility feeder with 2844 nodes.

In summary, the contributions of this paper are as follows:

1. it addresses coordination of OLTCs and SIs for optimal voltage regulation,

2. a novel linearization technique is proposed to convexify the optimization problem for higher computational efficiency,

3. it guarantees convergence and leads to more accurate voltage estimates,

4. it is robust against forecast errors,

5. it is scalable to handle multiple OLTCs and SIs coordination regardless of OLTC location.

The rest of the paper is organized as follows. Section 3.2 discusses the linearization technique for modeling the OLTC tap change and SI reactive power on distribution feeder voltage. Section 3.3 explains the formulation of the optimization. Section 4.4 provides details of the test feeder models, voltage regulation methods, and simulation scenarios. Section 3.5 presents simulation results followed by conclusions in section 4.6.

3.2   Model Linearization for Voltage Regulation

The goal of the optimization formulated in section 3.3 is to coordinate OLTCs and SIs for voltage regulation. In this section, we introduce the linearized model to represent

the relation between voltage and controllable parameters.

3.2.1 Linearization of Feeder Nodal Equation

Consider a distribution feeder with N nodes contained in the set $\mathcal{N}$. Its feeder nodal voltage equation can be written as:

$$\mathbf{V} = \mathbf{Z}\mathbf{I}, \tag{3.1}$$

where $\mathbf{V}$ and $\mathbf{I}$ are $N \times 1$ complex vector for voltages and net node current injections at all nodes ($\mathbf{V}, \mathbf{I} \in C^N$), and $\mathbf{Z}$ is the $N \times N$ feeder impedance matrix ($\mathbf{Z} \in C^{N \times N}$). A linear approximation of the perturbations in node voltage resulting from changes in impedance and current ($\partial \mathbf{V} / \partial (\mathbf{Z}\mathbf{I})$) leads to

$$\Delta \mathbf{V} = \Delta \mathbf{Z} \cdot \mathbf{I}_0 + \mathbf{Z}_0 \cdot \Delta \mathbf{I}, \tag{3.2}$$

where the subscript (0) represents unperturbed parameters. $\Delta \mathbf{Z}$ is a function of tap position changes of OLTCs and $\Delta \mathbf{I}$ results from current injection changes of PVs and loads. $\Delta \mathbf{V}$ is further derived by modeling the effects of OLTC tap changes on $\Delta \mathbf{Z}$ and current source changes on $\Delta \mathbf{I}$ which we cover in Section 3.2.2 and Section 3.2.3.

3.2.2 Modeling OLTC Tap Operation Effects on Voltage

An OLTC regulates voltage via changing tap position τ, which alters the ratio of the transformer secondary voltage with respect to the primary voltage (tap ratio a) and

changes the impedance matrix $\mathbf{Z}$. The tap ratio a is a linear function of τ,

$$a = 1 + \frac{\tau}{\tau_{\max}}(a_{\max} - 1), \tag{3.3}$$

where $a_{\max}$ is the maximum tap ratio corresponding to the maximum tap position $\tau_{\max}$. OLTC tap operation effects on voltage can be determined by modeling its effects on $\mathbf{Z}$, which is a function of tap ratio a.

In (3.2), $\Delta\mathbf{Z}$ is needed to determine $\Delta\mathbf{V}$. Considering an OLTC tap operation, which changes the tap ratio from a_0 to a, the corresponding impedance matrix change can be expressed as

$$\Delta\mathbf{Z} = -\mathbf{Y}_0^{-1} \cdot \Delta\mathbf{Y} \cdot \mathbf{Y}_0^{-1}, \tag{3.4}$$

where $\mathbf{Y}_0$ is the admittance matrix associated with the initial tap ratio a_0. $\Delta\mathbf{Y}$ is the admittance change due to change of OLTC tap ratio from a_0 to a.

Since $\Delta\mathbf{Y}$ is the only unknown on the right-hand-side of (3.4), $\Delta\mathbf{Z}$ can be determined if the corresponding $\Delta\mathbf{Y}$ can be modeled. Considering an OLTC connected between node i of the primary side and node j of the secondary side, only the elements associated with these two nodes are impacted by a OLTC tap change, i.e. only the following elements in $\Delta\mathbf{Y}$ are non-zero:

$$\Delta Y_{ii} = (a^2 - a_0^2)/z_T, \tag{3.5}$$

$$\Delta Y_{ji} = \Delta Y_{ij} = -(a - a_0)/z_T, \tag{3.6}$$

where z_T is the equivalent impedance of the transformer on the winding connected to node i. The non-linearity in (3.5) can be removed by a Taylor series expansion for a^2 around

a_0, yielding a linear expression,

$$\Delta Y_{ii} = (2aa_0 - 2a_0^2)/z_T. \tag{3.7}$$

More details on the derivation of (3.4) and the relationship between $\mathbf{Y}$ and a can be found in [68]. The derivation of (3.4) is based on the assumption of fixed current loads in [68], which does not accurately represent common loads [69]. In this paper, we apply a more common fixed power model for loads. However, the expression of (3.4) still applies since both $\Delta \mathbf{Z}$ and $\Delta \mathbf{Y}$ in (3.4) are direct results of OLTC tap changes and are only functions of tap positions.

3.2.3 Modeling Voltage Impacts of Current Sources

PVs and loads are the current sources. A change in their injected currents ($\Delta \mathbf{I}$) affects the feeder voltage profile per (3.2). The power injections of PVs and loads need to be specified for modeling their current injections into the feeder.

The power injections and current injections are related by

$$\mathbf{S} = \mathbf{P} + j\mathbf{Q} = \mathbf{V}\mathbf{I}^*, \tag{3.8}$$

where $\mathbf{S}, \mathbf{P}, \mathbf{Q} \in C^N$ are the vectors of complex power, real power, and reactive power injections at all nodes. $j := \sqrt{-1}$. $\mathbf{V}$ is the voltage vector and $\mathbf{I}^*$ is the conjugate of the net current vector. Expressing the parameters as the initial value plus a perturbation, $\mathbf{V} = \mathbf{V}_0 + \Delta \mathbf{V}$ and $\mathbf{I} = \mathbf{I}_0 + \Delta \mathbf{I}$, (3.8) can be rewritten as,

$$\mathbf{S} = (\mathbf{V}_0 + \Delta \mathbf{V})(\mathbf{I}_0 + \Delta \mathbf{I})^*. \tag{3.9}$$

Eq. (3.9) sets up the relation between $\Delta\mathbf{I}$ and the power injections of PVs and loads as needed for Eq. (3.2).

Substituting the real and imagery parts of $\mathbf{V}_0$, $\Delta\mathbf{V}$, $\mathbf{I}_0$ and $\Delta\mathbf{I}$ into (3.9) yields the real and reactive power injection as,

$$\mathbf{P} = (\mathbf{V}_{d0} + \Delta\mathbf{V}_d)(\mathbf{I}_{d0} + \Delta\mathbf{I}_d) + (\mathbf{V}_{q0} + \Delta\mathbf{V}_q)(\mathbf{I}_{q0} + \Delta\mathbf{I}_q), \tag{3.10}$$

$$\mathbf{Q} = (\mathbf{V}_{q0} + \Delta\mathbf{V}_q)(\mathbf{I}_{d0} + \Delta\mathbf{I}_d) - (\mathbf{V}_{d0} + \Delta\mathbf{V}_d)(\mathbf{I}_{q0} + \Delta\mathbf{I}_q). \tag{3.11}$$

where $\mathbf{V}_0 = \mathbf{V}_{d0} + j\mathbf{V}_{q0}$, $\mathbf{I}_0 = \mathbf{I}_{d0} + j\mathbf{I}_{q0}$, $\Delta\mathbf{V} = \Delta\mathbf{V}_d + j\Delta\mathbf{V}_q$, and $\Delta\mathbf{I} = \Delta\mathbf{I}_d + j\Delta\mathbf{I}_q$.

The unperturbed variables (subscript "0") are known. The terms with Δ symbol are the unknowns to be solved in the optimization. Imposing constraints of $\mathbf{P}$ and $\mathbf{Q}$ directly would result in a non-convex optimization problem due to products of two unknown optimization parameters (e.g. $\Delta\mathbf{V}_d\Delta\mathbf{I}_q$ in $\mathbf{P}$). To convexify the problem, $\mathbf{P}$ and $\mathbf{Q}$ are linearized and the constraints are implemented using $\Delta\mathbf{P}$ and $\Delta\mathbf{Q}$ ($\mathbf{P} = \mathbf{P}_0 + \Delta\mathbf{P} + \mathbf{P}_{\mathrm{err}}$, $\mathbf{Q} = \mathbf{Q}_0 + \Delta\mathbf{Q} + \mathbf{Q}_{\mathrm{err}}$).

Higher order non-convex square terms are dropped to yield

$$\Delta\mathbf{P} = \mathbf{V}_{d0}\Delta\mathbf{I}_d + \Delta\mathbf{V}_d\mathbf{I}_{d0} + \mathbf{V}_{q0}\Delta\mathbf{I}_q + \Delta\mathbf{V}_q\mathbf{I}_{q0}, \tag{3.12}$$

$$\Delta\mathbf{Q} = \mathbf{V}_{q0}\Delta\mathbf{I}_d + \Delta\mathbf{V}_q\mathbf{I}_{d0} - \mathbf{V}_{d0}\Delta\mathbf{I}_q - \Delta\mathbf{V}_d I_{q0}. \tag{3.13}$$

The higher-order non-convex terms constitute the real and reactive power errors $\mathbf{P}_{\mathrm{err}} = \Delta\mathbf{V}_d\Delta\mathbf{I}_d + \Delta\mathbf{V}_q\Delta\mathbf{I}_q$ and $\mathbf{Q}_{\mathrm{err}} = \Delta\mathbf{V}_q\Delta\mathbf{I}_d - \Delta\mathbf{V}_d\Delta\mathbf{I}_d$.

For load nodes, assuming a commonly used fixed power load model [70], the load power injections remain unchanged despite the perturbations. Therefore the power injec-

tion constraints for load nodes are

$$\Delta P_i = 0, \forall i \in \mathcal{N}^l, \tag{3.14}$$

$$\Delta Q_i = 0, \forall i \in \mathcal{N}^l, \tag{3.15}$$

where $\mathcal{N}^l$ is the set of load nodes.

For PV nodes, to maximize PV production real power curtailment is prohibited . The real power injections at the perturbed PV nodes then remain $P_{i0}, \forall i \in \mathcal{N}^{PV}$ and are determined by the available solar irradiance. The reactive power injections of the PV nodes are limited by the inverter rated power, $|Q_i| \leq Q_{i\max}, \forall i \in \mathcal{N}^{PV}$ as shown in Fig. 4.2. $Q_{i\max} = \sqrt{S_i^2 - P_i^2}$ is the maximum available reactive power of the SI, where S_i is the SI rated power, $\forall i \in \mathcal{N}^{PV}$. After the linearization, the constraints at the PV nodes become

$$\Delta P_i = 0, \forall i \in \mathcal{N}^{PV}, \tag{3.16}$$

$$|\Delta Q_i| \leq (Q_{i\max} - Q_{i0}), \forall i \in \mathcal{N}^{PV}. \tag{3.17}$$

Assuming that the PVs operate at unity power factor before reactive power perturbations ($Q_{i0} = 0$), the constraint in (3.17) becomes

$$-Q_{i\max} \leq \Delta Q_i \leq Q_{i\max}, \forall i \in \mathcal{N}^{PV}. \tag{3.18}$$

3.2.4 Linearization of voltage magnitudes

The magnitude of the complex node voltages can be calculated based on their real and imaginary parts as

$$|V|^2 = V_d^2 + V_q^2, \tag{3.19}$$
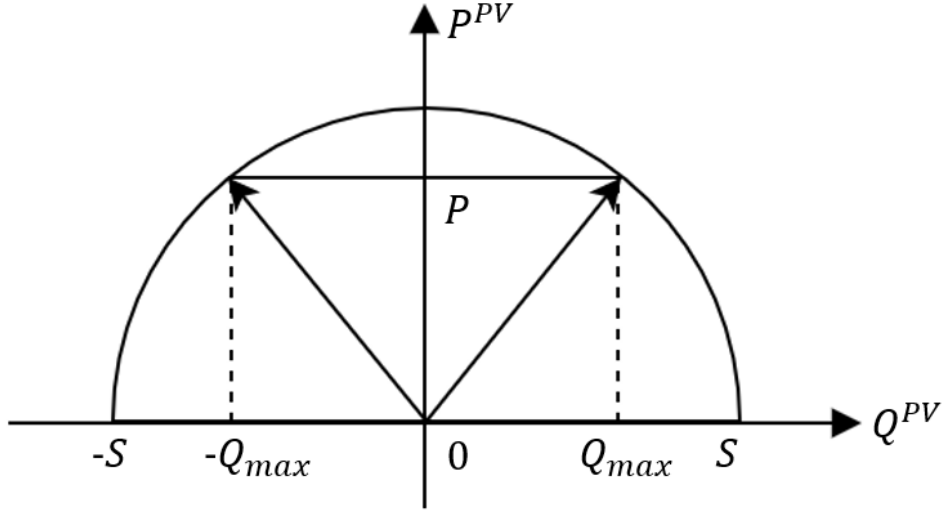
Figure 3.1: PV smart inverter output curve. P is the PV real power production, which is determined by the solar irradiance at each time step. Assuming no curtailment, given the SI rating S, the reactive power output can then vary between $-Q_{\max}$ and $Q_{\max}$.

where $V = V_d + jV_q$ is the complex voltage of an arbitrary node of the feeder.

Linearizing the nodal voltage magnitude in (3.19) around the initial point (i.e. $V_0 = V_{d0} + jV_{q0}$) yields $|V_0|\Delta|V| = V_{d0}\Delta V_d + V_{q0}\Delta V_q$. Then the voltage magnitude of an arbitrary node can be calculated as

$$|V| = |V_0| + \Delta|V| = |V_0| + |V_0|^{-1}(V_{d_0}\Delta V_d + V_{q_0}\Delta V_q). \tag{3.20}$$

This definition sets up an affine relation between the voltage magnitude of all nodes and the optimization parameters, which convexifies the optimization problem.

3.2.5 Implementation and Forecasts

Fig. 3.2 presents the flowchart of the implementation of the proposed voltage optimization. For tap operation minimization, the optimization problem is defined over a
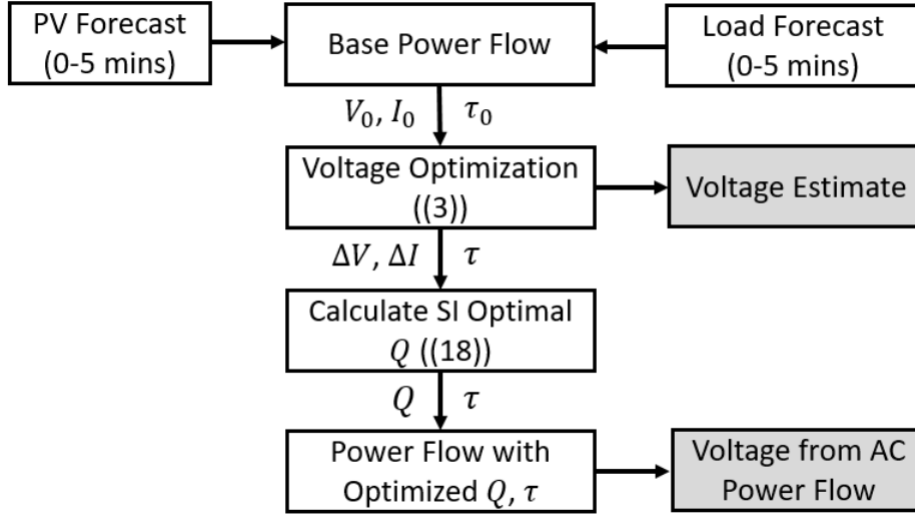
Figure 3.2: Flowchart of the proposed voltage optimization. PV and load forecasts are used to obtain the linearization voltages and currents $(\mathbf{V}_0, \mathbf{I}_0)$ for the next 5 minutes from an OpenDSS [2] base power flow simulations. Then, the voltage optimization per (2.17) is formulated and solved by interfacing with the CVX [3] and Gurobi solvers [4] using MATLAB, providing decision values for $\Delta\mathbf{V}$, $\Delta\mathbf{I}$ and τ. The optimal SI reactive power of the SI per (3.11) and the optimal tap positions τ are then input into another power flow. The voltage estimation accuracy using (3.20) is verified by comparing to the voltage results from the OpenDSS simulation.

5-min time horizon. $\mathbf{V}_0$ and $\mathbf{I}_0$ over the next 5 minutes are needed for modeling the effects of OLTC tap position changes and SI reactive power on voltage and they are obtained from a base power flow run by OpenDSS [2] using solar and demand forecasts. Sky imagers provide forecasts of PV availability throughout the feeder at high spatio-temporal resolution [59]. Load profile is from measured data at the substation provided by the utility. Forecasts are generated from the original data by adding different levels of random noise. Details of forecast construction are elaborated in Section 3.5.3. The optimal tap positions and SI reactive power set points are assumed to be delivered back to each OLTC/SI without communication delay.

3.3 Feeder-Wide OLTC and SI Optimization

In this section, we formulate the optimization for coordination of OLTCs and SIs. The goals are to mitigate voltage violations through minimizing voltage deviations and to reduce tap operations. The optimization objectives are formulated according to these two goals.

3.3.1 Optimization Model

The first objective function (J_1) is the sum of voltage deviations from 1 p.u. on the feeder during the optimization horizon

$$J_1 = \sum_{i=1}^{N} \sum_{t \in T} (||V_i(t)| - 1|), \tag{3.21}$$

where T is the set of time steps in the optimization horizon, and $|V_i(t)|$ denotes the voltage magnitude of node i at time step t (i is the node index, one node corresponds to one phase of a bus/a three-phase bus has three nodes). Minimizing J_1 achieves a more homogeneous and steady voltage.

The second objective function (J_2) counts the number of tap operations as,

$$J_2 = \sum_{p \in P} \sum_{t \in T} |\tau_{p,t+1} - \tau_{p,t}|, \tag{3.22}$$

where P is the set of all OLTCs and $\tau_{p,t}$ denotes the tap position of OLTC p at time step t. All tap changes over a defined time horizon T are aggregated in J_2.

Combining the two objective functions, the optimization can be formulated as:

$$\min \quad J = w_1 J_1 + w_2 J_2$$

$$\text{s.t.} \quad (3.2), (3.3), (3.4), (3.6), (3.7),$$

$$(3.14), (3.15), (3.16), (3.18), (3.20),$$

$$\tau_{p,t} \in \mathbb{Z},$$

$$\tau_{p,\min} \leq \tau_{p,t} \leq \tau_{p,\max},$$

$$|\tau_{p,t} - \tau_{p,t-1}| \leq \Delta TO_{p,\max}$$

The weighting factors w_1 and w_2 balance voltage regulation performance and total tap operations. Increasing w_1 will improve the voltage profile at the cost of more tap operations and vice versa. $w_1 = 1$ and $w_2 = 0.15$ are chosen in this paper through trial-and-error. This combination of parameters provide good performance on both test feeders. Details of weights factors selection are provided in Section 3.4.3.

3.3.2 Optimization Constraints

As presented in Section 3.3.1, (3.2) is included as an equality constraint to represent the linearized feeder nodal voltage equation. (3.3)(3.4)(3.6)(3.7) are equality constraints for modeling the relationship between impedance matrix change (ΔZ) and OLTC tap position (τ). (3.14)(3.15) are the fixed power load model constraints for load real power and reactive power, respectively.

In this work, real power curtailment is prohibited to maximize PV production, (3.16) is the corresponding equality constraint. As discussed in Section 3.2.3, the maximum

available SI reactive power injection is limited by the inverter rated capacity (Fig.4.2). (3.18) reflects the constraint on reactive power injection for each SI. The linearized voltage magnitude equation ((3.20)) is an equality constraint.

The remaining three constraints are OLTC tap position constraints. $\tau_{p,t} \in \mathbb{Z}$ indicates the tap position is an integer, where $\tau_{p,t}$ denotes the tap position of OLTC p at time step t and $\mathbb{Z}$ represents integer numbers. $\tau_{p,\min} \leq \tau_{p,t} \leq \tau_{p,\max}$ denotes the tap position is within $[\tau_{p,\min} \; \tau_{p,\max}]$, $\tau_{p,\min} = -16$ and $\tau_{p,\max} = 16$ are the minimum and maximum tap positions of OLTC p, respectively. $|\tau_{p,t} - \tau_{p,t-1}| \leq \Delta\text{TO}_{\text{p,max}}$ constrains tap position change within two consecutive time steps. Since OLTCs react slowly, $\Delta\text{TO}_{\text{p,max}}$ (1 tap operation per 30 sec) avoids unrealistic tap operation changes by limiting the maximum tap operations between two consecutive time steps.

3.4 Case Study

3.4.1 Distribution Feeder Models

To evaluate the proposed method, quasi-steady state simulations are carried out on two multi-phase unbalanced feeders, the modified IEEE 37 bus feeder and a real California utility feeder (feeder 10 in [60] as shown in Fig. 3.3). The feeder properties are summarized in Table 3.1. The IEEE 37 bus feeder is simulated for 24 hours with 30-sec resolution using measured solar profiles from a partially cloudy day. Due to computation time limitations for the large utility feeder, a 5-min simulation time step is used. The simulation is performed for a clear day.

Table 3.1: Test Feeder Properties.

Feeder	IEEE 37	Utility Feeder
# of nodes	120	2844
# of Loads	30	584
# of PV	30	203
Peak Load (MVA)	2.73	8.50
PV Penetration (%)	150	150
# of OLTC	1	1

For the IEEE 37 bus feeder, 30 PVs with DC power rating ranging from 23 to 206 kW and totalling $P_{\mathrm{pv}}^{\mathrm{peak}} = 4.1$ MW are randomly deployed on the feeder. The total PV penetration on the feeder is 150% by capacity: $PV_{\mathrm{Pen}} = \frac{P_{\mathrm{pv\_peak}}}{P_{\mathrm{load\_peak}}} \times 100\%$. 340 PVs with DC ratings varying from 7 kW to 458 kW are connected to the utility feeder, resulting in a total capacity $P_{\mathrm{pv\_peak}} = 12.8$ MW and also 150% PV penetration. 10% oversizing of AC power rating is assumed for the SIs on both feeders [71]. Both feeders contain one OLTC at the substation. The OLTC tap position can vary from $\tau = -16$ to $+16$ with voltage regulation capability of [0.9 1.1] p.u..

3.4.2 Voltage Regulation Methods

The proposed method is benchmarked against the widely-used conventional autonomous voltage regulation scheme (AVR). The two different voltage regulation strategies are summarized in Table 3.2.
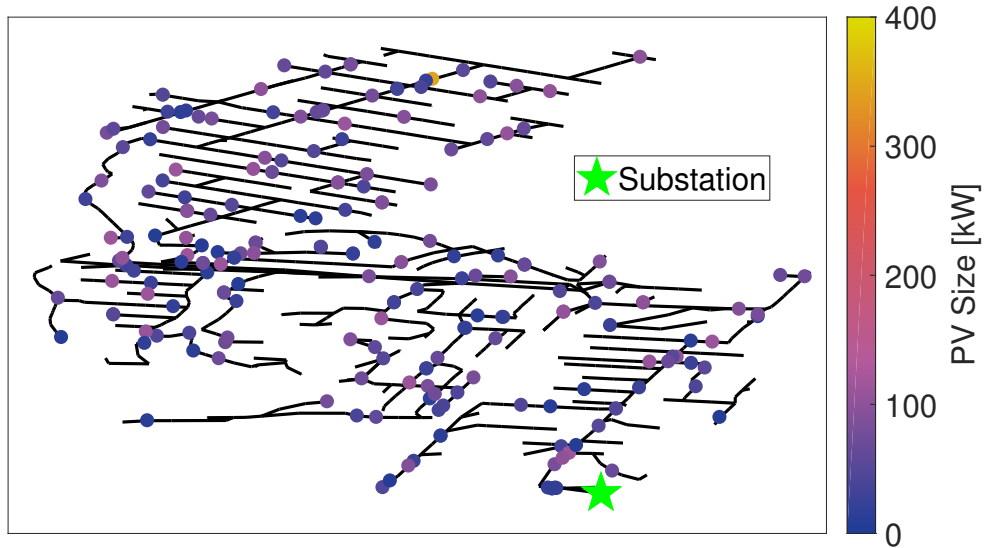
Figure 3.3: Feeder topologies of the California utility feeder. Black lines represent feeder lines. Each dot is a PV system and its color indicates its AC power rating. The OLTC is located at the substation (green star).

Autonomous Voltage Regulation (AVR)

In AVR, voltage control devices operate autonomously based on pre-defined rules or curves without coordination with each other. SIs output reactive power following the Volt-Var curve in Fig. 3.4, which is the recommended default Volt-Var curve by the California Public Utility Commission [5]. OLTCs change tap position to keep the deviation of the local busbar voltage from the preset reference voltage within certain limits. The OLTC reference voltage is set to 1.03 p.u. for IEEE 37 bus feeder and 1.02 p.u. for the utility feeder. The voltage regulation bandwidth is 0.0167 p.u. for both feeders. For better voltage regulation, the tap time delay is set to be 0 sec. All other OLTC parameters are set as the default OpenDSS [2] values.
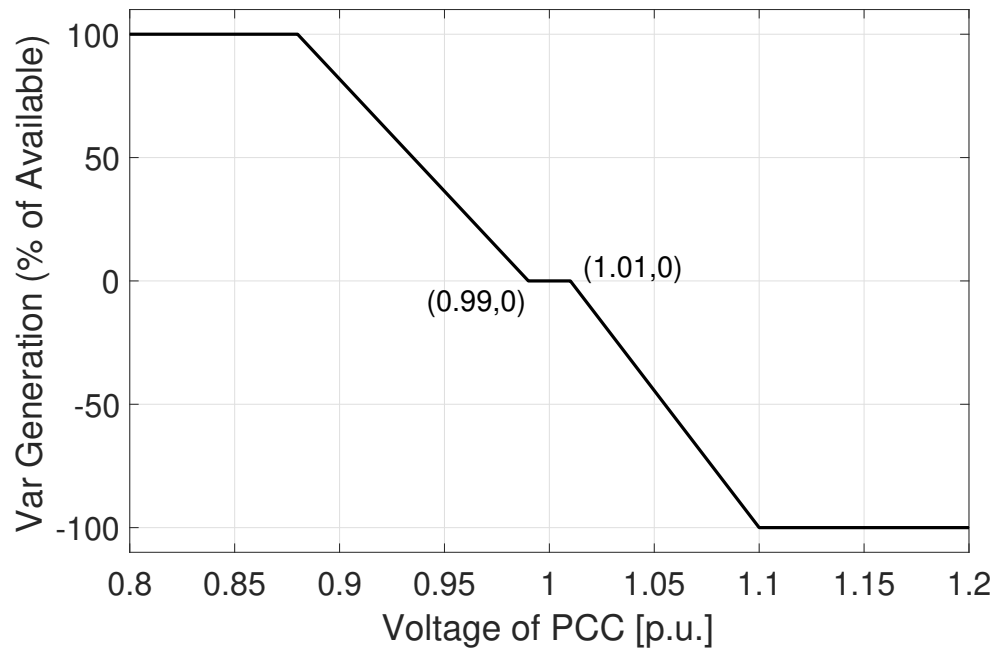
Figure 3.4: Volt-Var curve of SI adapted from [5]. The SI injects/absorbs the corresponding percentage of available vars based on the voltage at the point of common coupling (PCC). The available vars (Q_{max}) are limited by PV real power generation and SI rating as shown in Fig. 4.2.

Table 3.2: Summary of autonomous voltage regulation (AVR) and optimal voltage regulation (OVR).

	OLTC	PV
AVR (benchmark)	Autonomous control	Volt-var Curve
OVR (proposed)	Tap optimized	VAR optimized

Optimal Voltage Regulation (OVR)

For OVR, OLTCs and SIs are coordinated to minimize voltage deviations as described in Section 3.3. Per the optimization outputs, SIs participate in voltage regulation via reactive power absorption and injection and OLTC tap position are specified. A reference voltage is not needed as the OLTCs will follow the optimal tap position.

3.4.3   Selection of Weighting Factors for OVR

Since the optimization objective J is a weighted sum of J_1 and J_2, heavier weighting on J_1 will improve the voltage profile at the cost of more TOs and vice versa. Therefore, appropriate weighting factors should be chosen to achieve a desired trade-off between voltage profile and number of TOs. Several combinations of weighting factors (w_1, w_2) are tested with simulations on the IEEE 37 bus feeder on 150% PV penetration (Table 3.3).

As expected, larger weighting factors (w_2) on J_2 cause decreasing total TO, while voltage deviations generally increase. Relative to $w_2 <= 0.05$, $w_2 = 0.15$ provides a large reduction in TO without a significant increase in voltage deviations. And simulations with $w_2 = 0.15$ on the California utility feeder also show minimization of voltage deviations with a reasonable number of total TOs. Therefore, $w_2 = 0.15$ is used for both test feeders

Table 3.3: Case study of different objective function weights w_2 on the IEEE 37 bus feeder with 150% PV penetration. w_1 is fixed at 1. The mean voltage deviation is calculated for 8:00 - 17:00 of all nodes. The total TO is counted for the 24 hour day.

w_1	w_2	Mean Voltage Deviation (p.u.)	Total TO
	0.001	0.0170	94
	0.010	0.0170	91
	0.050	0.0172	38
1	0.150	0.0174	2

hereinafter.

The best combination of w_1 and w_2 for different feeders may vary due to the operator preferences between better voltage regulation or less TO, different locations of OLTCs, feeder topologies, distribution of PVs, etc. Local adjustments of the weighting factors are therefore recommended.

3.5 Distribution Feeder Simulations Results

3.5.1 Voltage Estimation Accuracy

Given that estimated node voltages are used in the optimization to determine optimal OLTC tap position and SI reactive power, we examine the errors resulting from the linearization of feeder nodal voltage equations ((3.2)), the admittance matrix (Section 3.2.2), power injection constraints (Section 3.2.3), and the voltage magnitude ((3.20)). Errors are defined as the differences in estimation of voltage magnitude from (3.20) versus

the non-linear AC power flow results from OpenDSS (Fig. 3.2)

$$E(t)_i = V_{\text{estimate}}(t)_i - V_{\text{OpenDSS}}(t)_i. \tag{3.23}$$

Fig. 3.5 presents $E(t)$ distributions for the IEEE 37 bus feeder. Since the voltage estimations match the AC power flow results closely, it can be concluded that the proposed model estimates voltage magnitudes accurately. The maximum error magnitude is 0.009 p.u. and the mean absolute error magnitude is always under 0.004 p.u.. Around noon when the distribution feeder is prone to voltage violations with high PV generation, the voltage estimation errors are less than 0.001 p.u.. At night when the estimation errors are relatively high, the distribution system is much less likely to experience voltage violations even with simple local Volt-Var functions (Fig. 3.7). And the proposed method can improve the night time voltage profile further as shown in Fig. 3.7. Therefore, the proposed method can effectively mitigate voltage violations despite somewhat larger voltage estimation errors at night.

3.5.2 Performance Under Perfect Forecasts

IEEE 37 Bus Feeder

Voltage Profile

Fig. 3.6 presents snapshot voltage profiles of the feeder around noon (11:32 h, medium loading of 0.84 MVA, large PV generation of 3.3 MW) and in the evening (21:00 h, heavy loading of 1.91 MVA, no PV generation). At noon, a voltage increase along the feeder results from reverse power flow caused by excess PV production. For AVR, the voltage
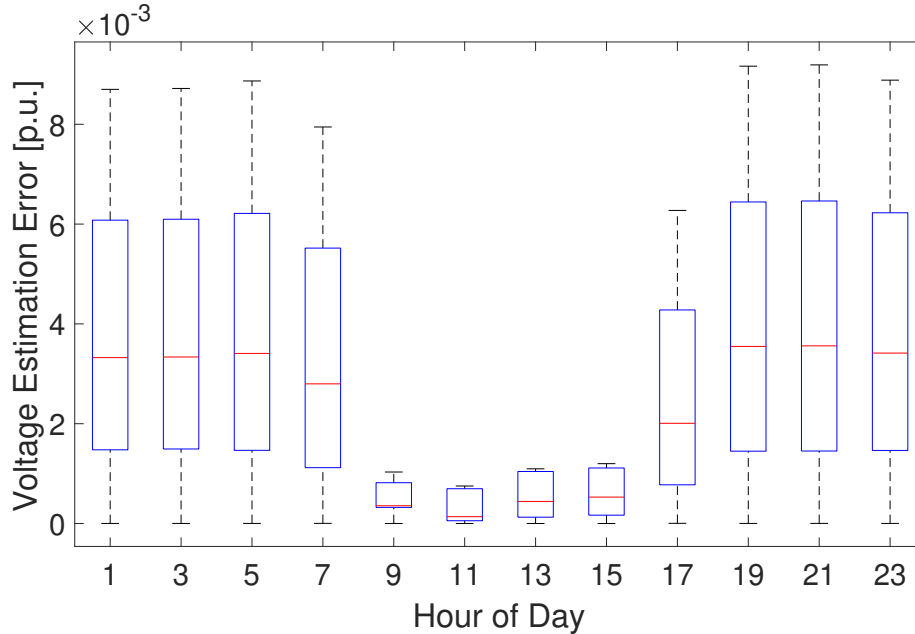
Figure 3.5: Box plot of voltage estimation errors for the IEEE 37 bus test feeder. For readability, the results are aggregated over two hours into 12 groups.

violates ANSI standards at the feeder end at 1.056 p.u. [7]. The over-voltage violation occurs in phases 1 and 2, while the voltage on phase 3 remains within [0.95 1.05] p.u.. At the feeder end, there are also large voltage imbalances across different phases with a mean voltage imbalance of 0.012 p.u. and a max of 0.030 p.u.

On the contrary, OVR keeps the voltage of all phases within the [0.95 1.05] p.u. ANSI limits. Due to limited available reactive power capacity around noon (at full active power, $Q_{\max} = 42\%$ of the rated power), the mean voltage unbalance stays the same and the max unbalance increase to 0.041 p.u. as a result of correcting the over-voltage issues. If PV curtailment was allowed, more reactive power support would reduce the voltage unbalance since OVR minimizes total voltage deviation, bringing all the voltages closer to 1 p.u..

At 21:00 heavy loading causes a large voltage drop with AVR. Again, voltage discrepancies between phases are large: the largest voltage difference occurs between phases 1 and 3 at the feeder end at 0.042 p.u., equivalent to 42% of the allowable voltage range. The mean voltage unbalance is 0.017 p.u.. With OVR, the voltages remain close to 1 p.u. across the entire feeder, resulting in a more desirable homogeneous (flat) voltage profile. The voltage unbalance is substantially reduced with a maximum of 0.014 p.u. (a 67% reduction compared to AVR) and a mean of 0.005 p.u.. OVR squeezes the voltage range on all phases toward 1 p.u. with coordinated reactive power support from SIs, reducing the voltage unbalance on the feeder. The favorable OVR results are enabled by coordination of OLTCs and SIs through optimization and also by unlimited reactive power support (Fig. 4.2) at night.

Fig. 3.7 compares absolute voltage deviation of all nodes on the feeder between AVR and OVR. For AVR, the mean voltage deviation is around 0.011 p.u. during periods without PV production. The voltage deviation mean increases when PV power production ramps up starting around 08:00 and reaches 0.031 p.u. at noon. Generally, voltages are scattered far around the mean value and the range is larger near noon due to high PV generation. The voltage deviations exceeded the 0.05 p.u. limit (over-voltage) for over one hour near noon. With OVR, the voltage deviations of all nodes are under the 0.05 p.u. limit, eliminating the over-voltage problems in the AVR case. The voltage deviation mean decreases to below 0.005 p.u. at night and is always below 0.01 p.u. during the day. The minimum average voltage deviations around 08:30 and 16:00 occur when PV generation balances load consumption minimizing power flow on the feeder. Like for AVR,
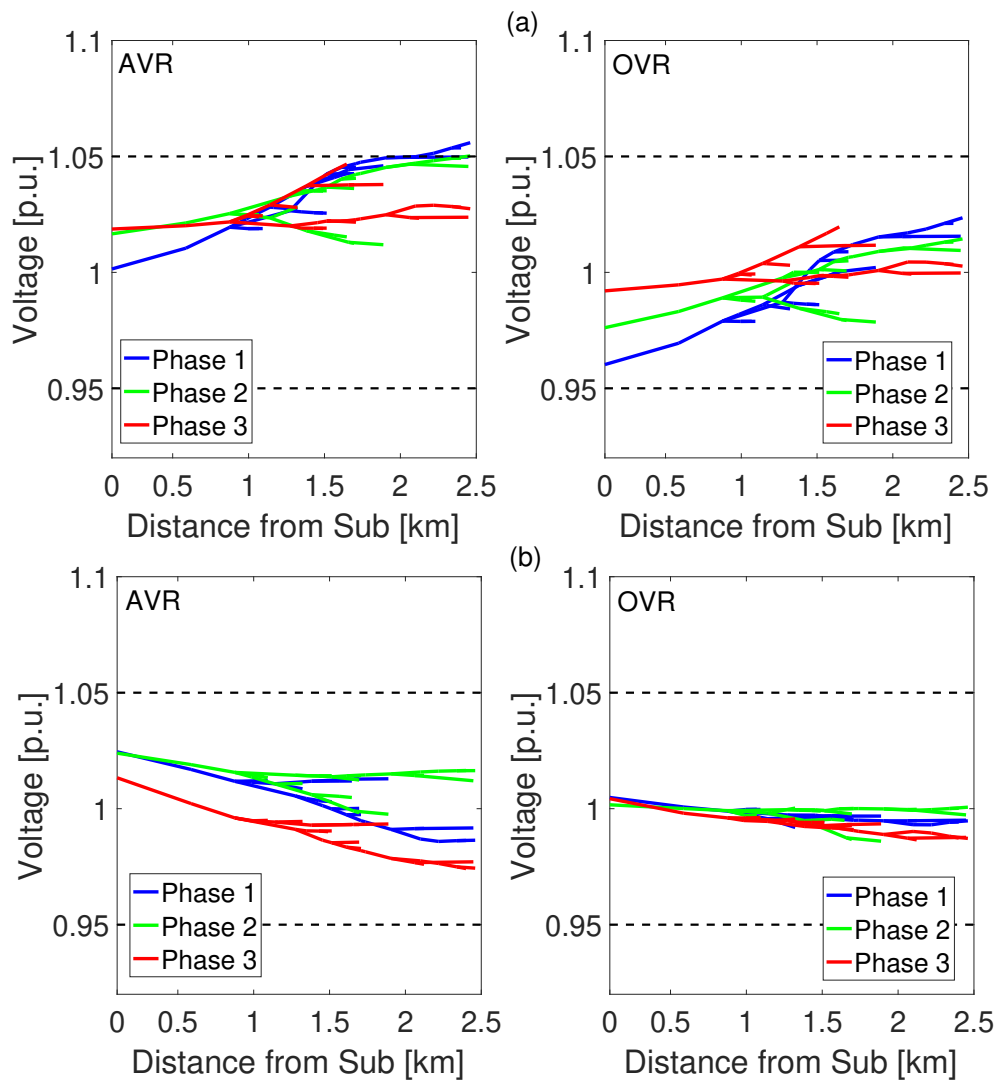
Figure 3.6: Feeder voltage profile at 11:32 (top, a) and 21:00 (bottom, b) for the AVR (left) and OVR (right) voltage regulation methods.

the OVR voltage deviation is larger during day time and peaks around noon. The noon peak is a combined effect of maximum power flow on the feeder (i.e. larger voltage change) caused by more PV power production and reduced available reactive power of SIs (Fig. 4.2).

OLTC Tap Operations

Fig. 3.8 presents the OLTC tap positions. For AVR, the tap position is set high (+9) during the night with no PV production compensating the voltage drop on the feeder. During the PV production period, the tap position is lowered (+6) due to increasing voltage. Since the OLTC and SIs operate autonomously based on local voltage without coordination, the fluctuating PV generation (as indicated by Fig. 3.7) triggers three immediate up-and-down tap operations. In total, 10 tap operations occur during the day. With OVR, SIs provide optimized reactive power support in coordination with OLTCs, allowing a lower tap position setting without violating operation limits. Unnecessary tap operations are also avoided per objective J_2 (3.22) resulting in only 2 total tap operations, which is an 80% reduction when compared to AVR.

Large California Utility Feeder

Fig. 3.9 displays the voltage profile of the large utility test feeder with AVR and OVR. The mean AVR voltage deviation is around 0.010 p.u. at night and increases to 0.021 p.u. around noon. The feeder experiences over-voltages for about 2 hours when PV generation peaks. The largest voltage deviation is 0.053 p.u., corresponding to a 1.053 p.u.
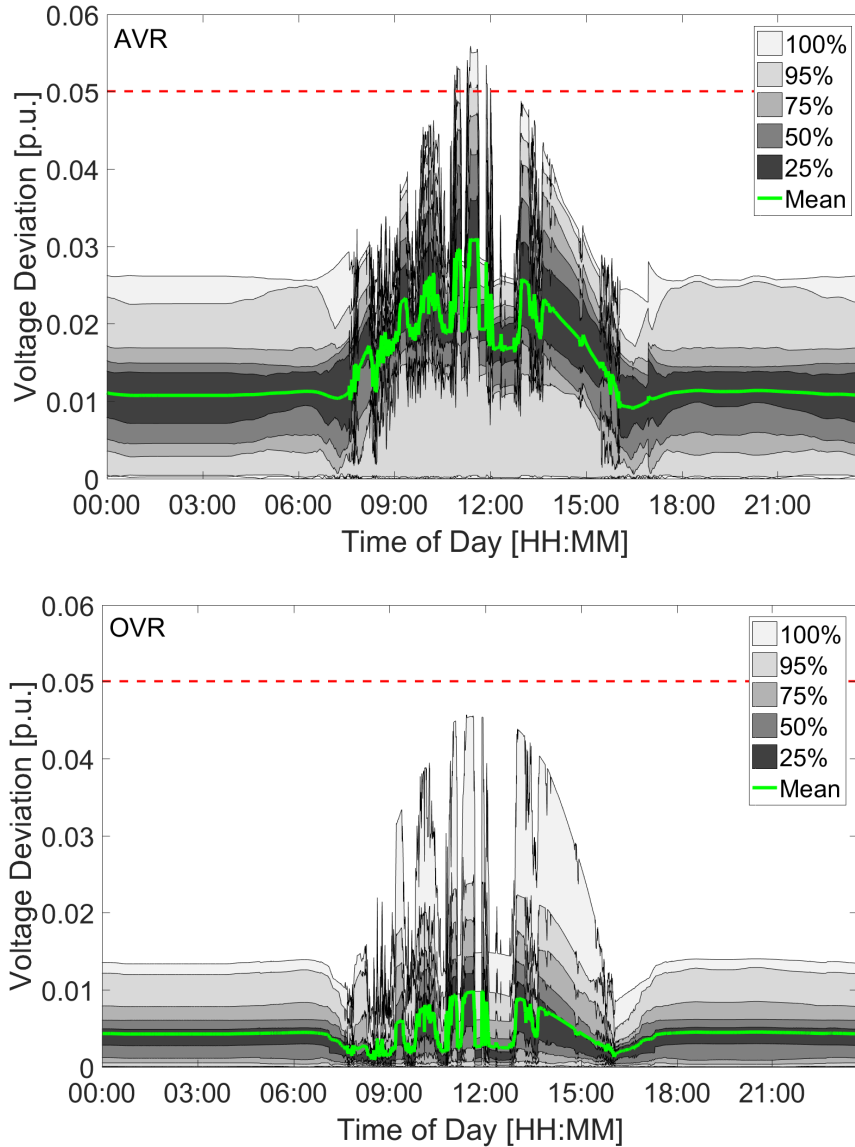
Figure 3.7: Distribution of the absolute values of feeder nodal voltage deviations from 1 p.u. for all nodes on the IEEE 37 bus feeder. top: AVR; bottom: OVR. The absolute values are plotted for consistency with $J_1(3.21)$. The red dashed line represents the [0.95 1.05] p.u. ANSI voltage limits. For the IEEE 37 bus feeder, all voltage deviations greater than 0.05 are over-voltages.
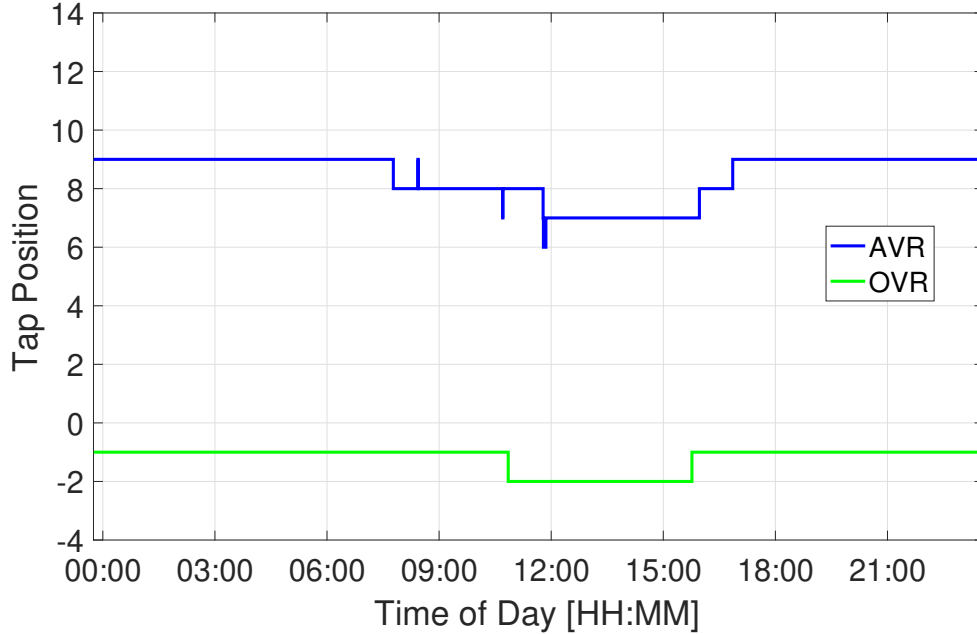
Figure 3.8: Time series of OLTC tap positions τ for the IEEE 37 bus feeder.

overvoltage. With OVR, the average nodal voltage deviation reduces to 0.002 p.u. at night and reduces to 0.010 p.u. near noon. All voltage deviations are under the 0.05 p.u. limit, indicating that the over-voltage issues for AVR are eliminated. The maximum voltage deviation decreases to 0.042 p.u., corresponding to a maximum voltage of 1.042 p.u.. Due to smooth PV generation of clear day the OLTC did not operate under AVR despite over-voltage issues on the feeder. With coordinated OLTC and SIs under OVR, 2 tap operations suffice to resolve the over-voltage problem for the entire day.

3.5.3 Performance with Forecast Errors

To evaluate the robustnes of the proposed OVR, multiple case studies are carried out on the IEEE 37 bus feeder assuming different levels of forecasting error. The PV and
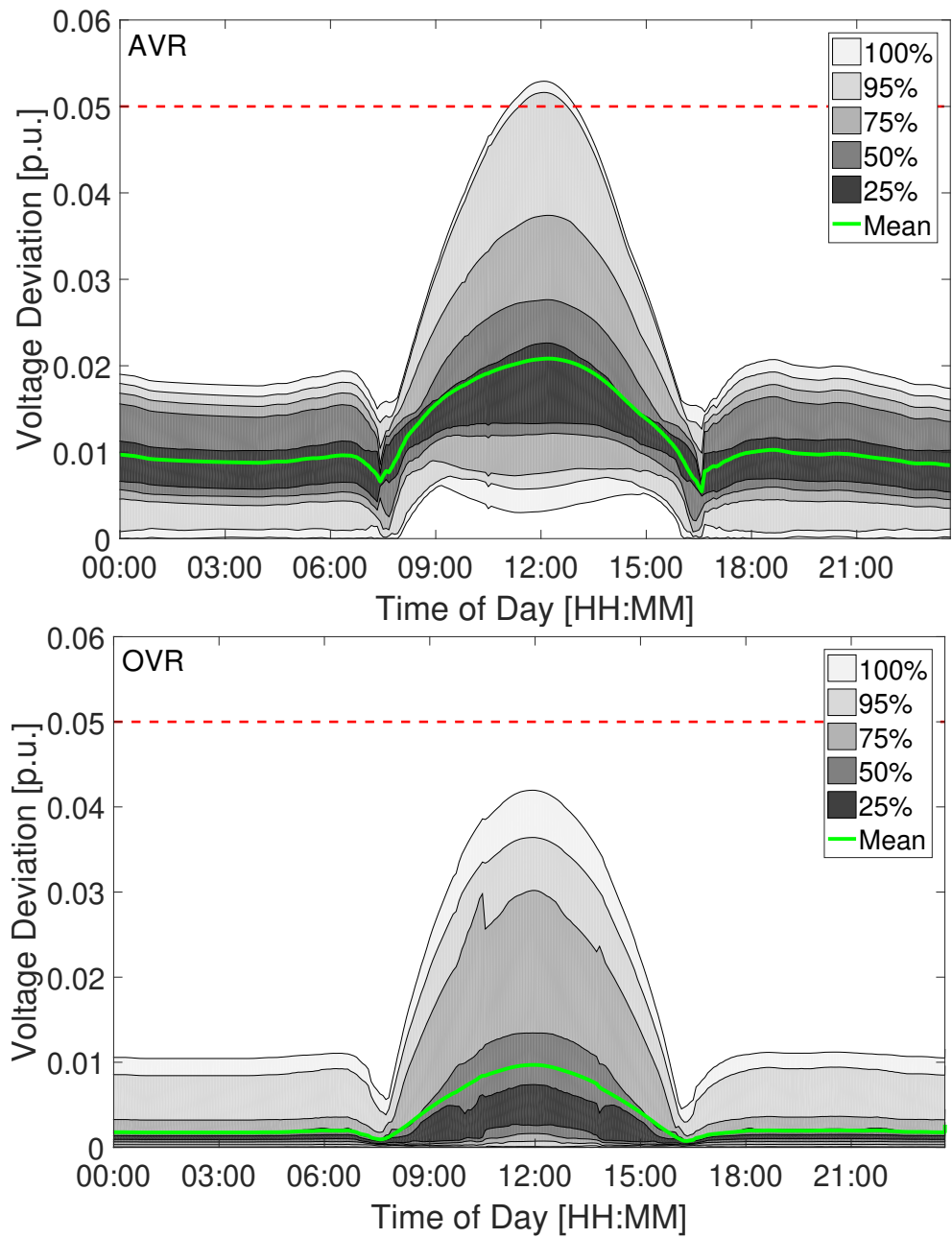
Figure 3.9: Distribution of absolute values of feeder nodal voltage deviation from 1 p.u. for AVR (top) and OVR (bottom) cases.
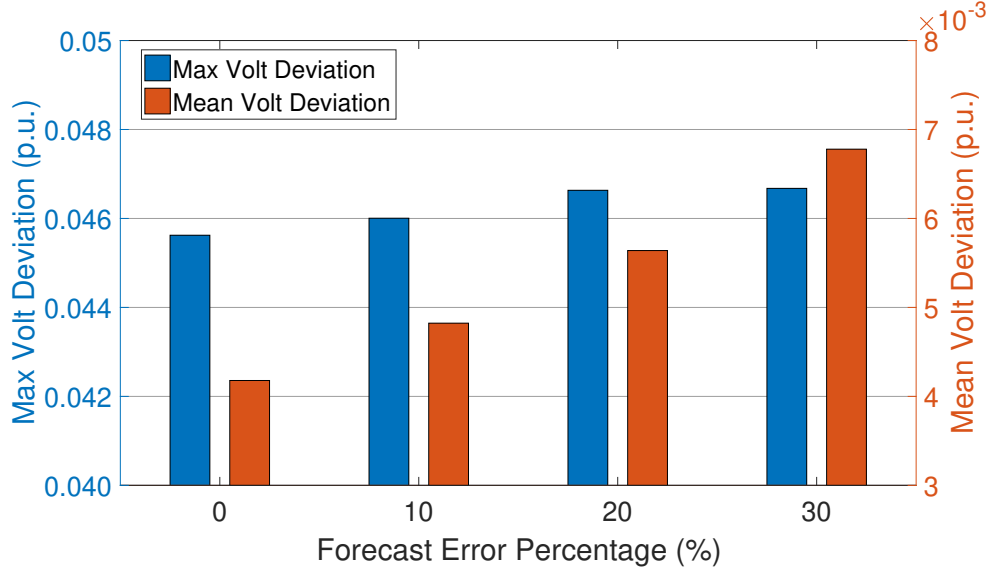
Figure 3.10: Maximum and average voltage deviation of the IEEE 37 bus feeder under different levels of forecast errors with OVR. Both quantities are calculated based on all nodal voltages for simulations of the same cloudy day as Section 3.5.2

load profiles with forecast errors are constructed using the following equation:

$$y(t) = (1 + \alpha\epsilon(t))y_{true}(t), \tag{3.24}$$

where $y(t)$ represents the forecasted PV output or load consumption at time step t, $y_{true}(t)$ is true PV/load profile for time step t. α is a scalar to represent the maximum error ratio in terms of $y_{true}(t)$ while $\epsilon(t)$ is a random number from an uniform distribution within [-1,1].

Fig. 3.10 presents the maximum and average nodal voltage deviations within 24 hr simulation period for IEEE 37 bus feeder with OVR for $\alpha = [0, 0.1, 0.2, 0.3]$. $\alpha = 0$ indicates perfect forecasts as in Section 3.5.2.

As shown in Fig. 3.10, the both maximum and average voltage deviations increase with larger forecasting errors. This is consistent with expectations that less accurate fore-

casts will lead to performance deterioration. Even with 30% forecast error, the OVR is still capable of keep the maximum voltage deviation (0.0467 p.u.) under 0.05 p.u., i.e. without voltage violations. In contrast, AVR fails to maintain e the voltage within [0.95 1.05] p.u. operation limits as shown in Fig. 3.7 (Note that since AVR does not require any forecasts, it is always tested with true PV and load profiles). With AVR, the maximum voltage deviation is 0.056 p.u., corresponding to an over-voltage of 1.056 p.u.. As for mean nodal voltage deviation, OVR keeps average voltage deviation under 0.0068 p.u. even with a forecast error of 30% while the average voltage deviation is 0.0135 p.u. for the AVR case. OVR significantly decreases voltage deviation per J_1.

3.5.4   Computation Time

Solving the optimization problem at an operational timescale would enable the control to be used in real time applications. Table 3.4 compares the average computation time in [8, 9] for the IEEE 33 bus feeder and IEEE 2500 node feeder with the OVR cases in this paper. For the IEEE 33 bus feeder with 99 nodes, 3 DGs, 2 ShCs and 1 OLTC, the average computation time is 40 s in [8] using an Intel Core i7-2600 @ 3.4 GHz processor. With the proposed OVR algorithm in this paper, however, the solution time is less than 1 second for the slightly larger IEEE 37 feeder with 120 nodes, 30 PVs and 1 OLTC using an Intel(R) Core(TM) i7-4700MQ 2.8-GHz processor. For the large feeders, the solution time for IEEE 2500 node feeder in [9] is 600 s with an Intel core i7-4710HQ @ 2.5 GHz processor, while our proposed OVR reduces computing time by 80% for a larger feeder on

Table 3.4: Comparison of average computation time (s) per time step in [8, 9] and OVR case study in this paper.

Test Feeder	# of nodes	Optimization	Solution time (s)
IEEE 33	99	[15]	40
IEEE 37	120	OVR	0.95
IEEE 2500	2500	[9]	600
Utility Feeder	2844	OVR	127

the PC with Intel (R) Core(TM) i7-4700MQ 2.8-GHz processor. While the computation cost comparison is not apples-to-apples, the results strongly favor our OVR approach which outperforms prior research by a large margin on larger feeders and comparable and even inferior computing resources.

Due to compatibility issue between CVX [3] and the newest version of Gurobi solver [4], Gurobi v6.5 is used in this paper; the solution speed could be further improved with the latest version Gurobi v8.1 [72].

3.6 Conclusions

A novel method of coordinating OLTCs and SI reactive power for voltage regulation was proposed. OVR is capable of coordination voltage regulation between multiple OLTCs and SIs. The proposed OVR is compared against conventional AVR through simulations on the highly unbalanced IEEE 37 bus test and a large California utility feeder. Results show that OVR can mitigate over-voltage violations, significantly reduce voltage deviations,

decrease voltage unbalance across phases, and avoid unnecessary tap operations. This is achieved by effective coordination between OLTCs and SI reactive power control. The robustness of the proposed OVR is also demonstrated on the IEEE 37 bus test feeder assuming different levels of forecast error. The computational efficiency of OVR is superior to prior methods and the solution time is compatible with real-time operation on large California utility feeder with 2844 nodes and 203 PVs even on a regular PC.

The text and data in Chapter 3, in full, is a reprint of the material as it appears in Coordination of OLTC and Smart Inverters for Optimal Voltage Regulation of Unbalanced Distribution Networks, Li, C., Disfani, V.R., Haghi, H.V., Kelissl, J., *Electric Power Systems Research*, 2020. The dissertation author is the primary investigator and author of this article.

Chapter 4

Data-Driven Online PV Smart Inverter Coordination using Deep Reinforcement Learning

4.1 Introduction

Renewable distributed generation (DG) adoption has seen significant increase recently due to the associated technical, economic, and environmental benefits [45]. However, DG adoption also presents various new challenges to grid operators. For instance, voltage violations can become a problem due to increasing penetration of variable DGs such as solar photovoltaic (PV) generators [60, 73].

Conventionally, distribution network operators rely on on-load tap changers (OLTCs) and fixed or switched shunt capacitors/reactors to maintain appropriate voltages across

the network. OLTCs typically work in autonomous mode, following simple pre-defined rules based on local measurements. This simple voltage regulation scheme is effective for conventional centralized power supply with monotonously decreasing voltage profile along the feeder and slow voltage changes. However, the presence of large amount of renewable DGs on the distribution network can cause reverse power flow, leading to voltage increases along the feeder and possible voltage violations [48]. Due to their electro-mechanical nature, OLTCs are limited in the number of tap changes before preventive maintenance or overhaul is required. To reduce the number of tap changes, OLTCs are programmed to act with delays of 10s of seconds and therefore respond slowly. Therefore, OLTCs are less effective in controlling voltage with sub-minute PV variability. On the contrary, smart inverters (SIs) can rapidly respond to voltage regulation by modulating active and/or reactive power of PV systems at the point of common coupling (PCC) [46]. The commonly used SI Volt-Var functions, as defined in [13, 14, 74], are based on local droop curves, which define the SI absorption/injection of reactive power according to the local bus voltage. Local droop curves result in sub-optimal system performance due to lack of coordination.

Various studies have aimed to improve basic rule-based autonomous local voltage control schemes [17, 19, 67]. Reference [17] improve the sensitivity of voltage control to downstream voltage using feeder end measurements instead of local bus voltage for the control of tap switching. Voltage estimates from a sensitivity matrix are adopted to dynamically adjust OLTC voltage set points to accommodate SI outputs in [19]. OLTC and SIs are coordinated by iteratively updating their settings to achieve target voltage at

81

the SI in [67].

These improved rule-based voltage control methods are relatively simply to implement and can achieve partial coordination between different devices. However, optimization-based approaches can realize optimal voltage regulation to combat complicated voltage profiles caused by renewable DGs. Some previous works focus on coordination of SIs [64, 25, 28, 66]. Reference [64] applies dynamic weight-based collaborative optimization to dispatch SI reactive power for voltage deviation minimization. Optimal power flow (OPF) is formulated as a second order cone program to optimize SI reactive power for line loss reduction while meeting voltage requirements [25]. Reference [28] adopts the alternating direction method of multipliers (ADMM) to solve the OPF problem and find the optimal SI reactive power to reduce losses. ADMM-based algorithms are also employed in [66] to determine SI active and reactive power set points for voltage regulation.

Other works research cooperation between other devices as well as SIs [68, 75, 76, 29, 30, 31]. Reference [68] proposed a linearization model to optimize multiple OLTCs to minimize voltage deviations. OLTC tap positions and SI outputs (reactive power in [75, 76]; active and reactive power in [29]) are optimized concurrently to minimize voltage deviations. DGs and OLTCs are coordinated through optimization to minimize voltage deviations and network losses in [30]. SIs, OLTCs, and shunt capacitors are coordinated in [31] to meet voltage operation limits.

Despite optimization-based approaches and OPF methods accomplishing optimal voltage regulation, there are two major limitations. First, they require accurate distribution grid models including resistances and reactances, and the network topology, which are

not necessarily available for distribution networks [34]. Second, non-linear power flow constraints render the optimization problem computationally intensive, especially for large networks. Long run times limit the methods' practical application to address fast PV disturbances caused by moving clouds.

The success of reinforcement learning (RL), especially deep reinforcement learning (DRL) in various fields including AlphaGo [35] and robotics [77], has attracted interest in the power and energy community. There have been numerous works on applying RL/DRL for intelligent control and operation in power grids. Deep Q network (DQN) and Deep Deterministic Policy Gradient (DDPG) are used in [78, 79] for controlling discrete generator voltage setting points to maintain acceptable system voltages in response to load variations and line outages. Double Deep Q network (DDQN) is applied to optimal active power dispatch to achieve operation cost reduction in [80]. DDQN is also adopted in [81] to control grid topology change to maximize available transfer capabilities. Reference [82] uses the multi-agent DDPG method to adjust generator voltage set points continuously to solve the classic autonomous voltage control problem in the transmission grid. Reference [36] dispatches SIs, OLTCs, and capacitors at two timescales for distribution grid voltage control. Optimization is used for fast dispatch of SIs while slow OLTCs and capacitors are handled by DQN. Batch reinforcement learning is applied to achieve cooperation of OLTCs for voltage regulation [37]. Coordination between OLTCs and capacitors are studied with the policy gradient method for voltage violation mitigation and operation cost reduction [38, 39, 40]. Multi-agent DRL is also used in [42, 43] to dispatch SI reactive power and static Var compensators to address voltage violations. Reference [44] studies SI reactive

dispatch with the policy gradient method for voltage deviation reduction. Reference [41] coordinates OLTCs, capacitors, and generators to meet operation limits with Q-learning.

Of the works that use RL for power grid applications, references [36, 37, 38, 39, 40, 42, 43, 44, 41] focus on distribution voltage regulation. Within those, [36, 37, 38, 39, 40, 41] use RL/DRL for control of legacy voltage regulation devices with discrete settings (i.e. generator voltage set points, OLTC tap position, capacitor switches).

SIs are more suitable for mitigating frequent PV generation fluctuations due to their continuous outputs and fast response in comparison to legacy voltage regulation devices. While references [42, 43, 44] coordinate SIs with DRL, PV active power curtailment is not considered in the reward function design in [42, 43], which can lead to excessive curtailment. Reference [44] balances active power curtailment and voltage regulation. However, instead of directly determining optimal active and reactive power set points, incremental changes are employed, which can lead to insufficient responses to large PV ramps. Moreover, the performance is not validated against OPF.

In this paper, we propose a DDPG-based algorithm to coordinate multiple SIs with continuous outputs. The reward is carefully designed to balance voltage regulation and active power curtailment, in contrast to [42, 43]. Unlike OPF approaches, the proposed DDPG agent is data-driven and relies on little to no knowledge of the distribution network. The DDPG approach can reach decisions in milliseconds, fully leveraging the fast-response speed of SIs to deal with frequent and fast solar ramps. The DDPG method is validated against the autonomous Volt-Var scheme [14] and OPF (contrary to [44]) on the modified IEEE 37 bus feeder and the IEEE 123 bus feeder. Comprehensive tests are carried out

for a full year (8760 different scenarios) to demonstrate the effectiveness and robustness of the well-trained DDPG agent.

The rest of the paper is organized as follows. Section 4.2 introduces preliminaries of the distribution grid and SIs. The OPF formulation and DDPG implementation for coordination of SIs is presented in Section 4.3. Case studies are detailed in Section 4.4. Results and discussion are presented in Section 4.5, followed by conclusions in Section 4.6.

4.2 Preliminaries

4.2.1 Distribution Power System

From graph theory prospective, a distribution network with $N + 1$ nodes can be represented by a graph $\mathcal{G} := (\mathcal{N}_0, \xi)$, where $\mathcal{N}_0 := \{0, ..., N\}$ is the collection of all nodes (one node corresponds to one phase of a bus/a three-phase bus has three nodes), and $\xi := \{(m, n) \subset \mathcal{N}_0 \times \mathcal{N}_0\}$ is the collection of edges representing distribution lines of the grid. The distribution grid typically operates radially as a tree and is served by a substation (a.k.a. the root) indexed by $n = 0$. The primary side of substation can be treated as a slack bus, where voltage magnitude $|V_0|$ and angle θ_0 can be modeled as constants. The voltage for all $N + 1$ nodes is governed by the power flow equations:

$$\sum_{j=0}^{N} |V_k||V_j| \big(G_{kj} cos(\theta_k - \theta_j) + B_{kj} sin(\theta_k - \theta_j) \big) - P_k = 0, \qquad (4.1)$$

$$\sum_{j=0}^{N} |V_k||V_j| \big(G_{kj} sin(\theta_k - \theta_j) - B_{kj} sin(\theta_k - \theta_j) \big) - Q_k = 0, \qquad (4.2)$$

where $|V_k|$ and θ_k are the voltage magnitude and voltage angle at node k, respectively; G_{kj} and B_{kj} are the conductance and susceptance of the electrical line connecting nodes k and j; P_k and Q_k are the net active and reactive power injections at node k.

4.2.2 Smart Inverter for Voltage Regulation

A PV inverter is a type of electrical device that converts the direct current (DC) output of a solar panel into an alternating current (AC) output, which can then be fed into the AC grid through the point of common coupling (PCC). Under the new standards/rules [13, 14, 74], PV inverters are required to contribute to grid regulation via defined smart functions; this type of PV inverter is referred to as a smart inverter (SI) hereafter. A SI supports voltage regulation by modulating active and/or reactive power at the PCC; in other words, the SI can change the P_k and/or Q_k in (4.1,4.2) if node k has a PV connection. In this way, the SI can change the voltage for node k as well as other nodes, per (4.1,4.2).

A commonly used smart function is a Volt-Var droop curve, as shown in Fig. 4.1. Six unique points specify the shape of the curve, according to which the SI will absorb or inject the corresponding amount of reactive power (var) based on the voltage at the PCC. The active power production of PV can be curtailed to make headroom for var generation if the SI reaches its capacity limit as shown in Fig. 4.2. This scheme is called Volt-Var with var priority. With a Volt-Var droop curve, every SI operates autonomously and independently (i.e. without coordination with each other) based on its local PCC voltage only. While this brings simplicity in terms of implementation, it can also lead to undesired system performance. For example, since not all nodes of the power network are equipped

with SIs, some nodes may suffer from voltage violations even under the autonomous SI dispatch scheme. Meanwhile, some SIs may use excessive reactive power due to a lack of coordination with other SIs, resulting in unnecessary PV production curtailment.
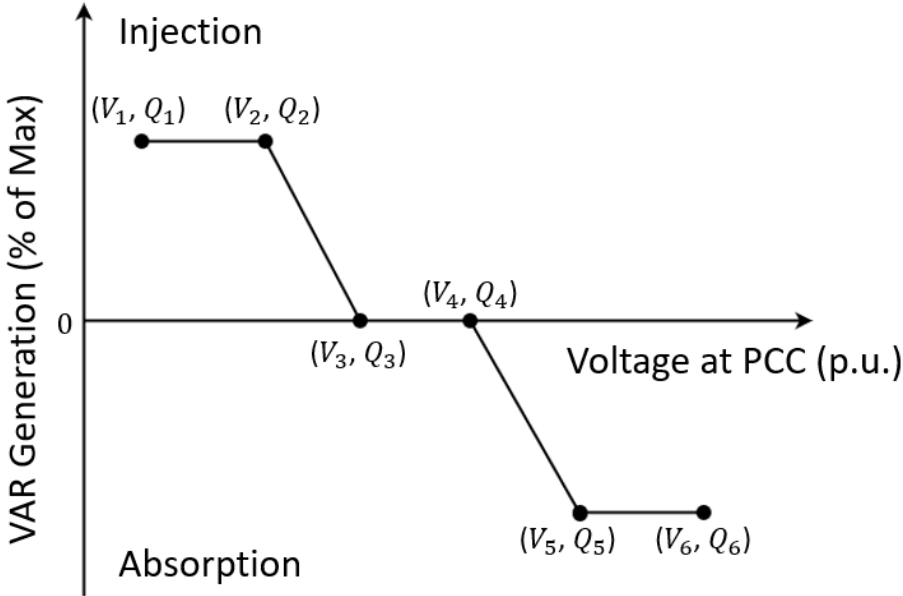
Figure 4.1: A typical Volt-Var droop curve of a smart inverter.

4.3   Problem Formulation

4.3.1   Reinforcement Learning Formulation

Reinforcement Learning

RL, especially DRL, has been shown to be capable of learning by interacting with complicated environments and achieve good performances on difficult control tasks, such as robot manipulation.
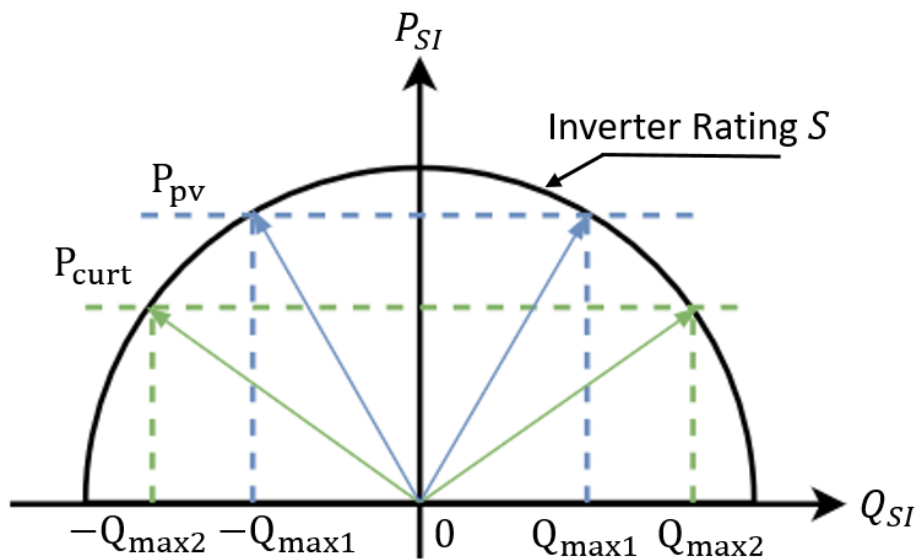
Figure 4.2: Smart inverter output curve. The complex power output of the SI is $S_{SI} = P_{SI} + iQ_{SI}$. S_{SI} is constrained by inverter rating S, meaning $P_{SI}^2 + Q_{SI}^2 \leq S^2$. P_{pv} is the available PV real power production determined by instantaneous solar irradiance, $\pm Q_{max1}$ is the corresponding maximum reactive power injection or absorption of the SI. If the real power is curtailed to P_{curt}, more headroom is made for modulating reactive power ($\pm Q_{max2}$).

The overall RL idea is presented in Fig. 4.3. An agent learns through interacting with an environment, E. At each time step, the agent receives the state of the environment s_t, takes an action a_t, and receives a scalar reward r_t. The agent learns a policy π, which maps states to a probability distribution over the actions $\pi : \mathcal{S} \to \mathcal{P}(\mathcal{A})$. This can be modeled as a Markov decision process with a state space $\mathcal{S}$, action space $\mathcal{A} = \mathbb{R}^M$, an initial state distribution $p(s_1)$, transition probability $p(s_{t+1}|s_t, a_t)$, and reward function $r(s_t, a_t)$. M is the dimension of the action space.

The agent uses the policy to explore the environment and generate states, rewards, and actions tuples, $(s_1, a_1, r_1, ..., s_t, a_t, r_t)$. The return of a state is calculated as the total discounted future reward from time step t and onwards, $R_t = \sum_{i=t}^{T} \gamma^{(i-t)} r(s_i, a_i)$, where $\gamma \in [0, 1]$ is the discount factor quantifying the importance attached to future rewards. The goal of the agent is to learn a policy that results in maximization of cumulative discounted reward from the start distribution $J = \mathbb{E}_{r_i, s_i \sim E, a_i \sim \pi}[R_1]$.

The action value function is defined as the expected total discounted reward after taking an action a_t in state s_t and thereafter following policy π:

$$Q^\pi(s_t, a_t) = \mathbb{E}_{r_{i \geq t}, s_{i \geq t} \sim E, a_{i \geq t} \sim \pi}[R_t | s_t, a_t]. \tag{4.3}$$

If the target policy is deterministic, it can be described as a function $\mu : \mathcal{S} \to \mathcal{A}$. The Bellman equation in Q-learning [83] can be expressed as:

$$Q^\mu(s_t, a_t) = \mathbb{E}_{r_t, s_{t+1} \sim E}[r_t(s_t, a_t) + \gamma Q^\mu(s_{t+1}, \mu(s_{t+1}))]. \tag{4.4}$$

Parameterizing the function approximators with θ^Q, the weights can be optimized by

minimizing the loss:

$$L(\theta^Q) = \mathbb{E}\big[(y_t - Q(s_t, a_t|\theta^Q))^2\big],\tag{4.5}$$

where $y_t = r(s_t, a_t) + \gamma Q(s_{t+1}, \mu(s_{t+1})|\theta^Q)$.

Deep Deterministic Policy Gradient Algorithm

Applying Q-learning ((4.4)) to continuous action space is problematic, as the greedy policy requires global optimization during policy improvement. The deterministic policy gradient (DPG) is more computationally tractable for problems over a continuous action space [84]. The DPG parameterizes the actor with a function $\mu(s|\theta^\mu)$. The critic $Q(s, a)$ is learned based on the Bellman equation as in Q-learning. Fig. 4.4 shows the structure of the deterministic actor critic network. The actor is updated via gradient descent to maximize the expected return from the start distribution J:

$$\nabla_{\theta^\mu} \approx \mathbb{E}[\nabla_{\theta^\mu} Q(s, a|\theta^Q)|s = s_t, a = \mu(s_t|\theta^\mu)].\tag{4.6}$$

In this paper, a similar approach is adapted from [85], which uses deep neural networks as function approximators for DPG. This approach is referred as deep deterministic policy gradient (DDPG).

4.3.2 Design DDPG Agent for Smart Inverter Coordination

The goal of a well-trained DDPG agent for SI coordination is to provide fast and effective actions for ensuring normal voltage performance and minimization of PV production curtailment. The actions are determined based on real-time measurements (states)
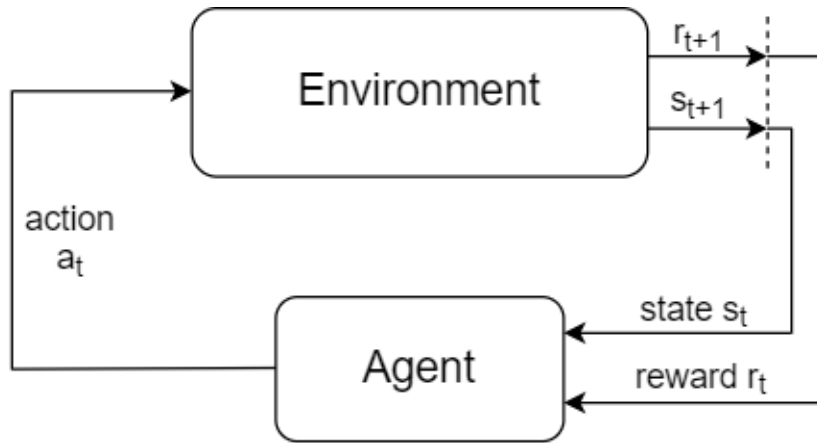
Figure 4.3: Schematic over-view of reinforcement learning.
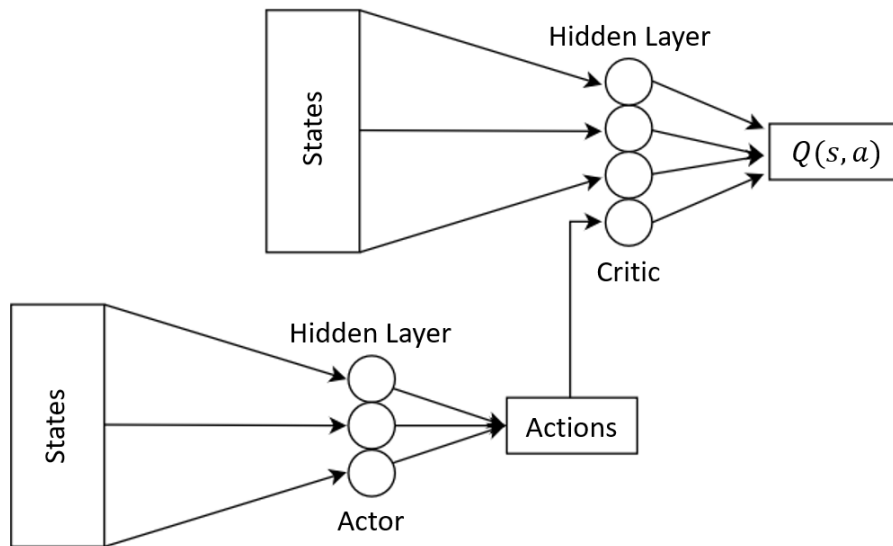
Figure 4.4: Deep deterministic policy gradient network. The actor suggest actions based on received states. The critic evaluates the actions provided the current states.

of the power grid from the supervisory control and data acquisition (SCADA) system or phasor measurement units (PMUs). In this paper, AC power flow (PF) is used to simulate the measurements from SCADA or PMUs. It is assumed that each node of the feeder is equipped with one measurement unit and PF solution information of all nodes are included as states. In the actual field application, to reduce costs, a selective group of important nodes can be chosen for measurement unit deployment.

The key concepts of episode, states, actions, and rewards are defined below:

1): Episode

The episode is a sequence of interactions between the agent and the environment in response to a specific grid condition/scenario (a combination of PV and load profiles). During an episode, the agent explores by suggesting actions and receiving resultant states and rewards until termination due to convergence or reaching the maximum number of steps. Each exploration step is also referred to as iteration.

2): State Space

The state s is defined as a vector containing power system information, including voltage magnitudes of each node as well as active and reactive power generation/consumption of PVs and loads. The state s belongs to the state space $\mathcal{S}$.

3): Action Space

SI reactive power outputs are actions. Through PV active power curtailment, each SI can adjust its reactive power output continuously from $-S$ to S (Fig. 4.2) or [-1,1] p.u. after normalization.

The action space $\mathcal{A}$ is spanned by action combinations of all SIs.

4): Reward

When applying RL to control, the reward scheme needs to be carefully designed to achieve proper system performance. Since the objectives are to mitigate voltage violations and minimize PV generation curtailment, the reward scheme is composed of two parts: (i) A large penalty for violating voltage limits; and (ii) a negative reward proportional to total reactive power dispatched by SIs. The reward associated with total reactive power is used to achieve regulation for both day time (possible curtailment) and night time (no curtailment).

The first part of the reward is assigned according to the voltage profiles. To differentiate voltage profiles, several voltage operation zones are defined (Fig. 4.5): a normal zone (0.95 - 1.05) p.u., a violation zone 1 (0.9 - 0.95 or 1.05 - 1.1) p.u., and a violation zone 2 (< 0.9 or > 1.1) p.u.. These zones are defined according to the grid operation limits in ANSI standards [7]. Assuming $|V_k|_{norm} = \frac{|V_k|}{V_k^{nom}}$ is the normalized voltage magnitude at node k, where $|V_k|$ is the voltage magnitude at node k and V_k^{nom} is the nominal voltage of node k. The voltage reward associated with $|V_k|_{norm}$ for node k in the jth iteration is:

$$
R_V(j,k) = \begin{cases} 0, & \text{if } |V_k|_{norm} \in \text{normal zone} \\ Penalty_1 & \text{if } |V_k|_{norm} \in \text{violation zone 1} \\ Penalty_2, & \text{if } |V_k|_{norm} \in \text{violation zone 2.} \end{cases} \tag{4.7}
$$

In other words, the corresponding voltage reward is zero if the node voltage is in the normal zone, and large penalties (i.e. negative rewards) will be assigned if the node

voltage is out of the operation limits.
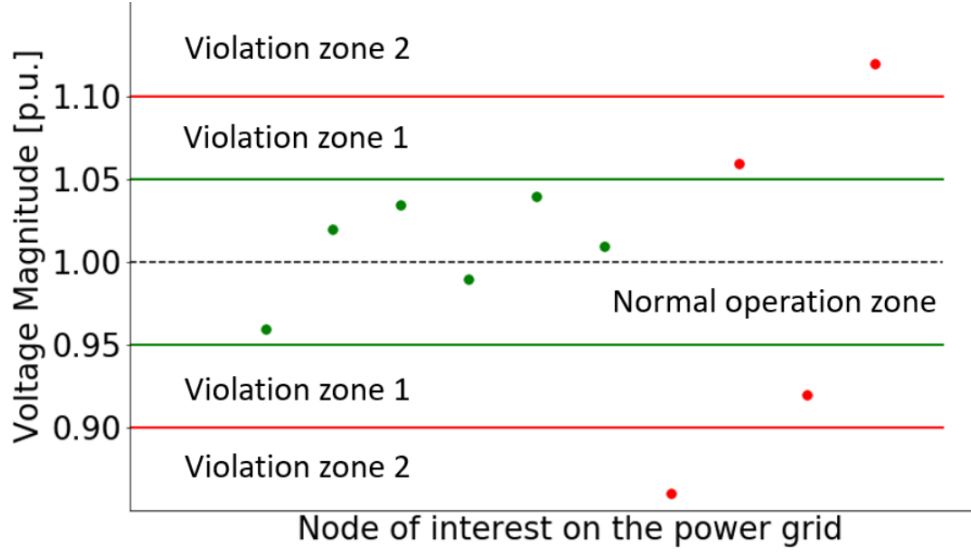
Figure 4.5: Definition of voltage profile zones. Each dot represents voltage of one node. The corresponding total voltage reward for this example is $2 \times Penalty_1 + 2 \times Penalty_2$.

The second part of the reward is assigned based on reactive power utilization. The objective is to minimize PV production curtailment, which is achieved by minimizing reactive power utilization. The reward for reactive power utilization is defined as:

$$R_Q(j) = \sum_{i=1}^{M} C \times (1 - q_i), \tag{4.8}$$

where $q_i = |Q_i|/S_i$ is the reactive power utilization ratio of the ith SI (i.e. the absolute value of action for the SI); M is the total number of SIs; C is a positive constant chosen to scale the reward. The value of C must be tuned to fit different power system configurations for desirable performance. The total reward for j^{th} iteration/exploration step of the episode is:

$$R(j) = \sum_{k=0}^{N} R_V(j, k) + R_Q(j), \tag{4.9}$$

where $\{0, ..., N\}$ are the indexes for all nodes.

4.3.3   Training of DDPG

DDPG is trained according to the procedures displayed in Fig. 4.6 with the following key steps:

Step 1: Initialize and solve power flow and assemble state vector: At the beginning of one episode, a new grid operation condition (a combination of PV and load profiles) is randomly generated. The PF is solved to obtain the system information and assemble the state vector. The PF is performed by the AC power flow solver OpenDSS [2], which takes in load consumption and PV generation, solves the corresponding PF equations (4.1,4.2), and finds voltages at each node.

Step 2: DDPG agent suggests actions: The state vector containing the system information (node voltage, active and reactive power consumption/generation of SIs and loads) is fed into the DDPG agent. The agent suggests actions, which are reactive power outputs of SIs.

Step 3: Execute actions and evaluate rewards: The environment (the SI in OpenDSS) take the suggested actions, producing the resultant state by solving another PF. The corresponding reward for that state is evaluated. If the termination criteria defined below are met, the training for this episode is terminated and the trained DDPG is stored for later use. If the termination criteria is not met, we return to **Step 2**, update the agent policy, and repeat the process until the termination is reached.

The training for one episode terminates if: 1) the reward for the exploration/iteration step converges, meaning the reward difference between current iteration and last iteration

is within 0.5% of highest reward in theory ($C \times M$ according to (4.9), i.e. the reward if agent uses zero reactive power and there are no voltage violations) for five consecutive iterations (the convergence is not checked until 200 iterations are performed for each episode, i.e. each episode runs at least 200 iterations); or 2) the maximum number of iterations (1000) is reached.

4.3.4 Optimal Power Flow Formulation

To benchmark the performance of the DDPG approach, an equivalent OPF problem is formulated and solved. Since the goal is to minimize reactive power usage and subsequently PV generation curtailment, the OPF objective is defined as follows:

$$\min \qquad \sum_{i=1}^{M} (-P_i^{\text{pv}} + wQ_i^{\text{pv}}), \qquad (4.10)$$

where M is the total number of PVs/SIs, P_i^{pv} is the PV active power production, Q_i^{pv} is the reactive power generation, and w is a weighting factor. As shown in Fig. 4.1, the constraint for every SI is: $(P_i^{\text{pv}})^2 + (Q_i^{\text{pv}})^2 <= S_i^2$, where S_i is the SI power rating.

The current mismatch equations are used to relate nodal voltage with active and reactive power injections from each load and PV unit. The current mismatch equations are [86]:

$$\Delta I_k = I_k^{\text{calc}} - I_k^{\text{sp}}, \qquad (4.11)$$
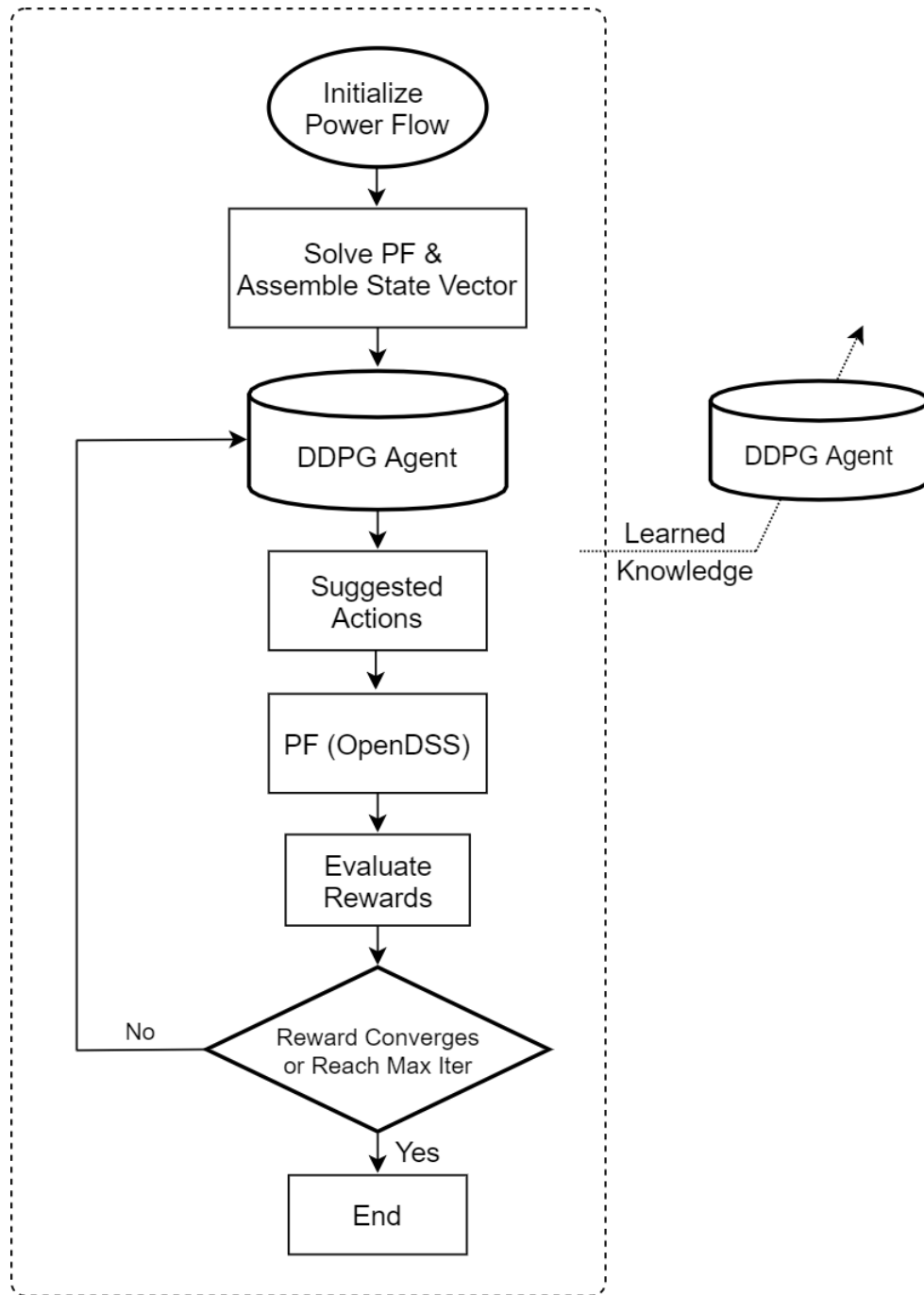
Figure 4.6: Flowchart of training a DDPG agent.

$$P_k^{\text{sp}} = \text{Re}(V_k)\,\text{Re}(I_k^{sp}) + \text{Im}(V_k)\,\text{Im}(I_k^{sp}), \tag{4.12}$$

$$Q_k^{\text{sp}} = \text{Im}(V_k)\,\text{Re}(I_k^{sp}) - \text{Re}(V_k)\,\text{Im}(I_k)^{sp}, \tag{4.13}$$

$$\text{Re}(I_k^{\text{calc}}) = \sum_{j=1}^{N}[G_{ki}\,\text{Re}(V_i) - B_{ki}\,\text{Im}(V_i)], \tag{4.14}$$

$$\text{Im}(I_k^{\text{calc}}) = \sum_{j=1}^{N}[G_{ki}\,\text{Im}(V_i) + B_{ki}\,\text{Re}(V_i)], \tag{4.15}$$

where ΔI_k is the mismatch between the calculated current injection I_k^{calc} and the specified current injection I_k^{sp} at node k, V_k and I_k are the voltage phasor (complex) and current phasor, respectively, P_k^{sp} and Q_k^{sp} are the specified active and reactive power injection for node k, and G_{ki} and the B_{ki} are the conductance and susceptance from the nodal admittance matrix.

The specified nodal active and reactive power injections at node k are defined by:

$$P_k^{sp} = P_k^{pv} - P_k^{l}, \tag{4.16}$$

$$Q_k^{sp} = Q_k^{pv} - Q_k^{l}, \tag{4.17}$$

where P_k^{pv} is the PV active power injection; P_k^{l} is the load active power consumption; Q_k^{pv} is the PV reactive power injection, and Q_k^{l} is the load reactive power consumption.

The basis of the OPF formulation is to force the current mismatches from (4.11) to equal zero; i.e. the following constraint is imposed:

$$\Delta I_k = 0. \tag{4.18}$$

The source bus is modeled as a slack bus by constraining its voltage magnitude and angle

Table 4.1: Properties of modified IEEE 37 bus feeder.

# of Nodes	37
Peak Load (MVA)	2.74
# of Loads	25
# of PVs	5
DC Rating of PVs (MW)	6
AC Rating of SIs (MVA)	5

to be constants determined by the voltage at the primary side of substation:

$$V_{\text{slack}} = V_{\text{slack}}^{\text{sp}}. \tag{4.19}$$

The voltage constraints at the other nodes are the [0.95, 1.05] p.u. ANSI limits [7]:

$$0.95 \leq \frac{|V_k|}{V_k^{\text{nom}}} \leq 1.05, \tag{4.20}$$

where V_k^{nom} is the nominal voltage of node k. After solving the OPF problem, the decision values (P^{pv}, Q^{pv}) are used to dispatch SIs.

4.4 Case Study

4.4.1 Case Study

The proposed DDPG agent is tested on the modified IEEE 37 bus feeder and modified IEEE 123 bus feeder. The properties of the IEEE 37 bus feeder are summarized in Table 4.1. There are 25 loads with a peak load of 2.74 MVA. Five 1.2 MW PVs are

Table 4.2: Summary of Different Control Strategies.

	SI Reactive Power Generation	SI Dispatch Scheme
No Control	No	N/A
Volt Var	Yes	local droop curve (Fig. 4.1)
OPF	Yes	coordinated by OPF solution
DDPG	Yes	coordinated by DDPG agent

randomly deployed, the AC rating of each SI is 1 MWA assuming 20% oversizing of solar array [87]. The resultant PV penetration is around 180%. The IEEE 123 bus feeder (Table 4.3) contains 85 loads with a peak demand of 7.7 MVA. Ten 1.2 MW PVs (each PV is equipped with 1 MVA SI) are added at randomly selected locations, achieving 130% PV penetration.

Four different control strategies are tested (Table 4.2): 1) **No Control**: The SI operates at unity power factor without any reactive power generation. 2) **Volt-Var**: Each SI operates autonomously according to the pre-specified local droop curve (Fig. 4.1) without coordination. 3) **OPF**: All SIs cooperate following the optimal solutions of the OPF problem ((4.10)). 4) **DDPG**: SIs are coordinated following the decisions made by the trained DDPG agent, as described in Section 4.3.

4.4.2 DDPG Agent Training Result

The training of the DDPG agent is performed following the procedures shown in Fig. 4.6. In the training stage, combinations of PV generation and load consumption are

randomly generated to present a mix of grid operation conditions/scenarios with low to high loading and PV generation.

Training is performed for 1,500 episodes for the IEEE 37 bus feeder case with 500,000 number of iterations in total (i.e. each episode terminates after approximately 330 iterations, on average). There are 245,310 parameters in total for the neural networks used for the IEEE 37 bus feeder case. The IEEE 123 bus case is trained for 800 episodes with around 387,000 iterations (i.e. each episode terminates/converges after 484 iterations, on average). Due to the larger and more powerful neural networks (874,820 parameters in total) used for the IEEE 123 bus case, the IEEE 123 bus requires less iterations/data samples to learn a good policy.

The training reward of 5 random experiments for the IEEE 123 bus case is plotted in Fig. 4.7. The reward R is normalized by the highest possible reward $C \times M$, therefore the reward upper limit here is 1. The reward starts at negative values, given that the grid experiences a large number of voltage violations and the DDPG agent has no prior knowledge on how to perform grid voltage regulation. The DDPG obtains an average reward greater than 0.8 after just 150 episodes, showing that the agent is learning efficiently. As learning progresses further after episode 150, the average rewards remains greater than 0.5 and almost always greater than 0.8 with small swings across different episodes. The episode reward fluctuations are due to differences in grid operation conditions for each episode. Since the grid operation condition/scenario is randomly generated for each episode, some episodes experience grid operation conditions with more violations. Since voltage violations occur in the beginning of these episodes and more reactive power

needs to be used to correct voltage violations, lower average episode rewards result.

The trained DDPG agent is used to perform grid voltage control for one year with 1 hour resolution (8760 different scenarios). To test the robustness of a DDPG that was trained solely on randomly generated episodes, online training is not applied. In other words, reward feedbacks after taking the suggested actions are not used to retrain and improve the DDPG agent during the test. Therefore, the DDPG agent makes decision solely based on the past experiences learned during the training phase. Contrary to the iterative process in the training stage, where the DDPG could iterate many times to reach an action with a high reward, in the test stage the agent has to provide effective actions within one iteration. The PV generation and load consumption profiles for the test are plotted in Fig. 4.8.
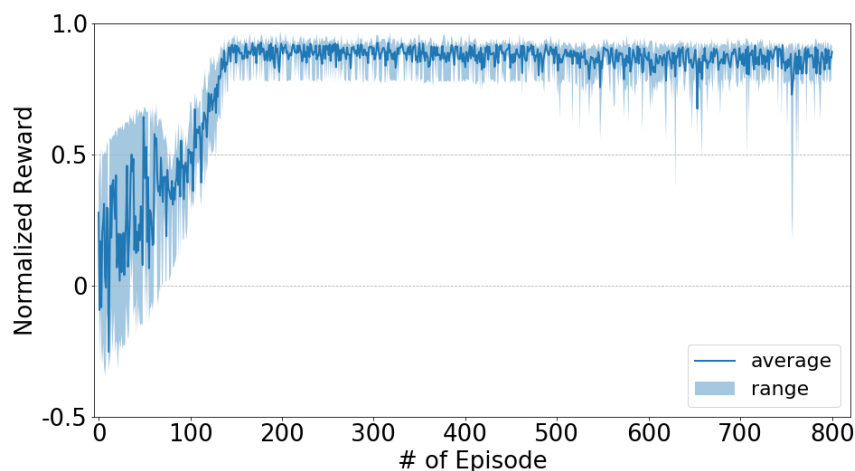
Figure 4.7: Reward during training process for the IEEE 123 bus feeder. The dark blue line represents the average reward of 5 experiments with different random seeds, and the shaded light blue area display the range of episode average reward (average of rewards of all iterations in the episode) of those 5 experiments.

Table 4.3: Properties of modified IEEE 123 Bus feeder.

# of Nodes	128
Peak Load (MVA)	7.7
# of Loads	85
# of PVs	10
DC Rating of PVs (MW)	12
AC Rating of SIs (MVA)	10
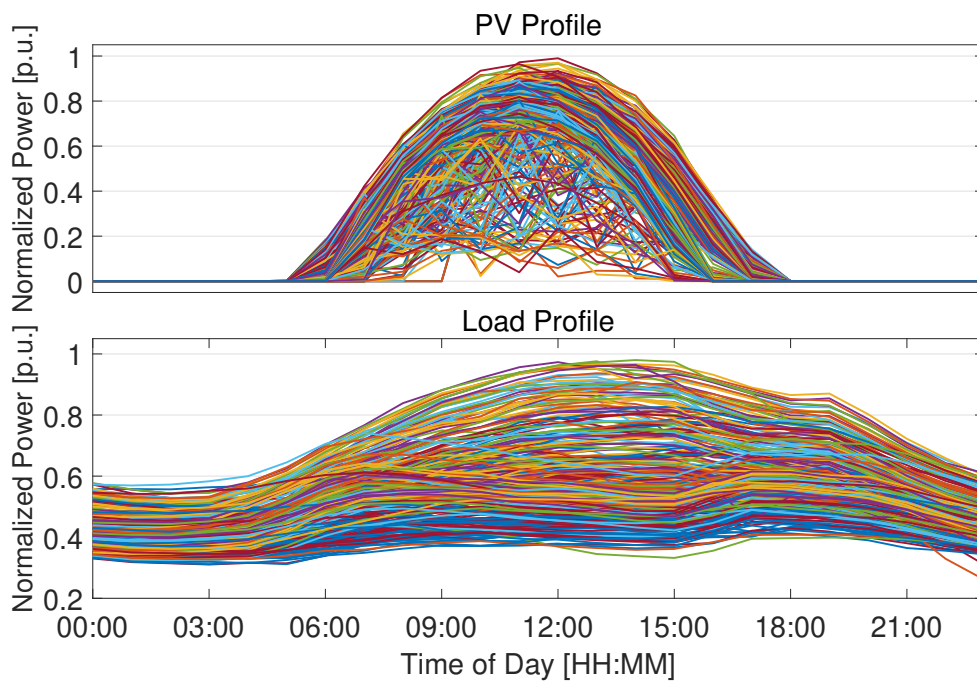
Figure 4.8: Normalized PV (top) and load (bottom) profiles used for tests. The PV generation profile is from public solar power datesets maintained by NREL [6]. The load profile is from the OpenDSS installation directory [2]. Single profile is used for all PVs and loads. 1 year (365 days) profiles are plotted here.

4.5   Results and Discussion

4.5.1   IEEE 37 Bus Feeder

Table 4.4: Summary of test results for IEEE 37 bus feeder. The value shown is the cumulative quantity of each parameter for 1 year.

	# of Under-voltages	# of Over-voltages	Max Volt [p.u.]	Min Volt [p.u.]	PV Curtailment (kWh)
No Control	1,797	6,998	1.067	0.921	0
Volt Var	0	0	1.040	0.966	15,252
OPF	0	0	1.050	0.950	1,291
DDPG	0	0	1.046	0.961	1,854

The node voltages of the IEEE 37 bus feeder are presented in Fig. 4.9. For the no control case (i.e. no reactive power generation from PVs), the feeder experiences both over-voltages and under-voltages. The total number of over-voltage violations, where one node voltage out of ANSI limits at any time step (a new scenario is applied at each time step) counts as one violation, is 6998 with the maximum voltage equaling to 1.0673 p.u. (Table 4.4). The total under-voltage occurrence is 1797 with a minimum voltage of 0.921 p.u.. With Volt-Var droop control (Fig. 4.1), all voltage violations are mitigated. The maximum voltage is brought down to 1.040 p.u. while the minimum voltage is increased to 0.966 p.u.. The OPF also eliminates all voltage violations. The maximum voltage and minimum voltage are 1.050 and 0.950 p.u., respectively, reflecting the voltage constraints imposed in (4.20). The proposed DDPG also solves all voltage issues, reducing the maxi-

mum voltage to 1.046 p.u. while boosting the minimum voltage to 0.961 p.u.. The results demonstrate that a DDPG agent is not only effective in voltage regulation but also robust in various operation conditions.

Reactive power generation by SIs to resolve voltage issues could lead to PV production curtailment due to the capacity limit as shown in Fig. 4.2. The normalized total PV curtailments due to reactive power utilization are plotted in Fig. 4.10. Since reactive power usage is prohibited in the no control case, the corresponding curtailment is always zero. For the Volt-Var, OPF, and DDPG cases, the active power of the SI needs to be curtailed to make room for reactive power generation. However, OPF and DDPG coordinate different SIs for voltage regulation, ensuring that reactive power is used more efficiently and less curtailment is incurred in comparison to Volt-Var. Relative to the Volt-Var case, DDPG reduces the curtailment by 88% (from Volt-Var 15,252 to DDPG 1,854 kWh) while OPF provides the optimal solution of most efficiently dispatching reactive power for voltage regulation and reduces the curtailment by 92% (from Volt-Var 15,252 to OPF 1,291 kWh). The difference in curtailment between DDPG and OPF is only 563 kWh for the 1 year test period, i.e. only 1.54 kWh per day. Therefore, DDPG approaches the optimal solution in minimizing reactive power to resolve voltage issues.

The non-linear and non-convex nature of the OPF problem renders it computationally intensive, limiting its practical application. On the contrary, a trained DDPG agent can map grid state information directly to SI actions, which requires only one feed-forward step of the neural network and is extremely efficient. Table 4.5 compares the mean solution time of both the OPF and DDPG methods. The solution time is the mean value of

Table 4.5: Solution time comparison on the IEEE 37 bus feeder.

Method	OPF	DDPG
Solution Time (s)	27.6	1.5×10^{-3}

solving 8760 different scenarios. For OPF, this is the time needed to solve the optimization problem. For DDPG, this is the time the DDPG agent takes to make decisions on SI actions after receiving grid state information. The solution time is not shown the Volt-Var method, as it is an autonomous local control scheme that acts essentially instantaneously.

The simulations are carried out on a PC with Intel (R) Core(TM) i7-4700MQ 2.8-GHz processor using Python 3.7. The OPF is formulated and solved using the KNITRO solver [88] with Pyomo interface [89]. The DDPG averages only 1.5 ms (CPU time) to make decisions while the OPF needs 27.6 s (CPU time) to get the solution (Table 4.5).

4.5.2 IEEE 123 Bus Feeder

Table 4.6: Summary of test results for IEEE 123 bus feeder. The value shown is the cumulative quantity of each parameter for 1 year.

	# of Under-voltages	# of Over-voltages	Max Volt [p.u.]	Min Volt [p.u.]	PV Curtailment (kWh)
No Control	7,832	19,865	1.066	0.906	0
Volt Var	100	0	1.040	0.946	58,703
DDPG	0	0	1.497	0.9503	7,277

The proposed DDPG is also tested on the larger IEEE 123 bus feeder. Since

Figure 4.9: Boxplot of node voltages of the 1 year test with 8760 scenarios on the IEEE 37 bus test feeder. For each case, the boxplot contains voltages of all nodes of all 8760 test scenarios (324,120 data points). Red dashed lines represent the [0.95,1.05] p.u. ANSI limits [7].
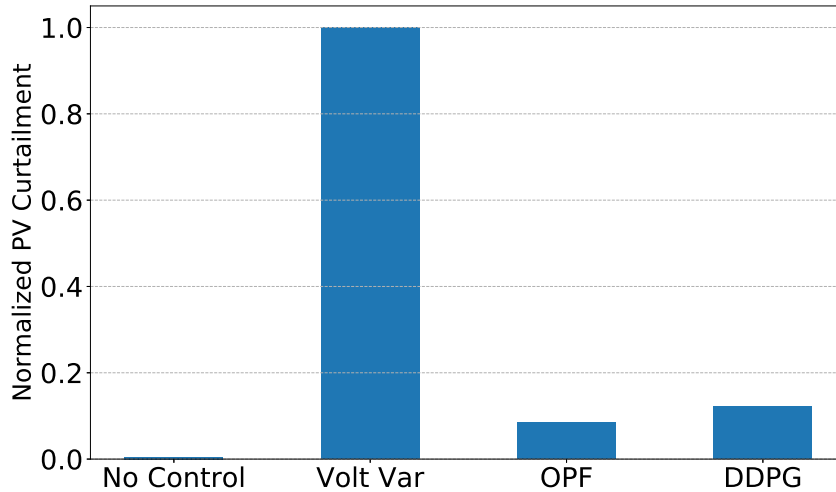
Figure 4.10: Normalized total energy curtailed during the 1 year test with 8760 scenarios for four different control cases on the IEEE 37 bus feeder. The energy curtailed is normalized with the energy curtailed of the Volt-Var case. The PV curtailment here is defined as the PV active power generation deficit between no control case (no reactive power utilization) and the other three cases (with reactive power generation), providing a direct comparison of Volt-Var, OPF, and DDPG on effective usage of SI reactive power.

107

academic license of the KNITRO [88] solver is limited to 300 variables and 300 constraints, the OPF is not compared here.

Fig. 4.11 displays nodal voltage distributions of the three remaining cases. Numerous voltage violations can be observed for no control case with a maximum voltage of 1.066 p.u. and a minimum voltage of 0.906 p.u.. There are 19,865 over-voltage and 7,832 under-voltage occurrences for the no control case (Table 4.6). The autonomous Volt-Var control eliminates all over-voltages, reducing the maximum voltage to 1.040 p.u.. However, there are still 100 under-voltages (Table 4.6) and the minimum voltage is 0.946 p.u.. With the proposed DDPG control, all voltage violations are resolved: the maximum voltage observed is 1.0497 p.u. and the minimum voltage is 0.9503 p.u.. The DDPG agent successfully learned a delicate strategy to utilize the minimal amount of reactive power to keep the voltage just within the ANSI limits. This demonstrates that imposing voltage "constraints" through large voltage violation penalties (Section 4.3.2) is an effective strategy to enforce voltage limits.

The curtailment of PV production due to reactive power utilization is displayed in Fig. 4.12. Since DDPG coordinates different SIs to utilize reactive power more efficiently, much less curtailment is incurred in comparison to the Volt-Var case. The total energy curtailed for the DDPG case represents a 88% reduction in curtailment (from Volt-Var 58,703 to DDPG 7,277 kWh, as shown in Table 4.6).

The average decision making time of the DDPG on the IEEE 123 bus feeder is 1.6×10^{-3} s (CPU time), which is almost the same as for the IEEE 37 bus feeder. This again demonstrates the solution speed advantage of the DDPG approach.
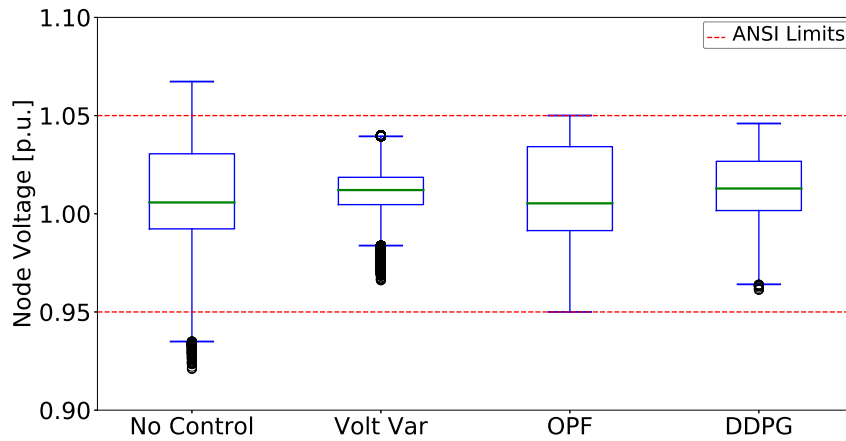
Figure 4.11: Boxplot of node voltages of 1 year test with 8760 scenarios on the IEEE 123 bus feeder. For each case, the boxplot consists of voltages of all nodes of all 8760 test scenarios (1,121,280 data points). Red dashed lines represent the [0.95,1.05] p.u. ANSI limits [7].
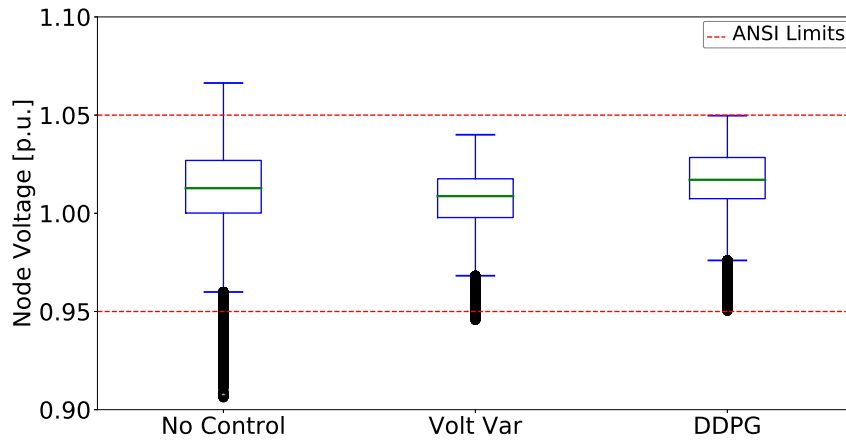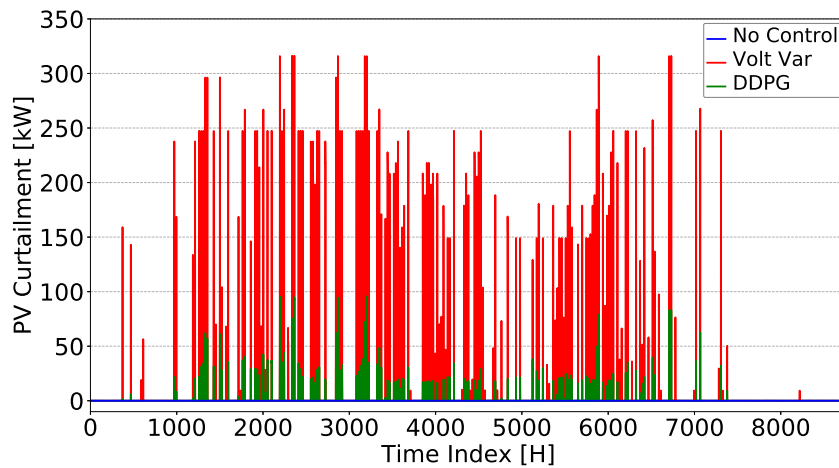

Figure 4.12: Total PV generation curtailment of each scenario/step of three different cases for the IEEE 123 bus feeder.

4.6 Conclusion

In this paper, a DDPG-based method is proposed to coordinate multiple SIs for distribution grid voltage regulation. Comprehensive tests with thousands of realistic scenarios are conducted on the IEEE 37 bus feeder and the IEEE 123 bus feeder to evaluate the trained DDPG agents. The proposed DDPG approach is compared against autonomous Volt-Var control and OPF. The results demonstrate that even without online reward feedbacks, a well-trained DDPG agent can use solely the knowledge accumulated in the training phase to make robust decisions under various operation conditions. As DDPG can coordinate different SIs, it is more effective in mitigating voltage issues with much less reactive power compared to autonomous Volt-Var control, achieving significant reduction in PV production curtailment. The decisions from DDPG are as effective as the optimal solutions from OPF in terms of resolving voltage problems; however, the DDPG results in a marginal increase in PV curtailment due to slightly more reactive power usage.

The OPF approach relies on accurate forecasting of future conditions, due to its large computation time, which would significantly increase for larger networks. While this paper assumes perfect forecasts for the OPF, forecast errors in actual applications can lead to performance deterioration for OPF including a failure to maintain ANSI voltage limits. On the contrary, (assuming fast communications), the DDPG is independent of forecasts, as it is capable of reaching decisions instantaneously.

The text and data in Chapter 4, in full, is submitted to *Journal of Renewable and Sustainable Energy* under the title Data-Driven Online PV Smart Inverter Coordination

using Deep Reinforcement Learning, Li, C., Chen, Y., Jin, C., Sharma, R., Kelissl, J.. The dissertation author is the primary investigator and author of this article.

Chapter 5

Conclusions and Future Work

5.1   Conclusions

In this dissertation, we focus on coordinated voltage regulation of distribution networks to facilitate high solar penetrations. Chapter 2 presented a novel way for coordination of multiple OLTCs via optimization. The optimization is formulated for selective critical buses to reduce problem size. Linearization techniques are proposed to remove non-linearities to speed-up the solution. Comprehensive simulations are carried out on two real California utility feeders using solar profiles at high temporal and spatial resolution. Results show that the proposed coordinated strategy can enable 67% more PV capacity compared to conventional autonomous OLTC control. Voltage estimates from the linearized equations are accurate with a maximum error of $O(10^{-3})$ p.u.. Results show that the proposed coordination method obtains solutions on operational time scales (below 30 s). The proposed method achieves voltage objectives while minimizing OLTC tap

operations, extending the lifespan of the OLTC.

Chapter 3 described coordinated voltage control with legacy OLTCs and emerging PV SIs, extending the method in Chapter 2. A set of linearization techniques are introduced to relax non-linear constraints in the optimization. The proposed method is validated on the IEEE 37 bus feeder and a large California utility feeder. Voltage violations are mitigated, voltage unbalance across phases is reduced, and unnecessary tap operations are avoided. Robustness is also validated against up to 30% forecast errors. The computational efficiency of the proposed approach is superior to prior methods.

Chapter 4 proposed a data-driven framework for SI coordination using deep reinforcement learning (DRL). The proposed DRL approach is compared with autonomous Volt-Var SI control and OPF solutions. Results show the proposed DRL can performs nearly as well as OPF, effectively mitigating all voltage violations and significantly reduce PV curtailments comparing to autonomous Volt-Var control. However, the DRL is a thousand times faster than OPF, enabling instantaneous SI coordination using real-time measurements rather than load and PV forecasts. Meanwhile, OPF is prone to performance deterioration with forecasting errors.

5.2 Future Work

In this dissertation, we focus on distribution network voltage regulation at "normal" states far away from critical points and around operation limits where the system is insensitive to perturbations and far from the point of voltage collapse (PoVC) (Fig. 5.1).
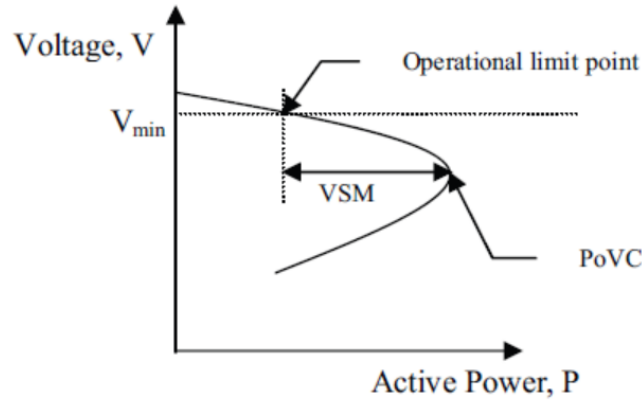
Figure 5.1: P-V nose curve.

However, the operation point could drift toward the sensitive edge of the nose curve during contingency situations [90], which could lead to increase of the error introduced by the linearization approximation applied in Chapter 2 and Chapter 3. Validating the performances within sensitive operation regions considering voltage stability could be an interesting extension of the current works in Chapter 2 & 3. , it would be worthwhile to validate the optimality gap resulting from the voltage approximation errors from the linearization compared to the optimization formulation without linearization.

In both Chapter 2 and 3, deterministic optimization is used to solve for optimal decisions without considering the stochastic nature of renewable solar generation and load uncertainties. On the contrary, chance-constrained stochastic optimization captures the probability of various scenarios and ensures balanced performances considering probabilistic load and PV forecasts [91, 92, 93], which is left for future work.

Optimization based methods requires accurate distribution network models, which are not necessarily available for distribution networks due to incorrect data for line param-

eters or network resistance variations from temperature changes [34]. Inaccurate distribution network models could cause suboptimal or even detrimental decisions. The work in Chapters 2 and 3 could be extended using robust optimization, which incorporates model uncertainties. However, as optimizations considering model uncertainties further increase computational costs [34], approaches to reduce the solution time should also be explored.

While the data-driven approach in Chapter 4 does not require distribution network parameters as inputs of the neural network, model uncertainties of distribution networks can have negative effects for reinforcement learning as well. That is because accurate distribution network models can generate high quality training data for offline training. To counter potential model uncertainties/mismatches and make the agent robust against errors, adversary training can be performed by adding model disturbances during the training phase [94].

A single DDPG agent is used to control all SIs in Chapter 4, which could give rise to scalability issues for large distribution networks due to increased state and action dimensions. Multi-agent reinforcement learning like multi-agent deep deterministic policy gradient (MADDPG) [95] could help to address this issue. In a multi-agent setup, multiple agents could coordinate to dispatch all SIs and each agent only needs to be responsible for one portion/cluster of SIs, reducing dimension and difficulty of the problem for each agent. Clusters of different SIs could be formed according to geographic locations [82].

Morever, standard DDPG may suffer from extrapolation error, errorneous estimate of action-value $Q(s, a)$ for unseen state-action pairs, due to mismatch in distribution of data induced by the policy and the distribution of data contained in the batch/finite

historical operation datasets [96, 97]. Batch-constrained reinforcement learning (BCRL) can be formulated to deal with the extrapolation error issue, which restricts the action space to force the agent towards to the policy generating the historical operational data.

Bibliography

[1] Growth of photovoltaics. [Online]. Available: https://en.wikipedia.org/wiki/Growth_of_photovoltaics#cite_note-epia-2016-1

[2] R. C. Dugan, "Reference guide: The open distribution system simulator (opendss)," *Electric Power Research Institute, Inc*, 2012.

[3] M. Grant and S. Boyd, "CVX: Matlab software for disciplined convex programming, version 2.1," http://cvxr.com/cvx, Mar. 2014.

[4] Gurobi Optimization LLC, "Gurobi optimizer reference manual," 2018. [Online]. Available: http://www.gurobi.com

[5] California Public Utilities Commission *et al.*, "Recommendations for updating the technical requirements for inverters in distributed energy resources, smart inverter working group recommendations," 2014.

[6] GE Energy, "Western wind and solar integration study," No. NREL/SR-550-47434. National Renewable Energy Lab.(NREL), Golden, CO (United States), Tech. Rep., 2010.

[7] "American national standard for electric power systems and equipment-voltage ratings (60 hertz)," *ANSI std. C84. 1-2011*, 2011.

[8] M. M. Othman, M. H. Ahmed, and M. M. Salama, "A coordinated real-time voltage control approach for increasing the penetration of distributed generation," *IEEE Systems Journal*, 2019.

[9] S. S. Guggilam, E. Dall'Anese, Y. C. Chen, S. V. Dhople, and G. B. Giannakis, "Scalable optimization methods for distribution networks with high pv integration." *IEEE Trans. Smart Grid*, vol. 7, no. 4, pp. 2061–2070, 2016.

[10] T. A. Short, *Electric power distribution handbook*. CRC press, 2014.

[11] M. Baran and F. F. Wu, "Optimal sizing of capacitors placed on a radial distribution system," *IEEE Transactions on power Delivery*, vol. 4, no. 1, pp. 735–743, 1989.

[12] R. Yan, B. Marais, and T. K. Saha, "Impacts of residential photovoltaic power fluctuation on on-load tap changer operation and a solution using dstatcom," *Electric Power Systems Research*, vol. 111, pp. 185–193, 2014.

[13] "Ieee standard for interconnection and interoperability of distributed energy resources with associated electric power systems interfaces," *IEEE Std 1547–2018*, 2018.

[14] California Public Utilities Commission *et al.*, "Rule 21 interconnection," 2018.

[15] M. Stifter, B. Bletterie, H. Brunner, D. Burnier, H. Sawsan, F. Andren, R. Schwalbe, A. Abart, R. Nenning, F. Herb, and R. Pointner, "DG DemoNet validation: Voltage control from simulation to field test," in *2011 2nd IEEE PES International Conference and Exhibition on Innovative Smart Grid Technologies*. IEEE, Dec. 2011.

[16] X. Liu, A. Aichhorn, L. Liu, and H. Li, "Coordinated control of distributed energy storage system with tap changer transformers for voltage rise mitigation under high photovoltaic penetration," *IEEE Transactions on Smart Grid*, vol. 3, no. 2, pp. 897–906, 2012.

[17] T.-T. Ku, C.-H. Lin, C.-S. Chen, and C.-T. Hsu, "Coordination of transformer on-load tap changer and pv smart inverters for voltage control of distribution feeders," *IEEE Transactions on Industry Applications*, vol. 55, no. 1, pp. 256–264, 2018.

[18] A. T. Procopiou and L. F. Ochoa, "Voltage control in PV-rich LV networks without remote monitoring," *IEEE Trans. on Power Syst.*, pp. 1–1, 2016.

[19] H. M. Maruf and B. H. C. Energy, "Impact of smart inverter functions on dynamic step voltage regulator settings for distribution voltage control," in *2019 IEEE Milan PowerTech*. IEEE, 2019, pp. 1–6.

[20] T. Senjyu, Y. Miyazato, A. Yona, N. Urasaki, and T. Funabashi, "Optimal distribution voltage control and coordination with distributed generation," *IEEE Trans. on Power Del.*, vol. 23, no. 2, pp. 1236–1242, Apr. 2008.

[21] N. Daratha, B. Das, and J. Sharma, "Coordination between OLTC and SVC for voltage regulation in unbalanced distribution system distributed generation," *IEEE Trans. on Power Syst.*, vol. 29, no. 1, pp. 289–299, Jan. 2014.

[22] ——, "Robust voltage regulation in unbalanced radial distribution system under uncertainty of distributed generation and loads," *International Journal of Electrical Power & Energy Systems*, vol. 73, pp. 516–527, Dec. 2015.

[23] A. Nguyen, M. Velay, J. Schoene, V. Zheglov, B. Kurtz, K. Murray, B. Torre, and J. Kleissl, "High PV penetration impacts on five local distribution networks using high resolution solar resource assessment with sky imager and quasi-steady state distribution system simulations," *Solar Energy*, vol. 132, pp. 221–235, Jul 2016.

[24] M. Kraiczy, T. Stetz, and M. Braun, "Parallel operation of transformers with on load tap changer and photovoltaic systems with reactive power control," *IEEE Transactions on Smart Grid*, vol. 9, no. 6, pp. 6419–6428, 2017.

[25] M. Farivar, R. Neal, C. Clarke, and S. Low, "Optimal inverter var control in distribution systems with high pv penetration," in *2012 IEEE Power and Energy Society general meeting.* IEEE, 2012, pp. 1–7.

[26] E. Dall'Anese, S. V. Dhople, and G. B. Giannakis, "Optimal dispatch of photovoltaic inverters in residential distribution systems," *IEEE Transactions on Sustainable Energy*, vol. 5, no. 2, pp. 487–497, apr 2014. [Online]. Available: https://doi.org/10.1109/tste.2013.2292828

[27] E. Dall'Anese, H. Zhu, and G. B. Giannakis, "Distributed optimal power flow for smart microgrids," *IEEE Transactions on Smart Grid*, vol. 4, no. 3, pp. 1464–1475, 2013.

[28] P. Šulc, S. Backhaus, and M. Chertkov, "Optimal distributed control of reactive power via the alternating direction method of multipliers," *IEEE Transactions on Energy Conversion*, vol. 29, no. 4, pp. 968–977, 2014.

[29] K. Christakou, J.-Y. LeBoudec, M. Paolone, and D.-C. Tomozei, "Efficient computation of sensitivity coefficients of node voltages and line currents in unbalanced radial electrical distribution networks," *IEEE Transactions on Smart Grid*, vol. 4, no. 2, pp. 741–750, jun 2013. [Online]. Available: https://doi.org/10.1109/tsg.2012.2221751

[30] A. Borghetti, M. Bosetti, S. Grillo, S. Massucco, C. A. Nucci, M. Paolone, and F. Silvestro, "Short-term scheduling and control of active distribution systems with high penetration of renewable resources," *IEEE Systems Journal*, vol. 4, no. 3, pp. 313–322, 2010.

[31] Q. Nguyen, H. V. Padullaparti, K.-W. Lao, S. Santoso, X. Ke, and N. Samaan, "Exact optimal power dispatch in unbalanced distribution systems with high pv penetration," *IEEE Transactions on Power Systems*, vol. 34, no. 1, pp. 718–728, 2018.

[32] F. Capitanescu and L. Wehenkel, "Experiments with the interior-point method for solving large scale optimal power flow problems," *Electric Power Systems Research*, vol. 95, pp. 276–283, 2013.

[33] F. Capitanescu, "Critical review of recent advances and further developments needed in ac optimal power flow," *Electric Power Systems Research*, vol. 136, pp. 57–68, 2016.

[34] K. Christakou, M. Paolone, and A. Abur, "Voltage control in active distribution networks under uncertainty in the system model: a robust optimization approach," *IEEE Transactions on Smart Grid*, 2017.

[35] D. Silver, J. Schrittwieser, K. Simonyan, I. Antonoglou, A. Huang, A. Guez, T. Hubert, L. Baker, M. Lai, A. Bolton *et al.*, "Mastering the game of go without human knowledge," *Nature*, vol. 550, no. 7676, p. 354, 2017.

[36] Q. Yang, G. Wang, A. Sadeghi, G. B. Giannakis, and J. Sun, "Real-time voltage control using deep reinforcement learning," *arXiv preprint arXiv:1904.09374*, 2019.

[37] H. Xu, A. D. Domínguez-García, and P. W. Sauer, "Optimal tap setting of voltage regulation transformers using batch reinforcement learning," *arXiv preprint arXiv:1807.10997*, 2018.

[38] W. Wang, N. Yu, J. Shi, and Y. Gao, "Volt-var control in power distribution systems with deep reinforcement learning," *IEEE SmartGridComm*, 2019.

[39] W. Wang, N. Yu, Y. Gao, and J. Shi, "Safe off-policy deep reinforcement learning algorithm for volt-VAR control in power distribution systems," *IEEE Transactions on Smart Grid*, vol. 11, no. 4, pp. 3008–3018, Jul. 2020. [Online]. Available: https://doi.org/10.1109/tsg.2019.2962625

[40] Y. Gao, W. Wang, and N. Yu, "Consensus multi-agent reinforcement learning for volt-var control in power distribution networks," *arXiv preprint arXiv:2007.02991*, 2020.

[41] J. G. Vlachogiannis and N. D. Hatziargyriou, "Reinforcement learning for reactive power control," *IEEE transactions on power systems*, vol. 19, no. 3, pp. 1317–1325, 2004.

[42] H. Liu and W. Wu, "Online multi-agent reinforcement learning for decentralized inverter-based volt-var control," *arXiv preprint arXiv:2006.12841*, 2020.

[43] D. Cao, J. Zhao, W. Hu, F. Ding, Q. Huang, and Z. Chen, "Distributed voltage regulation of active distribution system based on enhanced multi-agent deep reinforcement learning," *arXiv preprint arXiv:2006.00546*, 2020.

[44] R. E. Helou, D. Kalathil, and L. Xie, "Fully decentralized reinforcement learning-based control of photovoltaics in distribution grids for joint provision of real and reactive power," *arXiv preprint arXiv:2008.01231*, 2020.

[45] R. Walling, R. Saint, R. Dugan, J. Burke, and L. Kojovic, "Summary of distributed resources impact on power delivery systems," *IEEE Trans. on Power Del.*, vol. 23, no. 3, pp. 1636–1644, Jul. 2008.

[46] Z. K. Pecenak, J. Kleissl, and V. R. Disfani, "Smart inverter impacts on california distribution feeders with increasing pv penetration: A case study," in *PESGM, 2017*. IEEE, 2017, pp. 1–5.

[47] R. Caldon, M. Coppa, R. Sgarbossa, and R. Turri, "A simplified algorithm for oltc control in active distribution mv networks," in *AEIT Annual Conference, 2013*. IEEE, 2013, pp. 1–6.

[48] P. M. Carvalho, P. F. Correia, and L. A. Ferreira, "Distributed reactive power generation control for voltage rise mitigation in distribution networks," *IEEE trans. on Power Syst.*, vol. 23, no. 2, pp. 766–772, 2008.

[49] R. Yan and T. K. Saha, "Voltage variation sensitivity analysis for unbalanced distribution networks due to photovoltaic power fluctuations," *IEEE Trans. on Power Syst*, vol. 27, no. 2, pp. 1078–1089, May. 2012.

[50] R. Schwalbe, F. Herb, B. Bletterie, A. Abart, R. Pointer, and M. Stifter, "DG DemoNet: impact of volt/VAR control on increasing the voltage band reserve - results from field trial validations," in *22nd International Conference and Exhibition on Electricity Distribution (CIRED 2013)*. Institution of Engineering and Technology, 2013.

[51] X. Liu, A. Aichhorn, L. Liu, and H. Li, "Coordinated control of distributed energy storage system with tap changer transformers for voltage rise mitigation under high photovoltaic penetration," *IEEE Trans. on Smart Grid*, vol. 3, no. 2, pp. 897–906, Jun. 2012.

[52] M. Abdel-Rahman, F. Youssef, and A. Saber, "New static var compensator control strategy and coordination with under-load tap changer," *IEEE Trans. on Power Del.*, vol. 21, no. 3, pp. 1630–1635, Jul. 2006.

[53] M. Oshiro, K. Tanaka, T. Senjyu, S. Toma, A. Yona, A. Y. Saber, T. Funabashi, and C.-H. Kim, "Optimal voltage control in distribution systems using PV generators," *International Journal of Electrical Power & Energy Systems*, vol. 33, no. 3, pp. 485–492, Mar. 2011.

[54] Y. P. Agalgaonkar, B. C. Pal, and R. A. Jabr, "Distribution voltage control considering the impact of PV generation on tap changers and autonomous regulators," *IEEE Trans. on Power Syst.*, vol. 29, no. 1, pp. 182–192, Jan. 2014.

[55] J. H. Harlow, "Load tap changing control," Beckwith Electric Company, Tech. Rep., 1996.

[56] Z. K. Pecenak, V. R. Disfani, M. J. Reno, and J. Kleissl, "Multiphase distribution feeder reduction," *IEEE Transactions on Power Systems*, vol. 33, no. 2, pp. 1320–1328, 2017.

[57] H. Farhangi, "The path of the smart grid," *IEEE Power and Energy Mag.*, vol. 8, no. 1, pp. 18–28, Jan. 2010.

121

[58] C. W. Chow, B. Urquhart, M. Lave, A. Dominguez, J. Kleissl, J. Shields, and B. Washom, "Intra-hour forecasting with a total sky imager at the UC san diego solar energy testbed," *Solar Energy*, vol. 85, no. 11, pp. 2881–2893, nov 2011. [Online]. Available: https://doi.org/10.1016/j.solener.2011.08.025

[59] H. Yang, B. Kurtz, D. Nguyen, B. Urquhart, C. W. Chow, M. Ghonima, and J. Kleissl, "Solar irradiance forecasting using a ground-based sky imager developed at uc san diego," *Solar Energy*, vol. 103, pp. 502–524, 2014.

[60] C. Li, E. Ratnam, and J. Kleissl, "Distribution feeder hotspots," California Solar Initiative RD&D Program, Tech. Rep., 2016.

[61] D. Dohnal, "On-load tap-changers for power transformers-a technical digest," *Firmenschrift Maschinenfabrik Reinhausen*, vol. 6, no. 09, 2006.

[62] M. Group *et al.*, "The on-load tap-changer for maximum switching frequency–more switching operations without needing maintenance."

[63] C. Li, C. Jin, and R. Sharma, "Coordination of PV smart inverters using deep reinforcement learning for grid voltage regulation," in *2019 18th IEEE International Conference On Machine Learning And Applications (ICMLA)*. IEEE, Dec. 2019. [Online]. Available: https://doi.org/10.1109/icmla.2019.00310

[64] C. Cortés, H. V. Haghi, C. Li, and J. Kleissl, "Dynamic weight-based collaborative optimization for power grid voltage regulation," in *Solar World Congress 2019*. ISES, 2019.

[65] B. A. Robbins and A. D. Domínguez-García, "Optimal reactive power dispatch for voltage regulation in unbalanced distribution systems," *IEEE Transactions on Power Systems*, vol. 31, no. 4, pp. 2903–2913, 2016.

[66] E. Dall'Anese, S. V. Dhople, B. B. Johnson, and G. B. Giannakis, "Decentralized optimal dispatch of photovoltaic inverters in residential distribution systems," *IEEE Transactions on Energy Conversion*, vol. 29, no. 4, pp. 957–967, 2014.

[67] P. P. Singh, "Coordinated voltage control in active distribution network with on-load tap changer and solar pv system systems," 2019.

[68] C. Li, V. R. Disfani, Z. K. Pecenak, S. Mohajeryami, and J. Kleissl, "Optimal oltc voltage control scheme to enable high solar penetrations," *Electric Power Systems Research*, vol. 160, pp. 318–326, 2018.

[69] Z. K. Pecenak, V. R. Disfani, M. J. Reno, and J. Kleissl, "Inversion reduction method for real and complex distribution feeder models," *IEEE Transactions on Power Systems*, vol. 34, no. 2, pp. 1161–1170, 2018.

[70] W. H. Kersting, *Distribution system modeling and analysis*. CRC press, 2006.

[71] K. Turitsyn, P. Sulc, S. Backhaus, and M. Chertkov, "Options for control of reactive power by distributed photovoltaic generators," *Proceedings of the IEEE*, vol. 99, no. 6, pp. 1063–1073, 2011.

[72] Gurobi Optimization, LLC, "Gurobi 8 performance benchmarks," 2019. [Online]. Available: http://www.gurobi.com/pdfs/benchmarks.pdf

[73] Z. K. Pecenak, H. V. Haghi, C. Li, M. J. Reno, V. R. Disfani, and J. Kleissl, "Aggregation of voltage-controlled devices during distribution network reduction," *IEEE Transactions on Smart Grid*, pp. 1–1, 2020. [Online]. Available: https://doi.org/10.1109/tsg.2020.3011073

[74] Hawaiian Electric, Maui Electric, and Hawaii Electric Light, "Hawaiian electric rules," 2018.

[75] C. Li, V. R. Disfani, H. V. Haghi, and J. Kleissl, "Optimal voltage regulation of unbalanced distribution networks with coordination of OLTC and PV generation," in *2019 IEEE Power & Energy Society General Meeting (PESGM)*. IEEE, Aug. 2019. [Online]. Available: https://doi.org/10.1109/pesgm40551.2019.8973852

[76] ——, "Coordination of oltc and smart inverters for optimal voltage regulation of unbalanced distribution networks," *Electric Power Systems Research*, vol. 187, p. 106498, 2020.

[77] J. Kober, J. A. Bagnell, and J. Peters, "Reinforcement learning in robotics: A survey," *The International Journal of Robotics Research*, vol. 32, no. 11, pp. 1238–1274, 2013.

[78] R. Diao, Z. Wang, D. Shi, Q. Chang, J. Duan, and X. Zhang, "Autonomous voltage control for grid operation using deep reinforcement learning," in *2019 IEEE Power & Energy Society General Meeting (PESGM)*. IEEE, Aug. 2019. [Online]. Available: https://doi.org/10.1109/pesgm40551.2019.8973924

[79] J. Duan, D. Shi, R. Diao, H. Li, Z. Wang, B. Zhang, D. Bian, and Z. Yi, "Deep-reinforcement-learning-based autonomous voltage control for power grid operations," *IEEE Transactions on Power Systems*, vol. 35, no. 1, pp. 814–817, 2019.

[80] J. Duan, H. Li, X. Zhang, R. Diao, B. Zhang, D. Shi, X. Lu, Z. Wang, and S. Wang, "A deep reinforcement learning based approach for optimal active power dispatch," in *2019 IEEE Sustainable Power and Energy Conference (iSPEC)*. IEEE, Nov. 2019. [Online]. Available: https://doi.org/10.1109/ispec48194.2019.8974943

[81] T. Lan, J. Duan, B. Zhang, D. Shi, Z. Wang, R. Diao, and X. Zhang, "Ai-based autonomous line flow control via topology adjustment for maximizing time-series atcs," *arXiv preprint arXiv:1911.04263*, 2019.

[82] S. Wang, J. Duan, D. Shi, C. Xu, H. Li, R. Diao, and Z. Wang, "A data-driven multi-agent autonomous voltage control framework using deep reinforcement learning," *IEEE Transactions on Power Systems*, pp. 1–1, 2020. [Online]. Available: https://doi.org/10.1109/tpwrs.2020.2990179

[83] C. J. Watkins and P. Dayan, "Q-learning," *Machine learning*, vol. 8, no. 3-4, pp. 279–292, 1992.

[84] D. Silver, G. Lever, N. Heess, T. Degris, D. Wierstra, and M. Riedmiller, "Deterministic policy gradient algorithms," 2014.

[85] T. P. Lillicrap, J. J. Hunt, A. Pritzel, N. Heess, T. Erez, Y. Tassa, D. Silver, and D. Wierstra, "Continuous control with deep reinforcement learning," *arXiv preprint arXiv:1509.02971*, 2015.

[86] V. Rigoni and A. Keane, "Open-dsopf: an open-source optimal power flow formulation integrated with opendss," in *2020 IEEE Power & Energy Society General Meeting (PESGM)*. IEEE, Aug. 2020.

[87] N. Van Der Borg and A. Burgers, "Inverter undersizing in pv systems," in *3rd World Conference onPhotovoltaic Energy Conversion, 2003. Proceedings of*, vol. 2. IEEE, 2003, pp. 2066–2069.

[88] R. H. Byrd, J. Nocedal, and R. A. Waltz, "Knitro: An integrated package for nonlinear optimization," in *Large-scale nonlinear optimization*. Springer, 2006, pp. 35–59.

[89] W. E. Hart, C. D. Laird, J.-P. Watson, D. L. Woodruff, G. A. Hackebeil, B. L. Nicholson, and J. D. Siirola, *Pyomo-optimization modeling in python*. Springer, 2017, vol. 67.

[90] M. Alonso and H. Amaris, "Voltage stability in distribution networks with dg," in *2009 IEEE Bucharest PowerTech*. IEEE, 2009, pp. 1–6.

[91] H. Akhavan-Hejazi and H. Mohsenian-Rad, "Optimal operation of independent storage systems in energy and reserve markets with high wind penetration," *IEEE Transactions on Smart Grid*, vol. 5, no. 2, pp. 1088–1097, 2013.

[92] F. U. Nazir, B. C. Pal, and R. A. Jabr, "A two-stage chance constrained volt/var control scheme for active distribution networks with nodal power uncertainties," *IEEE Transactions on Power Systems*, vol. 34, no. 1, pp. 314–325, 2018.

[93] Z. Taylor, H. Akhavan-Hejazi, E. Cortez, L. Alvarez, S. Ula, M. Barth, and H. Mohsenian-Rad, "Battery-assisted distribution feeder peak load reduction: Stochastic optimization and utility-scale implementation," in *2016 IEEE Power and Energy Society General Meeting (PESGM)*. IEEE, 2016, pp. 1–5.

[94] H. Liu and W. Wu, "Two-stage deep reinforcement learning for inverter-based volt-var control in active distribution networks," *arXiv preprint arXiv:2005.11142*, 2020.

[95] R. Lowe, Y. I. Wu, A. Tamar, J. Harb, O. P. Abbeel, and I. Mordatch, "Multi-agent actor-critic for mixed cooperative-competitive environments," in *Advances in neural information processing systems*, 2017, pp. 6379–6390.

[96] Y. Gao, W. Wang, J. Shi, and N. Yu, "Batch-constrained reinforcement learning for dynamic distribution network reconfiguration," *IEEE Transactions on Smart Grid*, pp. 1–1, 2020. [Online]. Available: https://doi.org/10.1109/tsg.2020.3005270

[97] S. Fujimoto, D. Meger, and D. Precup, "Off-policy deep reinforcement learning without exploration," in *International Conference on Machine Learning*, 2019, pp. 2052–2062.